POLITECNICO DI TORINO

Master's Degree in Electronic Engineering

Master's Degree Thesis

Role of spatial filtering in the pre-processing chain of a BCI for non-responsive patients

Supervisors

Prof. Gabriella OLMO

Prof. Vito DE FEO

Candidate

Andrea BONOMI

12 December 2022

"E' l'affetto ciò che conta"

Abstract

Brain injuries represent a relevant current public health problem. Often, they lead to periods of unconsciousness, coma, or even death. Generally, individuals who exit from a period of coma survive in a non-responsive state, unable to voluntarily respond to external stimuli. For these nonresponsive patients, even though they accomplish movements, it is not trivial to establish and associate them with a level of consciousness, in order to interpret their intentions. This obstacle may easily conduct to misleading diagnoses. In order to obtain a more reliable diagnosis, it is essential to establish and develop methods able to enhance studies of various levels of consciousness in nonresponsive patients. In this thesis an innovative brain-computer interface (BCI) is presented, having the goal to analyze electroencephalographic (EEG) and electromyographic (EMG) signals, recorded from healthy individuals, to extract meaningful information about the intention to move while performing or imagining to perform motor tasks and to compare them with the ones retrieved from nonresponsive patients. This BCI is characterized by a pre-processing chain that aims at cleaning the raw EEG signals, extracting particular voltage waves called readiness potential (RP), which are analyzed and improved to be sent to a machine-learning algorithm, which will utilize them to perform a classification to execute differential diagnosis. The thematic nucleus of this thesis regards spatial filtering, which represents one of the blocks of the pre-processing chain that consists of an offline method to filter data in the spatial domain. Most specifically, the main analyses will deal with:

(1) a definition of the idea behind a spatial filter with a presentation of several pre-existent versions in literature;
(2) a classification of their principal features;
(3) an explanation of updates introduced in the previous versions of spatial filters to try improving them;
(4) several discussions about their performance in extracting a motor component called Lateralized Readiness Potential (LRP), in generating topographies of the scalp and modifying RPs of healthy people subjected to voluntary, semi-voluntary and involuntary tasks;
(5) final reflections regarding their role with advantages and disadvantages they bring to final RPs for machine learning algorithm.

In addition to that, this BCI is employed to study signals registered from hemiplegic patients to verify whether the motor intention on the hemiplegic side is preserved. Therefore, spatial filters are tested on data recorded from hemiplegic, as well.

Summary

Cadidate: *Andrea Bonomi*
Matricola: *s287689*
Supervisors: *Prof. Gabriella Olmo, Prof. Vito De Feo*
Title: *Role of spatial filtering in the pre-processing chain of a BCI for non-responsive patients*

Thesis purpose and brief description of the research area:

The challenge of the project consists in realizing the design of a low-cost non-invasive assessment method that, starting from electroencephalographic (EEG) and electromyographic (EMG) signals, can detect and distinguish different levels of consciousness in nonresponsive patients. The assessment method is a brain-computer interface which is characterized by a combination between a pre-processing chain and a machine learning algorithm. The pre-processing chain is characterized by several blocks that perform elaborations and analyses of the EEG signals to estimate the readiness potentials (RPs), which are specific voltage waveforms that highlights the intention of a subject to execute a motor task. The main idea is try to demonstrate that individual consciousness is correlated to the intention to move or even the imagination to move a muscle, so that RPs would become a valid bio-marker from which starts to establish a level of consciousness. After the calculation of RPs, they are sent to the machine learning algorithm, whose goal consists in classifying them to help conducting differential diagnosis on patients.
The aim of the thesis focuses on the improvement of some steps of the pre-processing chain, in particular on the spatial filters introduced to enhance the quality of the obtained Readiness Potential (RP), allowing a more accurate classification.

Personal contribution and results obtained

Before the beginning of this thesis, the function of spatial filtering was not employed in the pre-processing chain. Starting from literature's examples, they have been introduced and a list of features has been elaborated in order to estimate

its necessity. Firstly, spatial filters have been used as high pass spatial filters on healthy subjects and each of them demonstrated to be able to satisfy at least one of the following purpose:
(1) extract high spatial components of RPs useful to produce 2D topographies of the scalp to enhance the activity of some specific regions of the brain, even in cases where the signals were recorded from small EEG-cap.
(2) accentuate the slope between the peak of intention and the peak of the motor execution, which is an important feature for the machine learning algorithm to classify the quality of an RP.
(3) help visualizing an approximation of the lateralization of the readiness potential to establish the most active brain hemisphere.
Successively:
(4) initial standard filters have been updated in order to slightly improve the signal-to-noise ratio of the RPs where possible.
(5) they have been set to allow the user to choose among at least four types of spatial filters and to modify some parameters to tuning their functions accordingly to the nature of the input raw signal, so that they can be tested with signals recorded not only from motor tasks, but also other kinds of experiments.
They have all been tested and compared on the same healthy people subjected to voluntary, semi-voluntary and involuntary motor tasks to individuate two of them that were able to satisfy the greater number of the previous requirements and to be employed as low pass spatial filters, as well. The low pass versions provided:
(6) improvements of the RPs waveforms.
(7) enhancement of their signal-to-noise ratio.
They showed a good selectivity in filtering high or low spatial frequencies and they have been successfully tested on signals recorded from hemiplegic patients.

Acknowledgements

First of all, I would like to thank my mother for her unmatched support. If you had not convinced me to avoid giving up after the first suffered year of university, I would have not become an electronic engineer today. I am glad you decided to invest on me and helped me being a young man. I hope to make you feel proud.
Secondly, I would like to express my gratitude to the historical friends that remained closed and faithful to me during these journey, sharing ups and downs. In particular, I express my sincere gratitude to Marzia, for her endless encouragement, her ability to lighten my soul and our emotional conversations about life. I thank Giorgia, Lucia and Rosanna to be present in my life since the middle school and to be my endless sources of joy and laughs. I also thank Dario, Luca, Stefano B., Stefano G., Francesca, Mattia for the countless adventures that enriched these last years, making them so special. I am obliged to mention volleyball, the amazing sport that accompanied me during this trip, freeing me from stress and allowing me to know a lot of team mates I enjoyed unutterable moments with, especially after matches and training. Impossible to forget mentioning Cristina, Micaela and Viviana, three crazy girls I exalted and cried out with during these lasts months as thesis students.
I show extreme recognition to my supervisors for the opportunity they gave me to work on such an engaging project and for their helpfulness. Additionally, I show gratitude to all the teachers I met that pushed me over my limits and contributed to make me an engineer who can potentially do anything.
In conclusion, from the bottom of my heart, I sincerely thank every person that I have not already mentioned who, even for a short period of time, has been involved in this wild travel, from old friends that I lost to new I found, from lovers I encountered to people I did not have the time to become deep friends with. I am grateful for this thesis and for every person that loved me and believed in me. This master degree is dedicated to all of you and to my younger colleagues that deserve to realize their dreams.

Table of Contents

List of Tables

List of Figures

Acronyms

AI

Artificial Intelligence

BCI

Brain Computer Interface

BP

Bereitschaft Potential

CNV

Contingent Negative Variation

DOS

Disorder Of Consciousness

DTI

Diffusion Tensor Imaging

EEG

Electroencephalography

EMG

Electromyography

ERN

Error Related Negativity

ERP

Event Related Potential

fMRI

Functional Magnetic Resonance Imaging

ICA

Independent Component Analysis

LIS

Locked-In Syndrome

LRP

Lateralized Readiness Potential

MEG

Magnetoencephalography

MCS

Minimally Conscious State

MP

Motor Potential

MRCP

Movement Related Cortical Potential

MU

Motor Unit

MUAP

Motor Unit Action Potential

PMP

Pre-motion Positivity

RP

Readiness Potential

SF

Spatial filter

SMA

Supplementary Motor Area

SNR

Signal-to-Noise Ratio

PCI

Perturbational Complex Index

PET

Positron Emission Tomography

PSP

Post Synaptic Potential

TBI

Traumatic Brain Injury

TF

Transfer Function

TMS

Transcranical Magnetic Simulation

VS

Vegetative State

Chapter 1

Mistery of consciousness

The term consciousness immediately evokes more meanings to describe a wide range of mental phenomena. It indicates vigilance in terms of being wide-awake, but even awareness of oneself and of somebody's actions. It embraces the intention to perform an action and it manifests through body sensations (e.g. pain, pleasure) and sensory perceptions (i.e. sounds, colors), involving moods and emotions. It is hard to identify consciousness through standard laws of scientific investigation and verification, since they are strongly changeable from subject to subject. An interesting starting point is to view consciousness as a physical-chemical event generated by the brain. In this context, complications related to studies of consciousness can be divided into two main groups: easy and hard problems. Easy ones are related to neural mechanisms that can be explained by standard methods of cognitive science. The hard ones regard subjective experience, which adds an unpredictable parameter that ignores usual methods of neuroscience. Quoting the philosopher David Chalmers: *"In conclusion, theories so far have not solved the hard problem of mind and consciousness, namely how a physical brain can generate a non-physical essence."*[1],[2].
Progress in medical cures increased the number of people who survive painful brain damages [3]. Most commonly, they rapidly recover from coma in the first days after injury. Nevertheless, some of them permanently loose their main brain functions. When patients' recovery is quite slow, they tend to face different states of consciousness, implying situations in which they are awake but unaware (vegetative state) or they experience little moments of consciousness (minimally conscious state). Clinically speaking, the evaluation of these possible states is elaborated after the examination of two principal components of consciousness: **arousal** and **awareness**. Arousal is determined by spontaneous eye opening, while awareness is evaluated depending on responses to external stimuli. Awareness requires arousal, but preserved arousal levels do not imply awareness. Often, it is not trivial to produce reliable diagnosis based only on these parameters. On the other hand, other

elements can be taken into consideration in the studying of consciousness. Motor responsiveness is one of the first resources which enables to establish an important clinical evaluation of consciousness. Unfortunately, if patients suffer from diseases that impede motor movements (e.g. hemiplegia), study of consciousness becomes complicated. Consequently, it is crucial to find more objective diagnostic tools. In this context, the BCI presented in this thesis enters the scene. By analyzing cerebral signals produced during motor tasks, it tries to help quantifying the level of awareness in order to simplify the categorization of levels of consciousness.
In the next sections, a background scenario about the world of consciousness is provided. The path proposed in this chapter starts from introductory information regarding aspects involved in the concept of consciousness, a presentation of an existent evaluation scale with descriptions about disorders of consciousness and exploration of typical techniques employed in the methods of assessment. It concludes with an examination of a model that highlights the relevance of studying motor programming and cognition.

1.1 Neurological fragments of consciousness

Neurologically speaking, consciousness group a lot of aspects:

- *Level of vigilance:* it is the level of attention in experiencing psychic activities. Fluctuations of vigilance are controlled by reticular formation, which is situated in the median region of the brain stem.
- *Peripherals correlates of consciousness:* they are somatic alterations that cause fluctuation of vigilance and involve ocular movements, spontaneous and reflex body mobility, muscle tone and breath.
- *Electrical activity of the brain:* it represents the activation of the cerebral cortex. Ascending reticular projections are specialized in the modulation of cerebral electrical activity.
- *Contents of consciousness:* they emphasize elements of mental activity, such as thoughts, feelings, dreams that emerge in mind. Cerebral cortex is responsible for managing them. Most specifically, it can be schematized in two working areas: the first is called *specific*, which manages elementary functions such as execution of a movement. The second is called *associative*, which establishes connection between different regions of the cortex and performs integrative functions, such as processing sensory information or recognition of objects.
- *Self memory:* memories are stored from the hippocampus, the medial temporal cortex and the sensory associative areas. The associative cortex administers both short-term and long-term memory.

- *Selective attention:* it can be represented as the focusing of mental activity on something. It can be expressed in case of a voluntary choice of doing something of interest, such as solving a mathematical problem or in case a situation individuals are subjected to some stimulus, such as when they see the face of a person known in the crowd. Selective attention is controlled by posterior parietal, basal temporal and prefrontal associative cortical zones [4].

1.2 Levels of consciousness

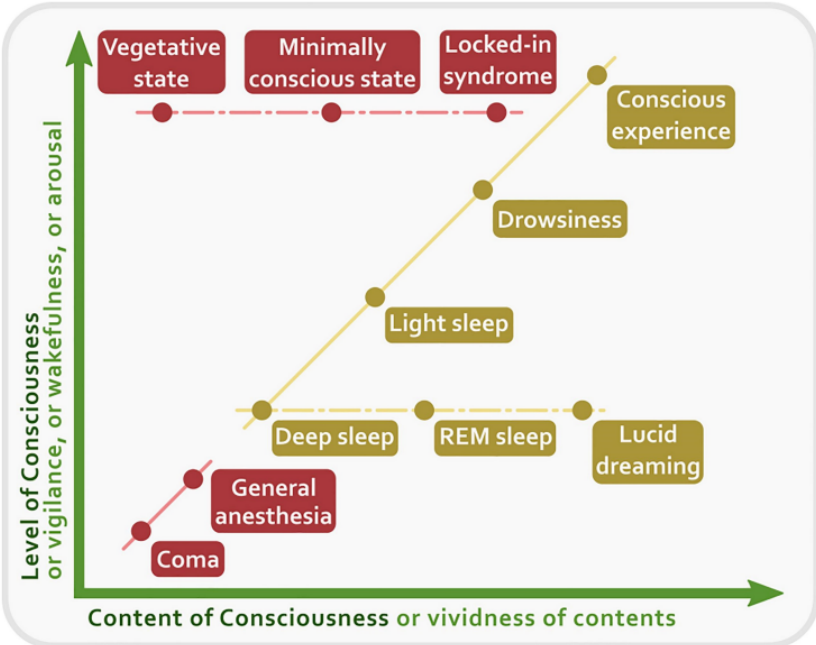

Figure 1.1: Scale to represent consciousness. The X axis represents the Content of Consciousness, while the Y axis represents the Level of Consciousness or wakefulness. Red color is used to identify clinical conditions to stabilize the level of consciousness, while yellow colour is employed for highlighting normal physiological states. The dots represent the Perturbational Complex Index [5].

Levels of consciousness can be measured by employing the Perturbational Complexity Index (PCI) shown in Figure 1.1. The two main relevant aspects put on the axis are content of consciousness and level of consciousness. The first highlights general awareness to recognise what happens in the surrounding environment. The second depicts a general state of vigilance, not strictly associated to awareness. PCI scale was introduced by Casali et al. (2013) and used to discriminate successfully levels

of consciousness in patients subjected to transcranial magnetic stimulation (TMS) evoked potentials measured with EEG.

1.3 Disorders of consciousness

Generally brain lesions that worsen consciousness are characterized by damages reported to reticular formation, reticular-thalamic-cortical pathways, cerebral cortex, and memory circuits. The main disorders of consciousness are presented:

- **Coma**: it is a state in which some functions are preserved, such as breathing and blood circulation, but the individual is not able to perform tasks, since it is not awake. Generally, it lasts a period of time that not exceed one month. After that, the person can completely recover consciousness either enter a vegetative state or in worst cases meet brain death. The origin of this state is due to several disruptions in the communication of neurons through electrical impulses belonging to the brain stem and the cerebral cortex (gray matter). Typical symptoms are: closed eyes, no responsiveness to environmental stimuli, impossibility to communicate, weakness in simple actions such as breathing, swallowing, coughing [6],[7].

- **Vegetative state (VS)**: severe dysfunctions of some hemispheres of the brain may cause this state where unconsciousness and lack of responsiveness are distinguished in the subject. Since brain stem and diencephalon are quite untouched, motor and neurovegetative reflexes, together with sleep-wake cycles are preserved. Differently from coma, through pain some motor involuntary response can be provoked, cranial nerves and spinal reflexes are intact. Even in this case, the subject is unable to execute tasks [8].

- **Minimally conscious state (MCS)**: it involves bad alterations of consciousness, but the subject demonstrates a minimal awareness of itself and of the surrounding environment. That is the main characteristic that distinguishes MCS from coma and VS. It manifests after one of the two previous disorders. It can last for a short period of time or accompany the patient til its death.

Locked-in syndrome is not a disorder of consciousness, even though paralysis of facial muscles and limbs can mislead, since they impede any reaction.

- **Locked-in syndrome (LIS)**: it is recognizable since subject is unable to move, speak, change facial expressions. Usually, only communication with a code based on blinking of eyes is possible. Patients are trapped in their body, but they are completely awake, preserving cognitive functions. For that reason, LIS is not placed in disorder of consciousness, since patients are not unconscious [7].

1.4 Instrumental assessment methods

The differential diagnosis of disorders of consciousness (e.g. to distinguish among VS, MCS and LIS) is very challenging, especially when patients with disorders of consciousness (DOCs) are unable to speak, move, complete a task or show a clear response to a stimulus. Paralysis, aphasia, fluctuations in arousal level, drugs' side effects, hard distinction between reflexive and voluntary movements are additional contributes that tend to increase clinical errors. Therefore, approaches purely behavioural are not enough. Fortunately, many more technology-based techniques exist to help defining subjects' states of consciousness, combining both temporal and spatial properties:

- **Positron Emission Tomography(PET)**: it is a medical imaging technique aimed at revealing activity and functions of thanks to the recording of the emission of positrons from radioactively labeled molecules. First of all, tracers are pre-prepared to be further injected into the bloodstream of the patient. They are specially-designed radioactive molecules generated in a cyclotron, a device that accelerates in a circular path charged particles through magnets and send them against ordinary atoms belonging to a particular chosen molecule (e.g. Oxygen-18). After these hits, the ordinary atoms become radioactive (Oxygen-18 becomes Fluorine-18) and the molecule, after being purified from a biological molecule synthesizer, gives birth to the tracer. After injecting the tracer into a vein in the arm or hand, its radioactive atoms starts loosing their radioactivity, freeing positrons that rapidly annihilate with electrons, realising gamma rays in opposite directions. The PET scanner is a big ring of gamma-ray detectors that, by recording them at each second, after each annihilation, it is able to reconstruct a three-dimensional activity map of the brain (Figure 1.3). These maps may be related to a specific DOC: comatose patients present a reduced metabolism from grey-matter, while reduced global metabolism of the brain emerged from patients in VS or MCS, whose awareness is severely deteriorated. PET studies also demonstrated that patients in MCS report a partial preservation of large-scale associative fronto-parietal network. To conclude, even though it provides absolute measures of the regional cerebral blood flow and it appears to be very reliable in distinguishing VS, MCS from LIS (Figure 1.2), it is an expensive technique, it requires time and precision to produce high quality tracers and it has a poor temporal resolution.

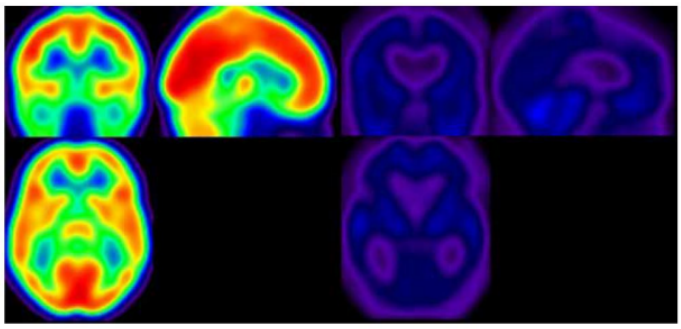

Figure 1.2: If the radio-activated molecule is fludeoxyglucose (FDG), it is possible to see on the monitor the levels of metabolism of the brain's tissue. The image shows the levels of metabolism represented with two colors: the red and yellow in the left identifies a high consumption of glucose, indeed images belong to an healthy subject; the blue color to the right reflect a low consumption of glucose and those images belong to a patient suffering from an unresponsive wakefulness syndrome.

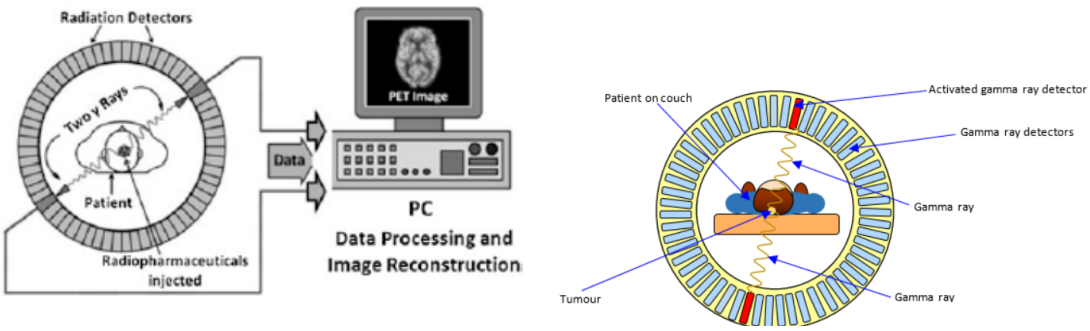

Figure 1.3: PET schematics.

- **Functional Magnetic Resonance Imaging (fMRI):** Magnetic Resonance Imaging (MRI) is the basis of this technique. Hemoglobin present in blood is essential to transport oxygen, a nutrient that neural cells need to survive. Hemoglobin can be subjected to chemical process that transform it into oxygenated or deoxygenated forms, depending on whether it is bound to or not to molecules of oxygen. These two forms showcase diamagnetic and paramagnetic properties respectively that can be exploited to elaborate some neural maps, representing the brain activity in specific regions. [9],[10]. Indeed, the flow of oxygen is greater towards neurons that are more stimulated by a mental process and viceversa. Consequently more blood will flow in the most active regions. This technique is employable for patients with DOC to

correlate their brain activities with residual cognition and awareness. Residual cognition can be identified even with imagined actions, without involving their concrete execution, helping the identification of a state of consciousness. For instance, Owen et al. conducted a recent fMRI study using mental imagery tasks (imagining playing tennis vs. spatial navigation around one's house) in a large cohort of 54 patients with DOCs. Despite the majority of them had been diagnosed VS/MCS after behavioural assessments, five patients showed the ability to understand spoken commands and to respond to them through brain activity rather than through speech or movement. Imagery tasks elicited distinguishable patterns of activation in specific regions of the brain, that have been compared with the results of studies in healthy volunteers doing the same tasks: imagine to play tennis elicits activity in the supplementary motor area, a region that houses imagination, while imagining moving from room to room in a house commonly activates the parahippocampal cortices, the posterior parietal lobe, and the lateral premotor cortices, regions that contribute to imaginary or real spatial navigation. These results depicted in Figure 1.4 provide evidence that some vegetative patients retain regions of preserved function and that in the absence of behavioural evidence, functional imaging provides a valuable tool to the assessment team.

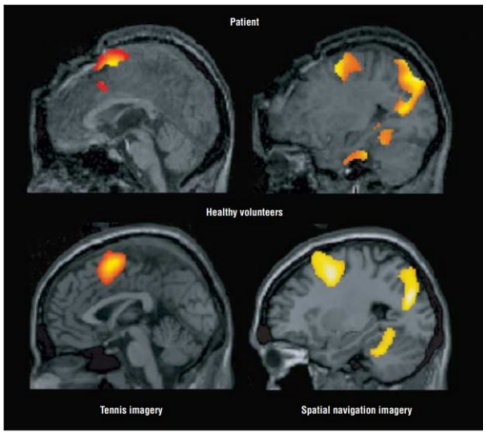

Figure 1.4: The figures depict the activity of the supplementary motor area while both an healthy and a patient imagine to play tennis (left) and moving from room to room in a house (right). In the upper images, a scan of a patient in a vegetative state shows the activation of the Supplementary motor area and the activation of parahippocamal gyrus, posterior parietal lobe and lateral premotor cortex during the two tasks. Comparing with the scans at the bottom, referred to an healthy subject, the areas and the intensity of activation are really similar among the healthy person and the patient.

- **Diffusion Tensor Imaging (DTI):** white matter tissue of the brain contains axons that form the connection between neurons. DTI images emphasize fibers of white matter to highlight which areas in the brain are strongly connected. This is useful to know from where to where the information travel inside the brain. Within white matter, hydrogen protons moves along the directions of axons. It detects differences in hydrogen atoms movements. Thanks to a MRI scan, a magnetic field aligns the hydrogen protons and disrupts their synchronous spinning around their own axis. Therefore they no longer spins with the same phase, indeed some will spin faster and some slower, depending on the applied magnetic field gradient. But in reality, they tend to move and consequently, if they are subjected to a magnetic gradient, they change location, as well. This causes a major diffusion of water, complicating the detection of a localized hydrogen proton's path inside the brain. On the contrary, regions with limited water diffusion can be indicative of neurological conditions, such as stroke. Since hydrogen protons are confined through an axon along only two directions, while they are able to travel along the axon's length, thanks to six magnetic field gradients at least, it is possible to individuate which are the preferential directions hydrogen protons follow in a 3D space. Flow of hydrogen protons through axon is called anistropic diffusion and the tendency to prefer a specific direction where to travel is measured by a factor called fractional anisotropy (FA). By using more gradients, spatial resolution improves. At the end, we have a picture like the one reported in Figure 1.5, where all the white matter tracks are depicted, where colors represent various directions in the 3D space.
  A positive aspect of this technique consists in utilising it even for patients that were sedated to perform *in vivo* detection or to study the shearing axons after a trauma of the brain. Fernandez-Espejo et al. employed DTI *in vivo* to assess a scheme of consciousness to distinguish twenty-five patients in VS and MSC from the diagnostic and etiologic point of view. He discovered that main differences were significantly highlighted in the regions belonging to the talamic and subcortical white matter areas among MCS and unresponsive patients. On the contrary, no differences were detected at the level of the brainstem. The results obtained from the DTI graphs combined with behavioural scores registered after each patient were subjected to a behavioural assessment allowed to classify the patients inside a specific category of DOC successfully. DTI helped emphasizing etiologic dissimilarities in patients in a VS. In conclusion, DTI demonstrated to work as an excellent bio-marker which can cooperate with behavioural assessment methods to classify the level of consciousness of injured patients.

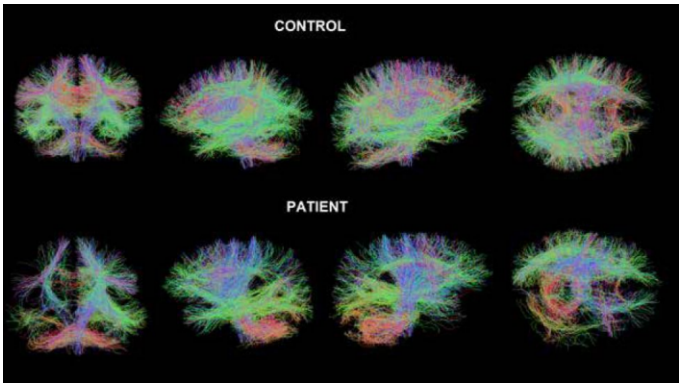

Figure 1.5: The sketches represent the neural maps produced from the usage of DTI. By looking at the neural tracks is possible to notice several structural damages in the patient's brain in a MCS (bottom) localized in the temporo-parietal region in the right hemisphere, where few neural paths are visible in comparison with the healthy volunteer (top). The colors help visualizing the directionality of water diffusion: in particular, red color specifies diffusion from left to right, green from anterior to posterior and blue from superior to inferior directions.

- *Electroencephalography and Transcrania Magnetic Stimulation (EEG-TMS):* EEG combined with Transcranial Magnetic Stimulation (TMS) appear useful in the consciousness assessment because it avoids all the issues that depend on the ability of the subject to understand and follow instructions, to communicate or to perceive sensory stimuli. TMS is non-invasive stimulation technique that uses electromagnetic induction to generate an electric current across the scalp and skull. Pulsed current is generated through a coil reported in Figure 1.6, which is put in proximity with patient's head, stimulating a subset of cortical neurons and modulating neural activity within the cerebral cortex. Perturbations provoked with TMS can be recorded from to measure the effects generated in the brain. In case of patients in VS, no response is detected after TMS by analyzing the EEG signals, emphasizing a breakdown of effective connectivity similar to the one observed in deep sleep and anesthesia. On the contrary, patients in MCS, showed complex EEG activation, involving distant cortical areas, similar to the activation recorded in patients in LIS and healthy awake subjects, even though no conscious behaviour is observable. The couple TMS-EEG appears to be a promising technique in the assessment of DOC patients, since they are not invasive, patients do not need to satisfy any task and they are easy techniques to apply.

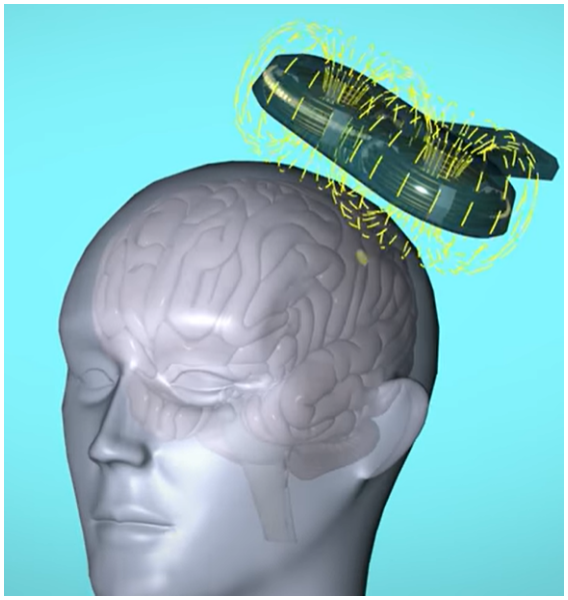

Figure 1.6: Sketch of TMS.

1.5 Conscious intention and motor cognition

Until now, state of consciousness has been the main sphere of interest in these sections. In order to investigate it better, it is necessary to link it to something easier to measure. The idea behind the project of this thesis is try to demonstrate the direct connection between the state of consciousness and the motor intention. Indeed, being aware of an action executed with free willing may correlate these two spheres. In particular, during the action that spans from thinking about a movement to when this is fulfilled, different moments of consciousness can be individuated:

- **Intention of the movement:** it is peculiar in subjects that are able to decide to move a muscle voluntary.
- **Consciousness of the intention:** it consists of the awareness of having previously decided which muscle moves.
- **Consciousness of the movement in progress:** that represents being conscious when the movement is happening.
- **Consciousness to have completed the movement:** being conscious of having finished the movement.

The consciousness about the motor cognition stimulates the front of the SMA and it is not influenced by the execution of the movement. Issues to SMA and parietal areas cause deficits of motor cognition and damage both intentionality and awareness. As a consequence, damages to motor cortex do not deteriorate awareness, which is strictly related to SMA, area devoted to programming movements.
Some researchers established a model to reproduce sequences of events happening in the brain before the execution of a movement (Figure 1.7). All begins with the *desired state*, which is what the subject desires to do. The model is characterized by the following blocks:

- **Motor planner:** it converts the desire state into two copies containing a sequence of commands necessary to realize it. The first copy is produced for the motor cortex that, following the commands, it is able to execute the movement. The second copy is sent to a *predictor*.

- **Forward model:** it is a predictor that generates a predicted state which consists of several sensory consequences due to the implementation of the movement. The predicted state is elaborated before the real execution of the movement happens.

- **Comparator A:** it compares the desire and predicted states. If they coincide, the subject experiences the "sense of agency", therefore the perception of doing the motor action. This perception is felt before the execution of the movement itself.

- **Comparator B:** it puts in comparison the predicted state with the *implemented state*. The latter derives after the activation of the primary motor cortex and the execution of the movement. If these two coincide, the subject is aware of having terminated a movement. Consequently, a damage regarding this comparator leads to a condition in which the patient is unaware of the paralysis that affects one or more muscles. This is what happens in hemiplegic individuals who suffer from *anosognosia* for **hemiplegia**, which will be better explained in chapter 5. Indeed, if comparator A is intact, the sense of agency is preserved, but they cannot feel they did not execute the muscular contraction.

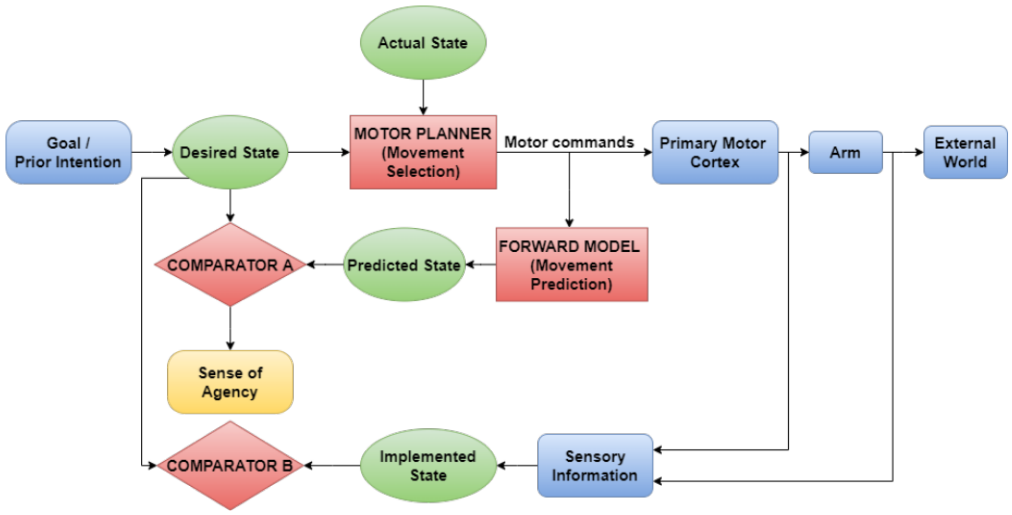

Figure 1.7: Computational model for movement execution..

This model emphasizes the interrelationship between motor cognition and conscious intention, distinguishing the difference between sense of being performing and having actually performed a muscular contraction. The recent challenge consists in studying the unconscious preparatory activity of the brain when there is the necessity to fulfill a movement.

Chapter 2

Detecting consciousness

2.1 Introduction to ERP

As said before, behavioural assessments are not enough to lead to reliable diagnosis regarding levels of consciousness, especially in non-responsive patients. Consequently, the following project aims at implementing an inexpensive and not invasive BCI, able to deliver neuronal commands to a robot controller, which interprets them to perform motor actions. Since consciousness is strongly correlated to the intention of performing voluntary movements, independently if the motor task is fulfilled at the end or just imagined, it is essential to start from recording and studying signals called **event related potential**.
Event related potential (ERP) technique provides a powerful method for exploring the human mind and brain. They are "event related", since they are electrical potentials which arise as a consequence of particular events. In 1929, a scientist called Hans Berger conducted a set of experiments and demonstrated that by putting an electrode above the scalp is possible to measure electrical activity of human beings. The signal registered must be amplified in order to depict a curve that shows changes in voltage over time [11]. This electrical activity is called the electroencephalogram or EEG. Nevertheless, EEG cannot be employed in its raw form to measure neurocognitive responses because it consists in a mix characterized by a wide range of neural sources of activity. Among them, there are neural responses related to sensory, cognitive and motor events. Since these responses are circumscribed to specific sphere of consciousness and can be reproduced by subjecting individuals to specific tasks, extracting them gains interest. To do that, an averaging technique is required combined with time-frequency analyses.
Speaking honestly, between 1965 and 1970, ERP technique drew a bad reputation among psychologists and neuroscientists because they were only employed to find new ERP components and responses, instead of employing them to solve a

more concrete goal. Nonetheless, as time progressed, thanks to the evolution of technology that introduced inexpensive computers and to the abrupt increasing of researches in cognitive neuroscience, ERP technique started becoming more and more popular. Even though other techniques appeared on the scene, such as PET and fMRI, ERP method did not vanish. On the contrary, it succeeded in distinguishing itself from the others because it provides information about human brain and mind, ensuring such a high temporal resolution that cannot be surpassed from other techniques. Most specifically, there are at least five main advantages of ERPs:

1. ERPs are easy and quick to compute with few analysis assumptions or parameters. It is possible to compare them to highlight different brain processes and electrophysiological dynamics arisen when an individual is subjected to tasks involving two different conditions.

2. They ensure high temporal precision, resolution and accuracy at each millisecond.

3. They allow to perform a fast check of the quality of data regarding single-subject data.

4. There is a very rich and decades-long literature of ERP findings a researcher can interpret and compare its results with.

5. They can be used as biomarkers: indeed, they are related to neurotransmission, represent an inexpensive technique and they can be recorded in animal models.

2.2 ERP neural origin

ERPs arise from postsynaptic potentials (PSPs), which are manifested when neurotransmitters bind to receptors, causing a varition in the flow of ions across the cell membrane. ERPs recorded from the scalp are not due to action potentials. Most specifically, a PSP is generated when a neurotransmitter is released from an axon's terminal at the apical dendrite of a cortical pyramidal cell, as shown in Figure 2.1. If the neurotransmitter is excitatory, the neuron's membrane is depolarized and becomes positive, so that a net negative charge is measured just outside the membrane, while a positively charged ionic current starts flowing from apical dendrite to cell body. When this current flows out the cell body and the basal dendrites, the membrane potential returns negative, determining a positive net charge in the extramembrane location, corresponding to these regions. These two opposite concentrations of charge put at small distance creates a dipole, which can be represented as a vector, whose arrow points at the positive terminal. On the

other hand, if the neurotransmitter is inhibitory or the generation of PSP happens at the cell body or basal dendrites, the dipole polarity is reversed. If this process happens in a wide range of similarly oriented neurons at the same time, all the PSPs are summed up and their sum travels through the brain, meninges, skull to reach the scalp at nearly the speed of light. Consequently, ERPs report a direct, instantaneous, millisecond-resolution measurement of neurotransmission-mediated neural activity. Their link with neutrotransmission allows to employ the ERP voltage waveforms as promising biomarkers in the pharmacological studies and treatments. As quoted before, the generation of a single PSP involves a creation of a tiny dipole that origins an oriented flow of current. ERP voltage waveforms can be measured at the scalp only when the dipoles from many thousands of similarly oriented neurons sum together. The orientations are important: different orientations of neurons in the same region lead to a destructive interference during the sum of electromagnetic fields originated from their dipoles, making their detection at distant electrodes impossible. On the other hand, similar orientations allow a constructive interference between electromagnetic fields originated from adjacent neurons, allowing the sum signal to reach the scalp. The most involved neurons in which constructive interference quite often happen are the **pyramidal cells** of the cerebral cortex. Indeed, these cells are oriented perpendicular to the cortical surface, therefore their dipoles sum together rather than canceling out. Consequently, scalp-recorded ERPs almost always reflect neurotransmission that occurs in these cortical pyramidal cells. Therefore, attention should be paid to the fact that they represent only a fraction of brain activity. ERP components can be either positive or negative at the electrode sites. The polarity depends on a combination of several factors and it cannot be used as an unique parameter to draw reliable conclusions regarding a specific ERP component. The superimposition of different dipoles can be represented quite accurately from a single equivalent current dipole. The voltage recorded on the surface of the scalp will be positive on one side of the equivalent dipole and negative on the other, with a single line of zero voltage separating the positive and negative sides. The voltage field spreads out through the conductive medium of the brain, helped by the high resistance of the skull and the low resistance of the overlying scalp, which lead to further spatial blurring [11]. Consequently, the voltage related to a single equivalent dipole appears broadly distributed over the surface of the scalp, especially for ERPs that are generated in deeper cortical structures. Differently from the electrical field, the magnetic field does not suffer from this blurring effect so much, since the skull is transparent to magnetism. For that reason, it is sometimes suggested to record the magnetic signal (from magnetoencephalogram or MEG) instead of EEG signals. Nevertheless, MEG recordings require very expensive equipment and are much less common than EEG recordings.

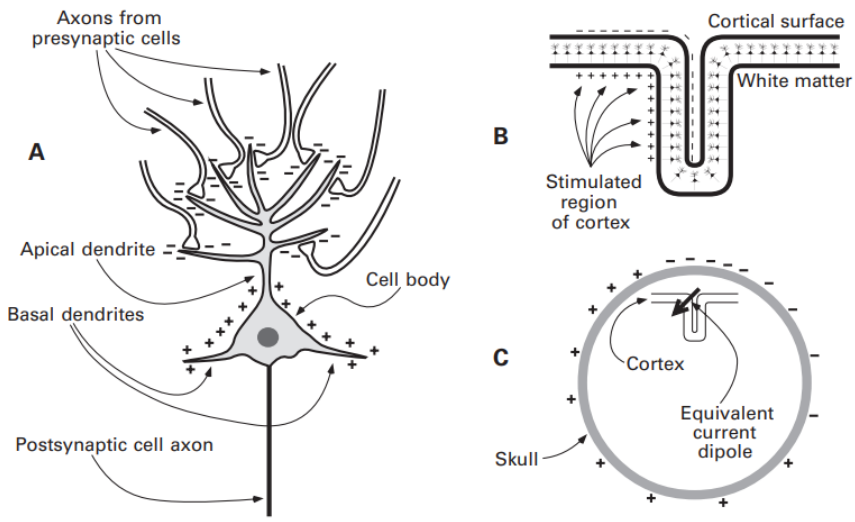

Figure 2.1: (A) Schematic pyramidal cell during neurotransmission. (B) Pyramidal cells contained in a folded sheet of cortex. The sum of individual dipoles happen when a region of this sheet is stimulated. (C) Single equivalent dipole obtain from the superimposition of dipoles related to single neurons. The arrowhead indicates the positive end of the dipole. The distribution of positive and negative voltages registered at the surface of the head depends on the orientation of the equivalent dipole. Between the positive and negative regions, there is the neutral line.

2.3 ERP limitations

The first drawback regards the so called *superposition problem*, because the ERP waveforms recorded on the scalp correspond to the sum of a lot of individual underlying components and it is hard to individuate each of them from this mixture. A consequence of this is the complexity in determining the specific neural generator locations that originate these underlying components. Secondly, a particular mental or neural process does not necessarily produce an ERP. In addition, they have a small amplitude of few μV in comparison to noise level, therefore many trials (from 10 to 500) of an experiment are necessary to reach satisfying statistical power and this is not trivial. Indeed, it requires time to instruct people to perform the task correctly and to record their EEG because ERP waves display in a time window that lasts around 8 s. They also require a well-determined onset of a stimulus corresponding to precise time-locking points. The onset represents the time instant in which the subject reacts to a stimulus by executing an action to complete the task proposed in the experiment. As explained in chapter 3, the onset in this case is represented by the motion of a finger from a patient. Therefore, EMG signal is

also recorded to define it. To be well detected, it requires to be sharp, otherwise, if the onset is difficult to determine because it is gradual or worse it is not present, ERP technique cannot be employed. More detailed explanations about consequence derived from bad detected onset are provided in chapter 5. In Table 2.1 is reported a comparison between ERP and the previous quoted alternative techniques, to have enhance the perspective about their ups and downs. Fundamental parameters are:

- **Invasiveness:** a typical invasive approach considers taking measurements through microelectrodes. They are supposed to be inserted into the brain, therefore their use is limited to animals and human patients that need neurosurgery. As regards PET, it requires to satisfy conditions per each subject to avoid reaching excessive levels of radiation. On the contrary, ERP and fMRI have not limitations on the amount of data which can be collected.
- **Spatial and temporal resolution:** spatial and temporal resolution are significant parameters that affect final ERP visualization, both over time and on the scalp, through images called topographies. Ideally, researcher would like to have both of them as high as possible, in order to distinguish each neuronal source from the others both in space and time. PET, fMRI have excellent spatial resolution around 1 mm and poor temporal resolution, while ERP experiences the mirrored condition. Indeed, ERP's time resolution is 1 ms or less under optimal conditions, while it has a poor spatial resolution owing to the infinite internal neural generators of underlying components that are mix together at the electrodes placed on the scalp. For that reason, ERP allows to answer questions about evolution of neural response that both PET and fMRI cannot. On the other hand, PET and fMRI does not suffer from superposition of different neuronal sources, therefore their results are more spatially localized.
- **Cost:** it always represents the biggest obstacle for researchers. ERP is the cheapest one because it does not need expensive supplies. PET is the most expensive because it needs radiative isotopes with short lifetime and medical personnel to prepare and inject the tracers. Even microelectrode recordings in non-human primates is quite expensive, due to daily costs necessary to maintain the animals. Costs often drives the final choice at employing a specific technique with respect to another. For that reason, ERP remains fairly attractive.

2.4 ERP challenges

The main challenge to face when dealing with ERP signals is what is called **volume conductance**. As explained in section 2.2, when a PSP occurs it generates a dipole.

Table 2.1: Comparison between techniques.

Technique	Invasiveness	Spatial res.	Temporal res.	Cost
ERP	Low	Poor	Excellent	Inexpensive
PET	Moderate	Good	Poor	Expensive
fMRI	Low	Good	Poor	Expensive
Microelectrode	High	Excellent	Excellent	Moderate

Immediately, an instantaneous electric field is determined and it gives birth to an electric current, which is a flow of charged particles (electrons and ions). Because many dipoles are concurrently created, they can be summed together and on the whole the scalp is divided in three portions: a positively charged, a negatively charged and an infinitesimally narrow neutral band that separates the previous two, as highlighted in Figure 2.2. Therefore, an equivalent electric current will flow from the deeper neuronal sources, passing through tissues, to the outer shell of the scalp. Every electron or ion pushes the neighbouring ones thanks to the instantaneous voltage generated by each dipole. This spread pushing phenomena is what defines volume conduction, because electricity does not just run between two poles of a dipole in a conductive medium, but spread all over the conductor. This is possible because tissue of the brain is a conductive material, but since the skull presents an intrinsic high resistance, the voltage increases and this spreading is more exacerbated. On one hand, it could be judged as a good phenomena, because thanks to EEG it is possible to record signals originated in regions far from the electrode placed on the scalp, even though it represents an attenuated version of the original one. On the other hand, each electrode detects a mix of attenuated components related to neuronal generators spread all over the brain, aspect which complicates the precise localization of a specific area of the brain related to a cognitive behaviour. Even in case just one single dipole is generated inside the brain, the different conductivity among tissues causes the signal to be dispersive and to be split up to travel less resistive paths to reach the superficial electrodes on the scalp. Consequently, the scalp distribution of an ERP component is usually very broad and if more dipoles are generated no single neutral band will be present. Volume conduction is the basis of the **inverse problem** that scientist of ERP often encounter. Reflecting on what was explained before, how is it possible to determine how many dipoles have been generated and where they are located by looking at a given voltage distribution all over a scalp?
This inverse problem, consisting in starting from the final result on topographies to retrieve the single neuronal sources is labelled as "undetermined" or "ill-posed" from mathematicians. Indeed, many configurations of dipoles can produce the same topographies, owing to volume conductance phenomena. A practical examples is

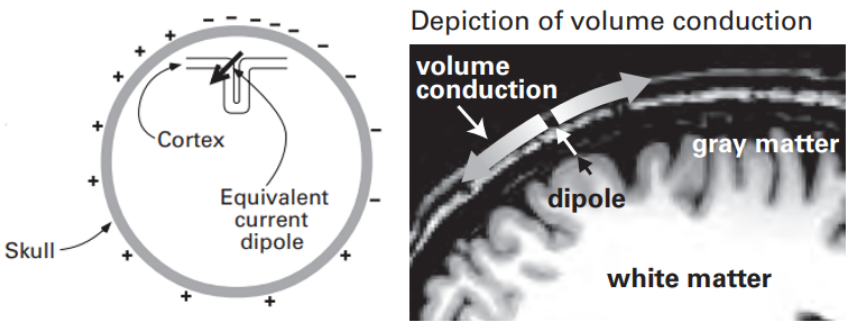

Figure 2.2: (Left) 2D model of the head with one equivalent dipole representing neuronal activation, where positive, negative hemispheres and neutral line are underlined. (Right) volume conductance representation.

reported in Figure 2.3. First of all, comparing A and B case in the picture, it can

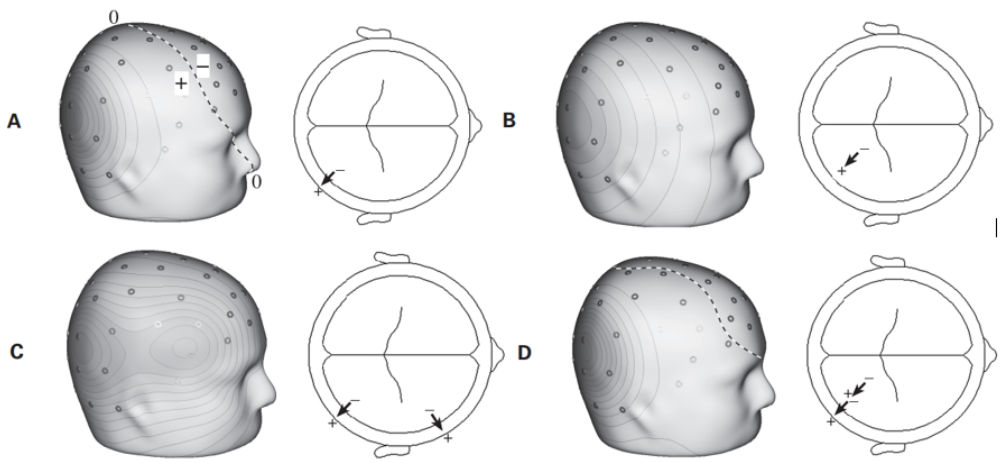

Figure 2.3: Comparison of four possible configurations of dipoles [11]

be noted that small spatial shifts of depth produce a great modifications in the voltage contour lines that detect ERP components. In the simplest case, if there is only one dipole, it can be individuated by looking the more intense region in the topography, where the voltage is maximum. Obviously, it is essential to check that the concentration of voltage is not due to noise or artifacts, which are useless peaks of voltage that cover and distort real information. Furthermore, deeper is the dipole generated and broader are the contour lines.
In case C we have two superficial dipoles, which are pretty distant between them, indeed they are well localized from EEG signal. Everything starts complicating in case D. At first glance, voltage distribution is very similar to case A, but this

time there are two dipoles, when superficial and when deep. The deeper one is covered by the superficial one, therefore, since EEG records well superficial neural activity, the final result in the topography is very similar to the one showed in case A, confirming that more than one solution satisfies the shape of the scalp distribution. Besides that, if deeper dipoles are shadowed by superficial ones, all the experiments stimulating those specific deep neural populations will not produce significant results. The worst scenario happens when the dipoles have different orientations, leading to partial or total destructive interference of the signals measured at the electrodes. Last aspect to keep in mind is the nature of the investigated component. Some ERP components, such as error-related negativity (ERN) which is not studied in this project, are very broader in comparison with others, therefore it can mask other dipoles or being interpreted both as a sum of dipoles or as if it is generated by a single dipole. For all these reasons, it is important to establish smart restrictions to the experiment in order to stimulate few ERP components to facilitate their detection, keeping in mind their nature and peculiar characteristic and making assumptions on where in the scalp they are supposed to activate.

2.5 EEG recording

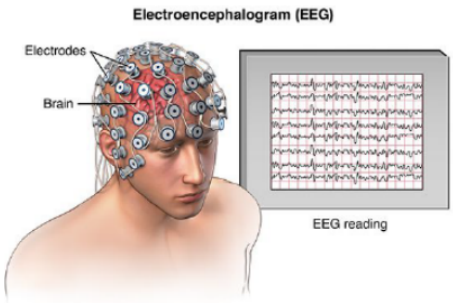

Figure 2.4: Sketch of EEG.

As mentioned before, EEG recording is the main approach to study ERP components. But, more precisely, why should anybody use EEG?
There are several reasons:

1. It is able to capture cognitive dynamics related to different fields that are manifested at various frequencies: from the quick cognitive, perceptual, linguistic, emotional and motor processes that may happen within tens to hundreds of milliseconds, to slower cognitive events that last from hundreds of milliseconds to a few seconds. Therefore, it showcases a high temporal resolution.

2. It directly measures neural activity. The voltage fluctuations of EEG directly reflect biophysical phenomena originated from population of neurons. Furthermore, oscillations that can be observed in the EEG signal implies neural oscillations in the cerebral cortex. Another attractive features is that it is multi-dimensional. EEG data comprise several parameters bound to different domains: time, space, frequency, voltage, power and phase. As said before, voltage over time brings to light neural activity instant by instant in real time. Space domain reveals how the measured components spread all over the scalp and how they are attenuated or not at each electrode, considering the inter-electrode distance. Frequency related to power and phase describes how the statistical power is distributed among the harmonics and how specific phase patterns can bring to light information about neural firing. All these elements combined together pave the way to test hypotheses that gain interest in the world of neurophysiology and psychology. Therefore, the brain can be described as a complex system that uses multi-domains to process, represent and transfer information.

Obviously, as everything in life, there is the dark side of the moon to consider. Which are the disadvantages of EEG?
EEG is not considered adapted to study precise functional localization and to test hypothesis regarding deep brain structures. Indeed, even though EEG manages to measure deep brain neural sources and showcases high temporal precision, resolution and accuracy, on the other hand its spatial precision, resolution, and accuracy are all relatively poor compared to previous analyzed techniques in section 1.4. Nevertheless, researchers have a degree of freedom in order to control it. Indeed, the spatial resolution of EEG is constrained by the number of electrodes. Most scientists employ at least thirty-two or thirty-four electrodes, as did in the experiments explained in this thesis. Ideally around to 256 electrodes is the best choice, even though it is harder to place and calibrate the entire montage above the scalp of the patient. Another trick to improve the spatial precision consists of introducing spatial filters in the pre-processing chain used to clean the EEG raw signal, such as the surface Laplacian or employing adaptive source-space-imaging techniques. Spatial filters represent the main topic of this thesis and they are fully explained in chapter 4. Above all, it is important to remember that each electrode does not measure only the activity of neurons directly below its location, but a complex mix of activities from a lot of brain regions, both near and far that location. Furthermore, the weight associated to a specific brain region, which contribute to compose the final EEG, depends on cortical anatomy and how much that brain region is active at a given point in time. For these reasons, it necessary to understand that brain networks are arranged with several spatial scales and, consequently, EEG cannot spatially sense neural activity at every depth in the brain. These scales are:

1. **microscopic scale:** it involves spatial areas of less than a few cubic millimeters. At this scale, neural columns, neurons and synapses can be found. EEG is not able to detect dynamics manifested at these dimensions, because the events do not give birth to electric field potential which are not powerful enough to be recorded from the scalp.

2. **mesoscopic scale:** it refers to cortex areas from several cubic millimeters to a few cubic centimeters. Only with helmet characterized by sixty-four electrodes and a pre-processing step involving spatial filtering techniques, the EEG can succeed in sensing dynamics arisen at this scale.

3. **macroscopic scale:** it comprises cortex regions that span many cubic centimeters. Even with few electrodes, EEG is able to sense dynamics at this scale. Indeed, in these cases, many scientists only employ from five to eleven electrodes, placing them in particular regions of the scalp above which the interesting neural populations should be activated from specific stimuli [12].

Now it is more clear that the number of electrodes should match the purpose of the experiment and it depends on which neural activity a researcher desires to record.
It is important to mention some of the most relevant voltage waves at various frequencies, which are contained in the raw EEG signal, because they often help to identify abnormal pathological rhythms related to a particular disease. They are classified depending on their amplitude, whose range is $(10 \div 500)\mu$V, their morphology, topography, symmetry and synchrony. They belong to specific frequency bands:

- *Delta waves (0.1 ÷ 4) Hz:* they have the highest amplitude, due to a strong synchronization from neurons which generate cortical potentials. They are manifested during deep sleep or in infants and comtose patients.

- *Theta waves (4 ÷ 8) Hz:* they are related to the subconscious activity and they appear during moments of deep relaxation and meditation. They stimulate the production both of serotonin, which increase relaxation and give relief from pain and cortical hormone, that helps improving memory and learning. They are more frequent in children under thirteen years old and they are considered abnormal in adults.

- *Alpha waves (8 ÷ 14)Hz:* they come up on both sides of the head and act like a bridge between conscious and subconscious state. They are present in adults while they are mentally relaxed with closed eyes.

- *Beta waves (13 ÷ 30)Hz:* they are related to thinking and conscious actions. They indicate an activation of the cortical areas an they are manifested

with talking, problem solving, judgement and decision making, which require attention and concentration.

- *Gamma waves (30 ÷ 100)Hz:* they combine sensory experience and memory. They activate in moments of full awareness and hyper vigilance.
- *Mu waves (7,5 ÷ 12,5)Hz:* they are originated in the motor cortex and are suppressed when a movement is executed with intention. They are useful for BCI because their absence is a flag that communicates when the subject has had the intention of performing a muscular contraction.
- *K-complex:* they are superimposed with theta waves and appear after a sensorial stimulus during deep sleep. They are characterized by high amplitudes.
- *Lambda waves:* they are stimulated during visual exploration, for instance when a person stares at blank surface or watches television.
- *Spike waves:* they are emerged mostly in children, usually in the delta waves range of frequency. They may appear in epileptic or brain injured patients.
- *Sleep Spindles (11 ÷ 15)Hz:* they are also known as "sigma activity". They appear during deep sleep [13].

2.6 EMG signal

Electromyography (EMG) is a technique that allows to measure muscle response or electrical activity of stimulated nerves of the muscle through a device called electromyograph. After the stimulation, a signal can be recorded, while in a resting state, muscle does not produce electrical activity. If contractions are electrically stimulated, the EMG signal generated is deterministic. On the other hand, if neurological activation of muscle fibers happens thanks to voluntary contractions, the EMG signal will be quite random. Muscular contractions take place in the motor unit (MU) and it is possible thanks to **actin** and **myosin**, two fundamental proteins placed in the functional muscular unit called **sarcomere**, where they are arranged parallel to each other. As highlighted in Figure 2.5, all starts from a stimulation of motor neurons. From the spinal cord depart several axons which drive an action potential towards them, in order to make some neurotransmitters bound to receptors for depolarizing their membranes. Successively, a PSP is generated and Ca^{2+} ions are released. They reach actin filaments and bound to the **tropomyosin**, a protein that blocks the junction sites that allow sliding and overlapping between actin and myosin. Thanks to these bonds, the junction sites are no longer blocked and small head placed on myosin's terminations can hook actin filaments by consuming an ATP molecule and make them slide, provoking a

reduction of the length of the sarcomere. After a lot of sarcomeres are shorten at the same time, muscular contractions of fibers take place. In rest conditions, overlap between the two proteins is no longer possible due to the presence of tropomyosin and the sarcomere restores its length, by relaxing muscles.

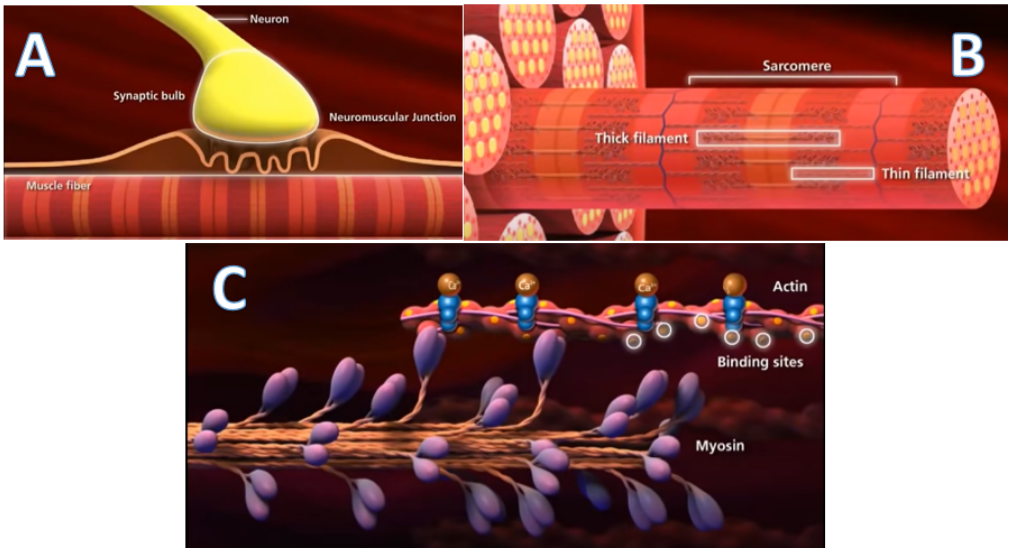

Figure 2.5: A) Motor neuron stimulation. B) Sarcomere structure. C) Actin and Myosin fibers with terminal myosin's heads attached to the actin's junction sites to perform sliding of actin above the myosin and Ca^{2+} ions bounded to tropomyosin molecules to let junction sites free.

Recording EMG signal is useful because it allows to examine cortical-muscular connectivity, to fix an onset (when subject performs movement) to estimate ERP and to identify trials in which individuals twitched the wrong muscles in a specific motor experiment. First step consists in putting an electrode near muscle fibers that are contracted, because, during the contraction a a depolarization of cells' memebranes of fibers happen, accompanied by a movement of ions, giving birth to a magnetic field that can be detected in a form of electrical potential, whose temporal excursion is known as **action potential** [14]. The sum in time and space of action potentials produced by the depolarization of each muscle fibers is called motor unit action potential (MUAP). It is influenced by the geometry of electrodes, the filtering behaviour of the tissue and how synchronously the action potentials are generated. In the electrode detection zone, there are contributions from a wide range of motor units that characterize a series of MUAPs. Since these MUAPs coming from different motor units are not all synchronous, their sum leads to a surface electromyographic raw signal, which is subjeted to a filtering operation, in order to obtain the final EMG and in case the single MUAPs related to different

motor units. The decomposed MUAPs in time from the raw EMG take the name of Motor Unit Action Potential Train (MUAPT), as depicted in Figure 2.6. In

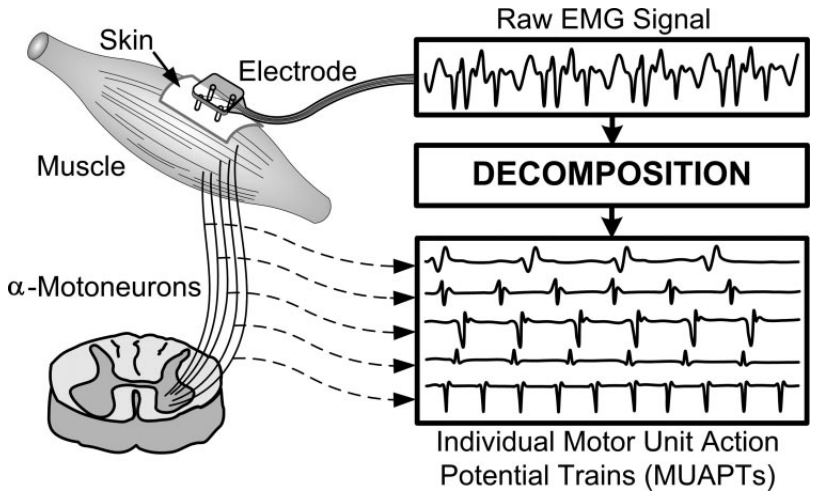

Figure 2.6: Sketch of EMG recording and decomposition of MUAPs to retrieve signal related to different MUAPs.

Figure 2.7 are represented two ways can be distinguished for measuring EMG:

- **Surface EMG:** the one used in this study, it exploits an array of electrodes to record muscular activity at the surface above the skin, therefore it is not invasive. The resulting signal consists of voltage potential differences between pair of electrodes in the array. Unfortunately, some drawbacks emerge: since it is a superficial measurement, behaviours of deepest fibers cannot be recorded. Furthermore, the adipose tissue between skin and muscles acts as a low pass filter. That means on the monitor, it will appear an EMG that will not reflect original amplitude and frequency, but a filtered version.
- **intramuscular EMG:** a monopolar needle is inserted in the patient and a reference electrode is placed above the skin. EMG is recorded faithfully and represent a muscular response of a precise localized motor units. On the other hand, patients feel pain and sterility and disinfection must be ensured.

2.7 RP and LRP

The equivalent dipole of a brain region can be considered an ERP component. The moment-by-moment changes in the magnitude of the dipole constitute the time course of the ERP component. Variations of brain activity related to psychomotor tasks are represented by **contingent negative variation** (CNV) and **readiness**

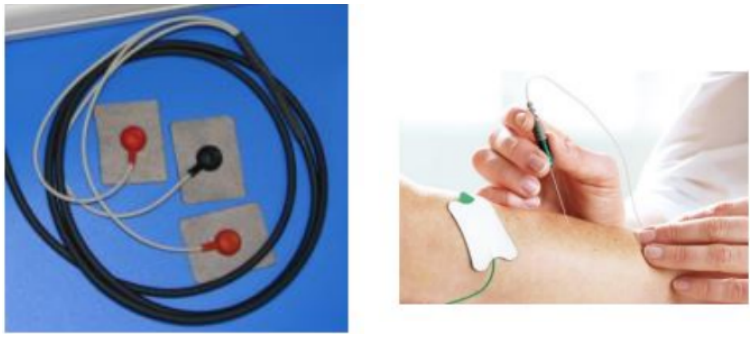

Figure 2.7: Surface EMG elecctrodes (left) and intramuscular needle (right).

potential (RP) or **Bereitschaft potential** (BP), which are specific ERP components. Kornhuber and Deeke in 1964 were the first scientists to discover RP in patients subjected to repeated, voluntary tasks in which they were supposed to flex the right index finger at a self-paced rate. Most specifically, they identified up to three components in the cortical signals, which are manifested before the EMG onset, highlighting preparation of the movement:

- **BP:** slow cortical negative trend detected 2 s or 1.5 s before the voluntary movement. Even if the movement is unilateral, this negativity appear in both left and right brain's hemispheres.
- **Pre-motion positivity (PMP):** bilateral cortical positive trend that arises around 80 ms before the EMG onset.
- **Motor potential (MP):** unilateral negative potential that becomes visible about 50 ms before the movement. This one can be detected only in the motor cortex area contralateral to the muscle moved.

MP and PMP are superimposed to BP, therefore sometimes can be hard to distinguish them clearly. Nevertheless, Shibasaki et al. proposed an other classification regarding BP, splitting it into two traces:

- **Early BP:** it reflects cognitive processes just like attention, preparatory state, intention to act that appears to be still unconscious. It represents the subconscious part of the readiness and it is bilaterally symmetrical in the two brain's hemispheres. It arises in in the pre-supplementary motor area (pre-SMA).
- **Late BP:** it starts from when the RP present a greater slope, ending up to a peak. It highlights the conscious part of readiness, involving conscious intention to act. It is affected by movement's precision, effort and complexity. Indeed, a

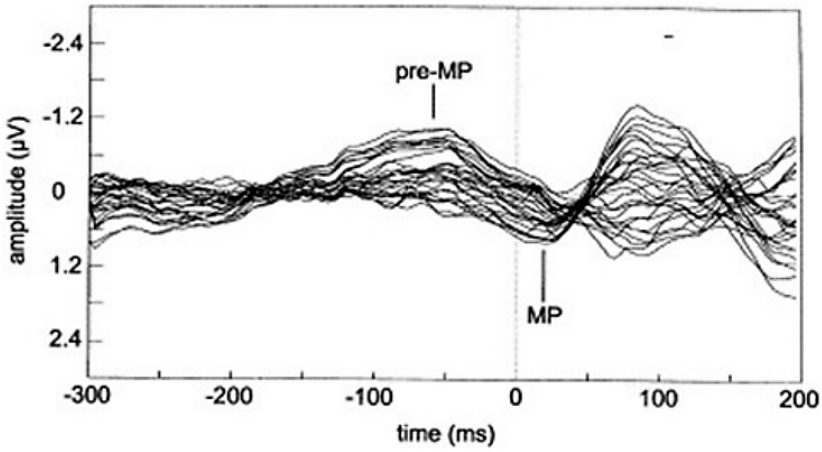

Figure 2.8: BP with PMP and MP.

more complex task involving more muscles increases the late BP amplitude. It showcases maximum voltage amplitudes over the contralateral primary motor cortex for hand movements, and at the midline for foot movements. The asymmetric distribution of voltage amplitude, which results higher over the contralateral motor hemisphere for movements of hand was identified by Coles as Lateralized Readiness Potential (LRP).

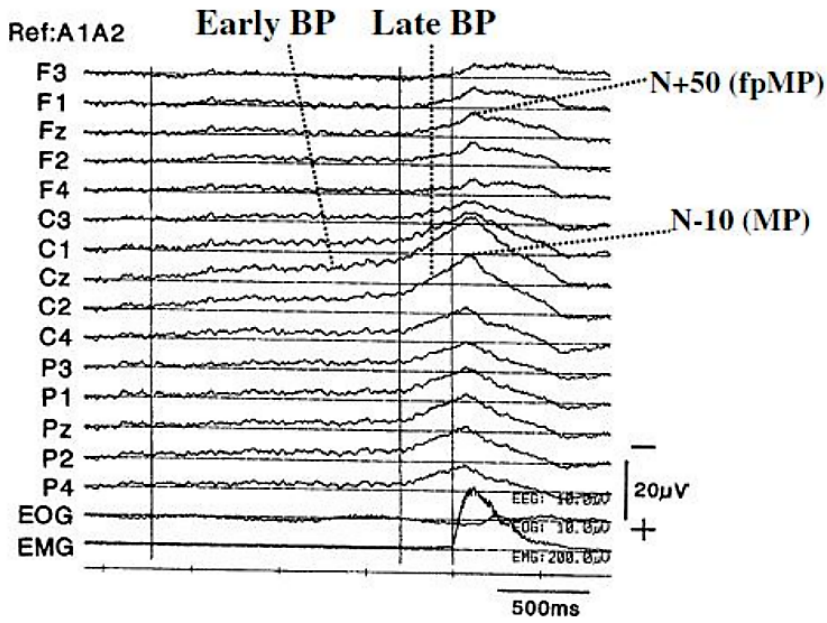

Figure 2.9: Early and late component of RP.

Being a Movement-Related Cortical Potential (MRCP), the BP is is time-locked to an event and acts as an index of motor preparation for a specific movement [15]. The BP signal may be influenced by a lot of factors relating to the subject, such as its level of intention, the selection of which muscle moves and whether it is free to move it, its preparatory state, pace in the repetition of movements, the effort it perceives, its ability to become accustomed to a determinate task and to fully understand it. To summarize, the RP or BP highlights the presence of a subconscious early activation of the brain, before being aware and conscious of both the intention and the preparation to move.
The Lateralized Readiness Potential (LRP) consists of a concentration of negativity in the hemisphere contralateral to the movement in case of hand motion, ispilateral to the movement in case of foot motion, registered in the BP, shortly before the onset of the unilateral motor response.
Contralateral and ispilateral are terms that describes the reciprocal sides between the muscle moved and the activated brain region to allow the movement [16]. Imaging to divide the brain in two hemisphere, it has been fully demonstrated that moving the right hand activates more the left hemisphere, while moving the left hand activates more the right one. Therefore a motion of hand produces a contralateral activation of the brain. On the other hand, moving right foot activates more the right hemisphere and viceversa, therefore there is an ipsilateral response of the brain to the movement of the feet. Generally, LRP tends to be maximum in motor cortex and SMA. The beginning of lateralization indicates when the subject decides which side perform the movement with. The main procedure to obtain LRP is through **double subtraction** of most involved electrodes: C3, C4 and Fc3, Fc4. More explanations about their location over the scalp will be explored later in chapter 3, for the moment it is sufficient to know that C3, Fc3 are placed in the left hemisphere of the brain, while C4, Fc4 in the right one. The first step consists in recording signals from patients subjected to two motor tasks, where in the first one they are obliged to move a muscle and in the second one they are forced to move the symmetric one (for instance left and right index finger). Next step consists in subtracting the samples recorded with the electrode placed in the ipsilateral hemisphere from the samples recorded with the electrode placed in the contralateral hemisphere of the brain. This operation is performed twice: one for the right and one for the left hand case. Unfortunately, from this first subtractions, an additional noisy component remains. It is called *bias* and depends from an intrinsic asymmetry in the activation of the two hemispheres of the brain. Indeed, it has been proved that individuals have characteristic biases in utilizing the left hemisphere more than the other for processing information. Due to the bias, it is not possible to report on a graph the true ERP component. Therefore, a successive subtraction between the two previous results are necessary, as shown in Equation 2.2. At the end, the true LRP is obtained because the bias term has

been cancelled, as shown in Figure 2.10

$$\text{LRP} = [(\text{RP}_{C3} - \text{RP}_{C4})|_{right} + \text{bias}] - [(\text{RP}_{C3} - \text{RP}_{C4})|_{left} + \text{bias}] \iff \quad (2.1)$$
$$\text{LRP} = [(\text{RP}_{C3} - \text{RP}_{C4})|_{right}] - [(\text{RP}_{C3} - \text{RP}_{C4})|_{left}] \quad (2.2)$$

Smaller amplitude of LRP have been registered in case of motor imagery conditions, as well. Its measurement in these conditions are particularly attractive in studies about hemiplegic patients.

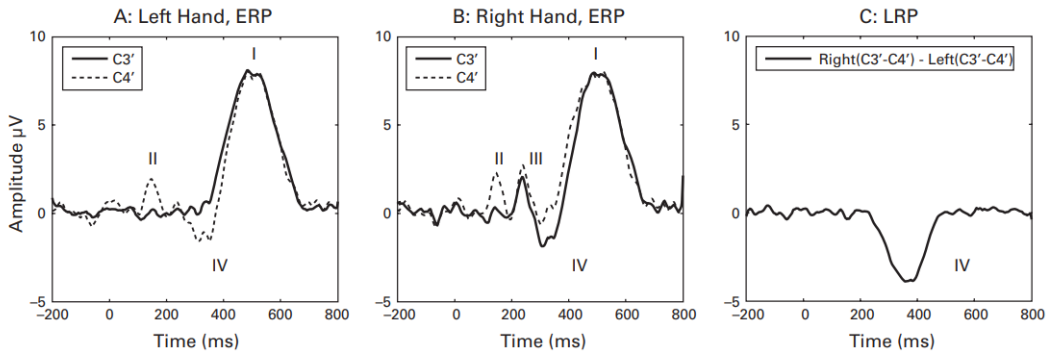

Figure 2.10: A) First task in which signals recorded from electrodes C3, C4 are reported. C4 is more negative because the movement of hand activates more the contralateral hemisphere that presents a greater negativity. B) Mirrored case of the previous one. C) Resulting LRP component obtained from the double subtraction. Every peak is numerated. IV peak indicates the LRP that in case A) and B), it is less evident.

2.8 Libet's experiment

The psychologist and neurophysiologist Benjamin Libet desired to demonstrate that the conscious experience is a result deriving from brain activity and not the contrary. Most specifically, he sustained that the brain acknowledges the movement that will be performed in advance with respect to the moment when the subject becomes aware of willing to do it, underlying a delay during the conscious experience of an event. The main experiment that inherited its name was based on asking the subjects of study to stare at a screen in which rotating spots and quadrants were displayed every 2560 ms and to move the right hand only when one of the spots entered one of the quadrants, claiming the exact moment when they felt the imminent urge to move the muscle. This moment emphasized when the subjects became aware of their intention to move the hand. After measuring both EEG

and EMG signals during the experiments, Libet denominated this time instant as "W judgment" and tried to compare it with the rising time of the readiness potential estimated by averaging all the EEG epochs which were time-locked to each EMG onset (the moment when the hand started moving). He discovered that *W* moment was 206 ms before the EMG onset, but the RP appearance was even hundreds of milliseconds before. The precocious upcoming of RP suggested that there is an unconscious neural process that anticipates and probably gives birth to the conscious intention whenever there is the desire to execute an action. Following this idea, Libet individuated at least three cerebral events that anticipated the movement: the unconscious raising of the RP that prepares the motor action called *C*, the previously quoted conscious decision to move the muscle *W* and the event corresponding to the muscular movement called *M*. Fixing at 0 ms the reference time when the muscle is contracted, the first recorded peak *C* appeared at 550 ms, followed by the *W* moment at 200 ms before the EMG onset. Despite following the personal gut would suggest the correct sequence of events would be *W*-*C*-*M*, in reality the correct chain is *C*-*W*-*M*. In conclusion, the onset of the RP indicates a preparation of the action from the brain that anticipates the awareness of the intention to execute a movement of 300 ms at least[17].
By doing a recap of what is the circuit of brain regions that are activated while individuals tend to perform a task, giving a look at Figure 2.12, it can be noticed that all starts with the intention to move which arises in the **prefrontal cortex** and in the **limbic area**. Then, electrical activity arises in the **presupplementary** and **supplementary motor areas**, whose job consists in programming the timing, the orders and the sequences required to execute the movement. On the other hand, **primary sensory cortices** sends the **premotor cortex** and the **parietal cortex** the external information which are used from the premotor cortex to select movements to execute. Premotor, supplementary and presupplementary areas are devoted to generating the early component of RP (BP1). Next, the information of the BP1's generation is transferred down via the motor cortex to **loops-basal ganglia** and **cerebellum** for checking and modulating the motor control over the motor execution. At the end, from these two, after crossing the **thalamus**, the information returns back to the premotor cortex, where the late component of RP (BP2). Concurrently, after the generation of BP1, an efferent signal arises and goes to the **posterior parietal cortex** to be compared with a sensory-propioceptive information (called corollary discharge). If the two are equal, in this region the sense of agency during the execution of the voluntary action takes place. This last process embodies the feedforward model. At the end, BP2 travels from the primary motor cortex to the spinal cord to reach the contralateral muscle (in case of hand motion) to stimulate its movement [18].

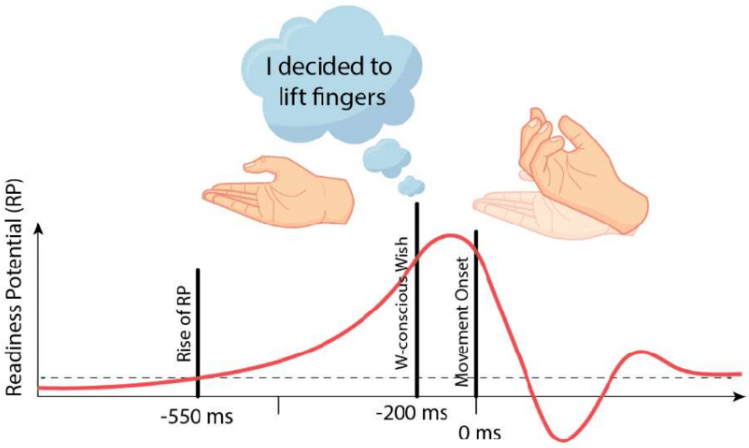

Figure 2.11: Readiness potential component evoked through Libet's experiment.

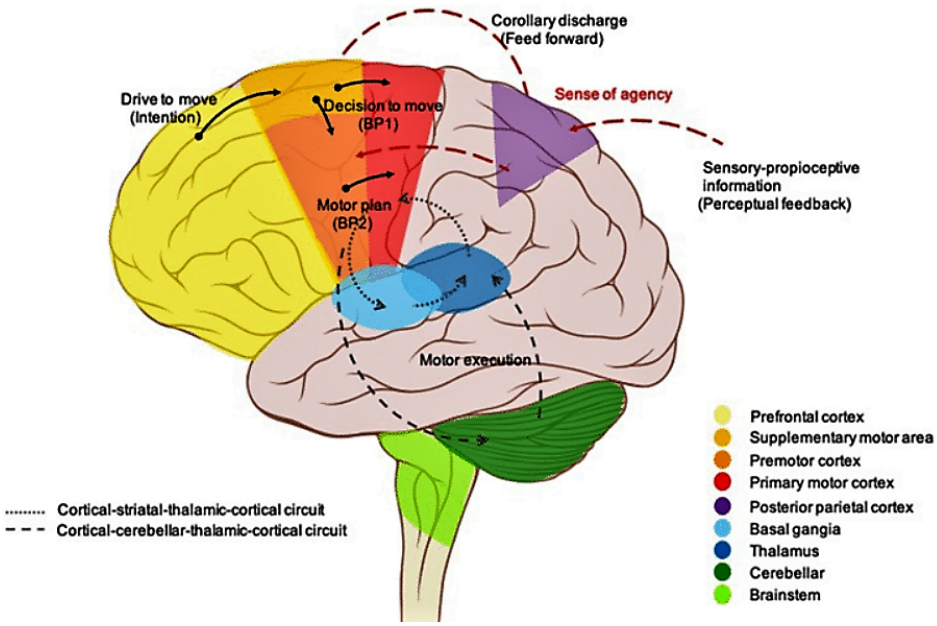

Figure 2.12: Brain circuitry for voluntary movement.

Chapter 3

Measurement of consciousness

At *Centro Puzzle*, in Turin, bio-signals have been recorded from both healthy volunteers and patients suffering from hemiplegia, aged between 18 and 65 years old. The experiments are not all equal, indeed they follow different protocols, which will be described in the next sections. After recording, potentials were shown on a screen thanks to the software called *Galileo NT*. For the sake of the project, three kinds of bio-signals have been registered:

- **Electroencephalography (EEG) signals:** an EEG cap with a varying number of passive Ag/AgCl electrodes (four, height or thirty-two) has been employed to measure them.
- **Electrooculography (EOG) signals:** two adhesive electrodes have been placed above and below each eye to measure blinking activity that produces an artifact in the EEG signal. Indeed, these ocular artifacts are registered to be removed successively from that.
- **Electromyography (EMG) signals:** several adhesive electrodes have been attached to regions near the muscles the patients contract. In the experiments belonging to the most recent protocol, they were put on the front and the back of the second phalanx of the index finger, because the task required to lift the right index.

3.1 Electrode montage

EEG signals are measured with electroencephalogram, characterized by many electrodes that register the electrical activity from the scalp. Between them and the

scalp there is a small layer of conductive gel (Ag-Cl) which improves the contact and reduce the impedance of the skin-electrode interface, which would contribute to volume conductance and dispersion phenomena. Usually, in order to obtain registered data which can be comparable with other studies, the 10/20 system or International 10/20 system is employed. It is one of the most employed methods to establish the location of scalp electrodes. The numbers "10" and "20" stand for the distances in percentage with respect to the total front-back or right-left distance of the skull, between adjacent electrodes (Figure 3.1). Every electrode is labelled with a letter to identify the site of recording and a number to specify the location in one of the two hemispheres. Odd numbers indicate left hemisphere, even numbers right hemisphere [19].

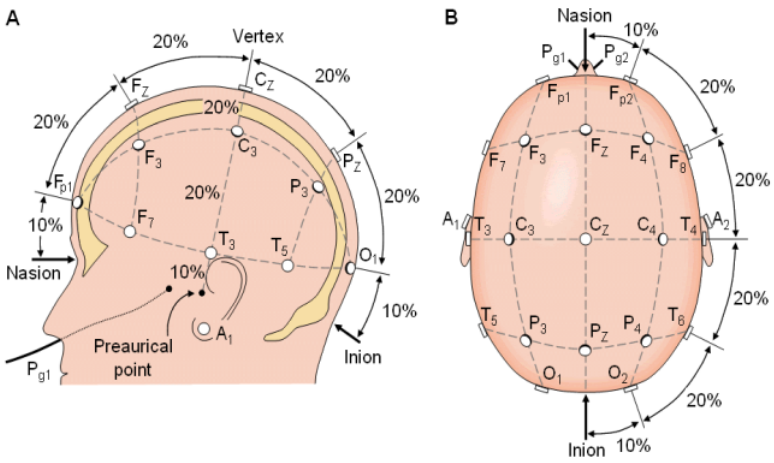

Figure 3.1: International system 10-20 for placing electrodes on the scalp.

Table 3.1: Electrode standard nomenclature.

Electrode	Lobe
F	Frontal
T	Temporal
C	Central
P	Parietal
O	Occipital

It is important to specify that letter 'C' is used for identification purpose only because a central lobe does not exist. Additionally, if a 'z' is present in the name, it indicates that the electrode lies on the midline, that divides the scalp in two halves seen from above. In Figure 3.1 are present two sketches of the montage.

3.2 Tasks and protocol

In the following subsections are describe the various protocol utilized to perform experiments on healthy and ill patients.

3.2.1 2012-2015 Protocol

The experimenter starts the clock timer displayed on the computer: after five seconds passed, the subject flexes the index finger of the right hand once every ten seconds for six minutes. At the end, the registered EEG signal continuous in time is divided into forty epochs, which are time window of same length. In addition to that, alternative tasks have been proposed:

- *Using the mouse:* in this topology, the subject clicks on a mouse button instead of bending the index.
- *Using both hands:* in order to remove the stereotyped movement effect, the subject utilizes both hands and the experimenter indicates which.
- *Short trials:* the experiment is repeated as the standard one, but each trial lalsts 5 s to confirm the idea that the subject becomes aware of the action to be executed after the brain has been already prepared for that action (Libet experiment described in 2.8).
- *Bimanual:* both hands are used concurrently. This kind of task is useful especially for patients suffering from *anosognosia for hemiplegia*. It consists of a transient condition which can damage either the right hemisphere of the brain or the left one in which there are population of neurons involved in the control of the motor area. Consequently, these subjects have a paralysis of the one of the two sides of the body and they are not aware of it! They feel they can move paralyzed hand and leg without problems. For that reason, in order to register EMG signal and retrieve a satisfying ERP, it is necessary to ask them to move both hands or legs, so that the movable muscle accomplishes the motion allowing to record signals derived from muscular contractions of fibers. The intention of moving the paralyzed muscle leads to an activation of a population of neurons living in the contralateral hemisphere (see 2.7 to recall the meaning of contralateral and ipsilateral) that generates an ERP that can be studied. In this thesis, patients suffering from hemiplegia have been analyzed. Most specifically, they have the right hemisphere of the brain injured, therefore they cannot perform motor tasks with their left side of the body. In cases where the left side is the hemiplegic, the center of language is compromised as well, impeding them to communicate their degree of awareness about their paralysis.

3.2.2 2015-2018 Protocol

In these sets of experiments, a simple movement must be executed, while observing a clock on a screen: after five seconds, the movement should be repeated every ten seconds, for six minutes and forty seconds, in order to retrieve an EEG signal divided into forty epochs at the end. The movements required are: flex of the index finger, voluntary movement of the foot or leg, coordinate movement of both hand and leg and finally the patellar reflex of the knee. The last one verifies the integrity of medullar neurons. Sensory neurons connected to the patella transmit the action potentials generated after their stimulation to the spinal chord, from which a response is sent to the efferent motor neurons that transmit the responsive pulses to contract the patella. In some cases, the patients have been blindfolded to avoid any influence of the external environment on them and it was the experimenter to watch the clock and tell them when they would be able to perform the movement.

3.2.3 2018-2019 Protocol

The subject moves only index finger and EMG signal is recorded. Neurologically healthy volunteers perform tasks divided into three sections:

- *Voluntary task:* after hearing a sound, the person can perform the movement in a time window that does not overcome thirteen seconds. This constraint allows to enclose the action in a fixed time frame by leaving the subject the freedom to act. Consequently, moments of acting vary from person to person and from trial to trail.

- *Semi-voluntary task:* the subject executes the movement, but this time, as soon as he/she hears the acoustic cue.

- *Involuntary task:* it tests an involuntary muscular contraction, therefore the experimenter hits softly the patella of the subject with a gavel, when he perceives the acoustic cue which cannot be listened by the subject.

Every experimental session is characterized by forty repetitions for each task and the acoustic signal is randomized to avoid adaptation by the subjects which would modify the expected final RP. Indeed, when the brain becomes accustomed to a task, it tends to enhance some cerebral components and to suppress others.

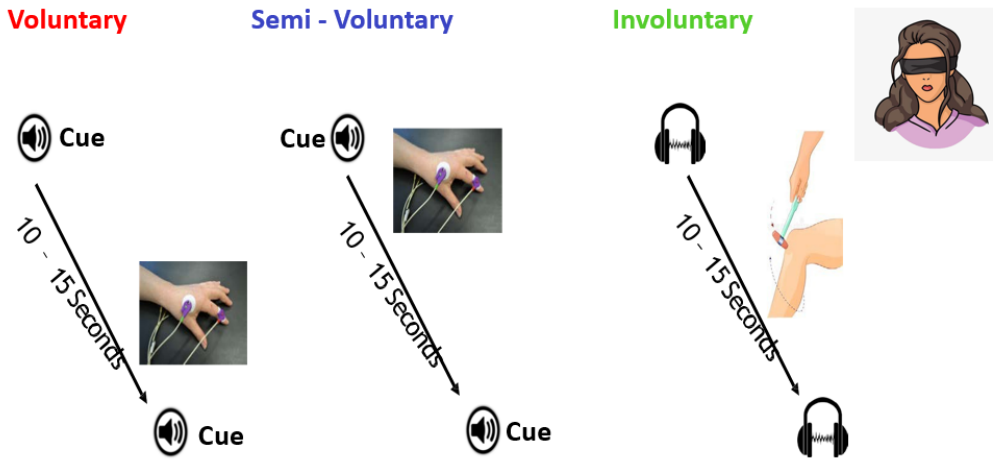

Figure 3.2: 2018 Protocol for EEG, EOG and EMG recordings (voluntary, semivoluntary and involuntary task).

3.2.4 Classification of the dataset

To distinguish various dataset, string of characters have been elaborated to label each protocol, considering the topology of task performed, the name of the subject, the type and method employed to acquire the biological signals and the specification of the instrumentation involved. In these experiments a Labjack is employed, which is a USB measurement and automation device that provides digital inputs and outputs and it is responsible of generatng the acoustic trigger to punctuate the movement, while it is connected to a DAQ. Bboth the EMG signal and the Labjack signal were evaluated through a scale ranging from 0 to 3, where 0 indicates a poor quality, while 3 indicates a good quality of the two signals. The EMG signal quality depends on the amount of noise and the variability of the signal itself.
The strings of characters are constituted with:

- **8 characters** bearing the anonymized name of the subject, sequentially there are the first letter of the name, the first letter of the surname, the last digit of the recording year, the last two digits of the year of birth, the month of registration and the character 0/1 if the subject is male/female (in case of homonymy, the last character is placed equal to 2).
- **5 characters** for the EEG electrode mounting: 32C18 is the acronym for the 32-electrode mounting ("32 Channels 2018"), while OBE12 is the one with bridge electrodes ("Bridge Electrodes 2012")
- **4 characters** indicating the protocol used for the control group: A18C for the 2018 protocol ("After 2018 Controls"), B18C for the 2015-2018 protocol

("Before 2018 Controls") and VOPC refers to the data of the 2012-2015 protocol ("Very Old Protocol Controls").

- **3 characters** to describe the condition of the subject: the acronym FOL refers to blindfolded subjects, while UNF to non-blindfolded
- **5 characters** to identify the type of task performed: voluntary, semi-voluntary or involuntary, indicated respectively by VOL18, SEM18 or INV18
- **4 characters** s for the task: RFOF for right forefinger, LFOF for left forefinger, BFOF for bimanual forefinger, RMOU when clicking the mouse with the right hand, RLEG for right leg, LLEG for left leg, RFOO for right foot, LFOO for left foot, RHLE for right hand and leg, LHLE for left hand and leg
- **4 characters** to indicate the channel used for EMG: EMG1 for channel 1, EMG2 for channel 2, EMGX for channel without any number.
- **4 characters** to discriminate signal quality for EMG and Labjack, therefore: E + 0/1/2/3 for EMG and L + 0/1/2/3 for the Labjack (in protocols prior to the 2018 protocol, the last two characters correspond to L0, as LabJack is not present).

3.3 Experimental setup

In this section, the materials and the preparation stage are described, according to the last protocol, drafted in 2018. Before starting with the recording phase, it's important to carefully fix the instrumentation in a suitable way, in order to acquire a legible signal trace (Figure 3.2). Such instrumentation is composed by:

The instrumentation employed for the 2018-2019 protocol is:

- **Data Acquisition device:** Galileo Suite, EB Neuro with Brain Explorer (BE) amplifiers.
- **Galileo Software:** for processing and display the EEG traces.
- **Stimulation system:** Labjack and OpenSesame software for the acoustic signal.
- **Synchronization system:** Labjack and photocoupler circuit.
- **Recording tools:** EEG cap, adhesive electrodes (4 for EOG signal and 2 for EMG signal), the ground electrode for EMG (placed on the wrist for voluntary and semi-voluntary tasks or on the ankle involuntary task), 2 earlobes reference electrodes for EEG.

- **Additional accessories:** TEN20 (conductive paste), NUPREP (abrasive paste), conductive EEG gel, a syringe with a blunt needle.

Figure 3.3: Experimental setup in "Centro puzzle", Turin.

Firstly, the subject is invited to sit on a raised chair to avoid touching the floor with the feet, condition necessary especially for the experiments involving patellar reflexes and while he/she is sitting, biological signals will be recorded. Secondly, two computers are required to conduct the studies. One runs the *OpenSesame* software that allows to start the tasks by emitting the acoustic signal thanks to the LabJack, the other runs the *Galileo NT* software, which is connected to the EEG-cap and shows the acquired bio-signals that can be processed and exported, as well. Both computers are placed out of the sight of the subject, so that it is not influenced by looking at the screens. EMG and EOG sensors and electrodes on earlobes, wrist or ankle for involuntary tasks are mounted using TAN20 paste. Successively, the EEG-cap is placed on the scalp, trying to collocate the Cz electrode in the middle of the surface of the head, in the point where longitudinal and latitudinal lines obtained connecting inion with nasion and the two earlobes cross together. After that, the head's skin is cleaned with an abrasive paste called NUPREP, in order to remove dead cells and sebum. Finally, a conductive EEG gel is employed to fill the

inner part of the montage, through a syringe with a blunt needle.

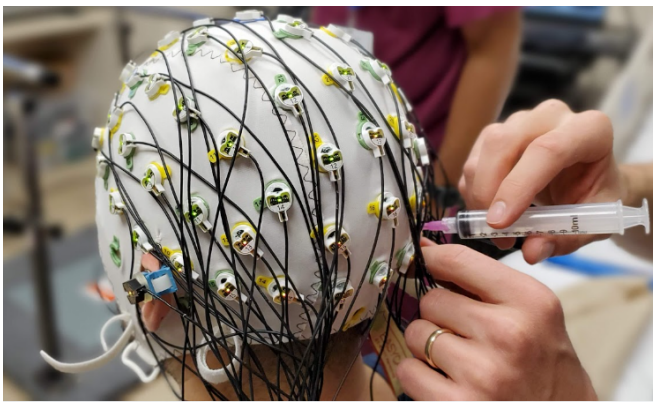

Figure 3.4: Filling the EEG-cap.

3.4 Software for signal processing

At this point, biosignals have been collected and made compatible to be processed in MATLAB. The signals are elaborated starting from a free toolbox called EEGLAB [20], in which a plug-in called MRCPLAB has been specifically created with all the necessary functions to perform the signal processing for this project.

3.4.1 MRCPLAB

MRCPLAB is the plug-in devoted to analyzing movement-related cortical potentials (MRCPs) recorded from the software *Galileo NT*. In this subsection, a brief summary about all the functions involved in the pre-processing chain for recorded signals is presented. For deeper details about each function recalled in the project, a manual has been written for the purpose. When the software is active, it displays a menu with the following voices:

- **Import/Save Data:** by clicking on it, two other voices appear.
  Import from ASCII file and filter allows to import a new dataset, in a format already compatible with the plug-in and to save it as a *.set* file. In particular, EEG, EOG and EMG signals are imported and temporally filtered and a pop up window appears, asking the users to enter some information:
  - The sampling frequency (set to 0 to read it from the file).
  - The epoch duration in seconds in which the signal has been divided. For dataset belonging to 2018-2019 protocol user must insert "0" because the discriminant signals is the cue sound provided by LabJack. On the

contrary, for all the others, the value to insert is "10" because each epoch lasts ten seconds.

- The epoch definition, in milliseconds, which is set from −5 s to 3 s.
- the channel on which the EMG signal is detected, which may be EMG1 or EMG2. It was also used another channel, called 'Pulsante' for the acquisition of the EMG signal, that must be entered in this box if the dataset name reports the EMGX as EMG channel.
- The name of the cue channel, which is the Labjack for experiments conducted on healthy volunteers.
- In the end, the user can choose whether to obtain a graph with the EMG trace or the EMG with the cue channel signal.

Import from .sets file allows to open a previously uploaded dataset, in order to save time and have all the information about the signals already well organized in structures.
At the end, three different datasets are created: the first contains the EEG signal filtered, the second the EEG, EOG, EMG signals filtered and the third the EOG, EMG signals filtered.

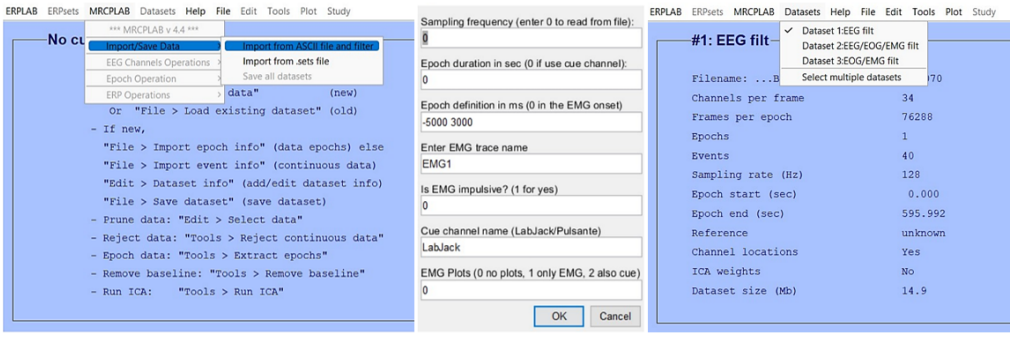

Figure 3.5: Import/Save Data pop up window.

- **EEG Channel Operations:** by clicking on it, several functionalities can be executed:
  - *Channel data scroll:* for visual analysis of EEG signals related to all channels.
  - *Seek noisy channels:* for detecting noisy channels to remove further, relying on channel statistics.
  - *Select or reject data:* it permits to get rid of the noisy channels previously found. It cancels portions of data and epochs.

- *Artifact correction:* it corrects the signal by removing distortion, disturbs and all useless information that typically produces large voltage peaks in the EEG signal. To do that, it employs the Independent Component Analysis (ICA).

- *Interpolate electrodes:* previously removed channels are substituted with new ones, resulted from an interpolation between their adjacent channels. Two interpolation methods have been implemented: the nearest-neighbor interpolation, replacing one site with the average of the neighboring sites, and the spherical spline interpolation that takes into account all of the electrode sites.

- *Spatial filtering:* it allows the user to choose among several spatial filters to apply to the EEG signal. It is useful to enhance the weakness recalled in section 2.3. Indeed, after their application, it is possible to distinguish the neural generators inside the brain and their specific locations. Most specifically, user can choose among different spatial filters and decides which version employ:

  * *SLSF:* it executes the small laplacian spatial filter and the user can specify the number of neighbouring electrodes (four or eight) with (selecting "0") or without (digiting "1") the update on the signal-to-noise ratio.

  * *LLSF:* it executes the large laplacian spatial filter and the user can specify the number of neighbouring electrodes (four or eight) with (selecting "0") or without (digiting "1") the update on the signal-to-noise ratio.

  * *CARSF:* it executes the common averaged spatial filter. Number of neighbouring electrodes is not a user's choice because it depends on the size of the montage. The update on the signal-to-noise ratio does not count for this kind of filter.

  * *SSIF:* it executes the spherical spline interpolating patial filter. It considers all the electrodes of the montage and it does not take the update of the signal-to-noise ratio into consideration.

  To apply spatial filters with the updates, it is necessary to estimate the signal-to-noise ration of the raw RP before calling these functions.

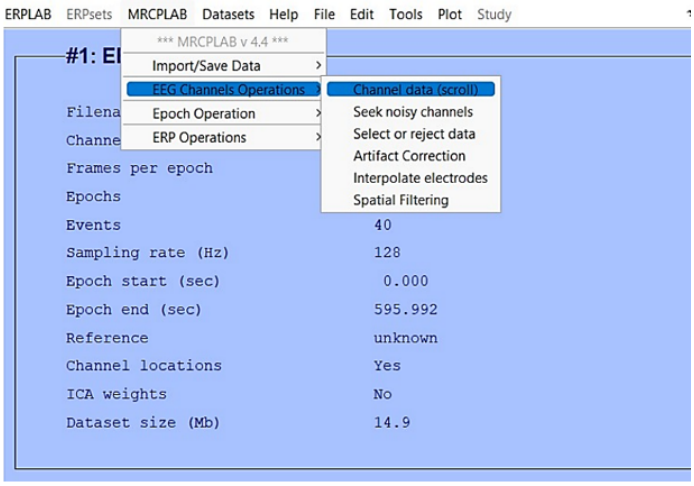

Figure 3.6: EEG Channel operation, pop up window.

- **Epoch Operations:** by selecting this voice, others will open:
  - *Epoch calculation:* it starts from the time instants related to the several ONSETS in the EMG signal to build around them the epochs, that go from 5 s before and 3 s after it. Consequently, the number of epochs coincide with the number of ONSETS, which is the number of time the patient has moved the muscle of interest. Additionally, it executes the removal of the baseline, which is a low frequency fluctuation that emerges in the first part of each epoch, when the subject has not received the stimulus yet.
  - *View topography and energy consideration:* it provides graphs related to topographies of ERP from EEG signal epoched in time and a table that reports all ERP energy contributes. It also provides a graph that reports the $\sqrt{2 \cdot V_H V_L}$ contribute, to have an idea of the selectivity of the spatial filters between high and low passed versions. After clicking on this function, a first menu will ask which results user desires to see (from raw or high, low filtered signals). Then, a second window will ask some specifications, for instance the time instants in which generates the topographies.
  - *Jitter compensation:* it is employed to align the epochs, whose samples are affected by delays, allowing a statistical average aimed at obtaining ERP as much reliable as possible.
  - *SNR estimation and ERP visualization:* the signal to noise ratio (SNR) vector can be computed and users can choose to realize picture related to ERP elaborated previously by the RIDE algorithm. Users can obtain

graphs regarding single channels, averaged lines of single channels, noise and SNR images and difference waves between couple of symmetric electrodes in the two brain hemisphere by selecting the respective voices and typing the proper digits.

Chapter 4

Spatial filtering

Spatial filters represent one of the most popular techniques aimed at improving the raw EEG signal from a spatial point of view. Indeed, ERPs suffer from poor spatial resolution, therefore it is not possible to identify neuronal generators which are responsible of particular responses of the brain, owing to the issue related to volume conductance. This phenomena causes a dispersion of the signal all over the scalp, complicating the classification of single motor components, which result useful to distinguish more or less activated population of neurons in patients who suffer from diseases affecting brain, providing a relevant help for medics to establish their state of consciousness and the most effective cures. For all these reasons, it is important to employ a method to overcome those spatial weaknesses related to ERPs. The main aim of this thesis consists in testing some known spatial filters used in literature, improving them and comment results both on healthy volunteers and hemiplegic patients. Most specifically, various spatial filters are compared considering several features, trying to highlight advantages and disadvantages in their application in the pre-processing chain of MRCPLAB.
This chapter is organized by four initial sections to introduce what is a spatial filter, reporting some pre-existent examples, an explanation of the tuning of the spherical interpolating spatial filter and pseudocodes utilised in the project. In section 4.5, first results obtained by applying spatial filters known in literature can be found, with a preliminar conclusion on them at the end. In section 4.6, several results on healthy individuals performing voluntary tasks are listed, in order to compare the old and updated versions and try establishing at least two spatial filters that show better qualities to introduce in the pre-processing chain to be employed on other dataset belonging to different protocols and experiments. Indeed, section 4.7 contains the results after the application of the chosen high spatial filters on a dataset belonging to the 2015-2018 protocol and on dataset belonging to 2018-2019 protocol, involving semi-voluntary and involuntary tasks. section 4.8 is the last of this chapter in which results are listed, after the application of the updated SLSF

as low spatial filter.

4.1 Spatially unfiltered RPs

First of all, it is significant to recall that the EEG signal is characterized by voltage samples recorded for a period of time at each electrode that composes the entire montage. As stated in 2.4, the different resistance of tissues characterizing the brain provokes a dispersion of the signal corresponding to a certain neuronal population that tends to spread all over the scalp. Consequently, each electrode measures the same components of the generated signal, but scaled differently in amplitude, depending on the physical distance between each electrode and the activated region inside the brain. After an average step, it is possible to obtain RPs measured from each electrode, which are vectors of voltage samples recorded at each time instant in temporal window that goes from $-5\,\mathrm{s}$ to $3\,\mathrm{s}$. Before introducing spatial filters, it may be useful to define some important features that helps highlighting the quality of a general RP signal. The best way is to start with a RP which is not spatially filtered. In order to distinguish this kind of signals from other spatially filtered versions, in this thesis they will be called *raw RPs*. The important features to look for can be summarized in two categories:

- **Shape:** ideally, the RPs should be similar to the one illustrated in 2.8. At the beginning of the epoch, the baseline should be $0\mu V$, representing the inactivity of the brain. Then, it should be identified the negative peak of the intention before 0 ms, which involves the early and the late components. 0 ms is the time instant that coincides with the ONSET of the EMG signal, after which a positive larger peak indicating the motor activation of the muscle should appear to go back to $0\mu V$ again, after the motor tasks is finished.

- **SNR:** the signal-to-noise ratio is an important quality-marker because it testifies if the signals recorded from the channels are reliable or only noisy waves. To simplify the classification of the SNR, three different lines have been traced inside a time window equal to t_w = [-1000 ÷ +1000]ms, which is where the two peaks of intention and of muscular movement arise. The criteria is:

  - *Thick lines:* applied when $SNR \geq 6\,\mathrm{dB}$, which is the best case.
  - *Thin lines:* which appear when $3\,\mathrm{dB} \leq SNR < 6\,\mathrm{dB}$, symbolizing a middle quality of the signal.
  - *Dashed lines:* when $SNR < 3\,\mathrm{dB}$, which is the worst case, where there is a lot of noise.

In this case, EEG signals recorded from a voluntary healthy subject has been taken into consideration. The dataset analyzed is named "MI993011-32C18-A18C-UNF-VOL18-RFOF-EMG1-E2-L2". In Figure 4.1 are reported the RPs of both the single seven electrodes mostly involved in motor actions and the lines referred to different brain areas retrieved by averaging small groups of them. In Table 4.1 are reported the electrodes included in each line. Looking at Figure 4.2 as well, the RPs successfully satisfy the shape and SNR standards. In Figure 4.3 the noise power is presented.

Table 4.1: Definition of lines on the scalp.

Lines	Included electrodes
Motor	Cz, C3, C4
Pre-motor	Fcz, Fc3, Fc4
Right	C4, Fc4
Left	C3, Fc3
Median Rosto Caudal	Cz, Fcz, Pz

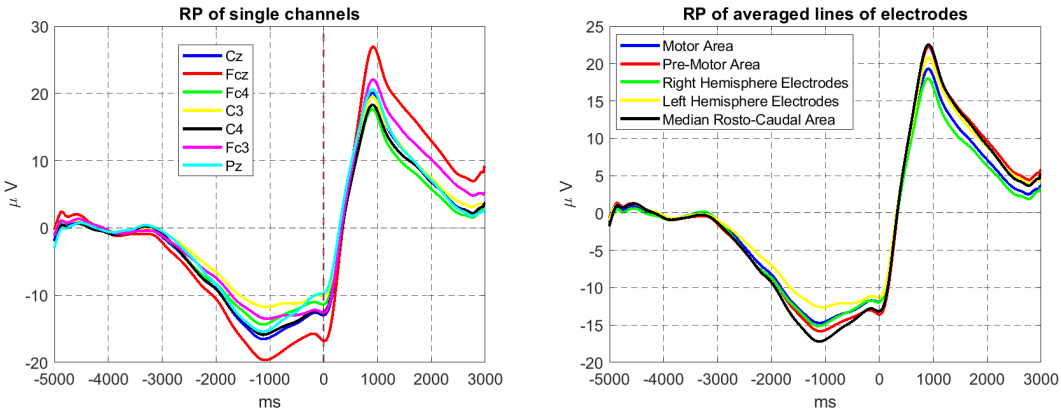

Figure 4.1: Single channels and averaged lines showing RPs.

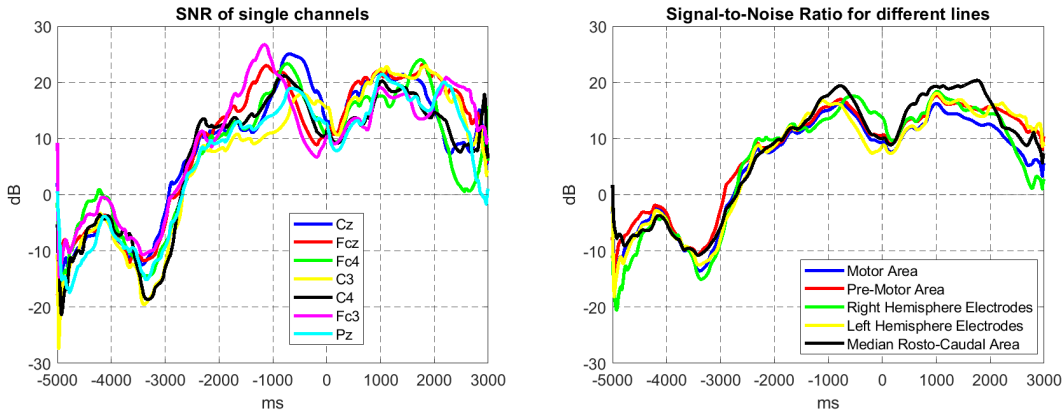

Figure 4.2: SNR of single channels and averaged lines.

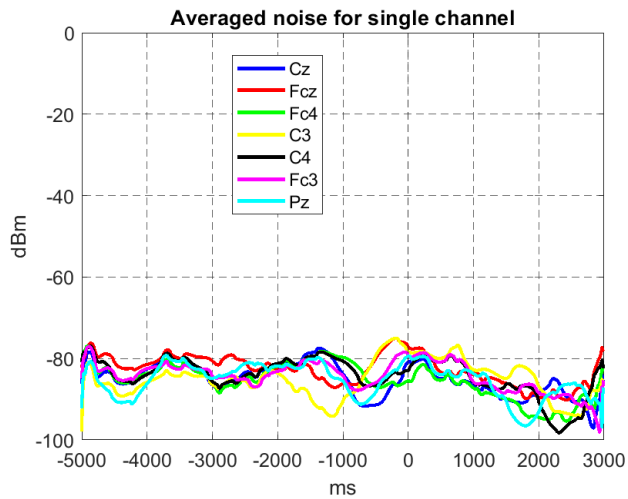

Figure 4.3: Power of noise of single channels in time.

The temporal resolution of 1 ms is the point of strength of the RP technique. From Figure 4.1, it is possible to distinguish the negative peak of the subject's intention to perform the movement and the positive peak related to when the subject is performing it. Unfortunately, no clear information about which is the most active region of the brain can be deduced. A way to overcome this issue is to view the RPs of all these electrodes on the scalp concurrently, by producing a topography. A topography is an image that reports a voltage spatial distribution at fixed time instant. From the topographies shown in Figure 4.4, some contour lines circumscribed around few electrodes emphasizes some regions with respect to others but essentially only mono-color scalps appear. This demonstrates the spreading of the signal because each electrode measures a voltage potential difference similar

to the others, due to the phenomena of volume conductance. Consequently, even though it is clear where intention of performing the movement and muscular motion of the subject occur in time, it is impossible to spatially identify additional information about which electrodes registered a higher neuronal activation in comparison with others, complicating the search of motor components revealing specific brain activity, such as LRP. At this point, the object of the research are fundamentally two:

1. Localize neuronal sources, establishing the most active channels.
2. Improve final RP and some of its features useful from a classifier based on a machine learning algorithm.

In order to satisfy the first purpose, high spatial filtering operation is investigated, while for the second purpose low spatial filtering operation is employed.

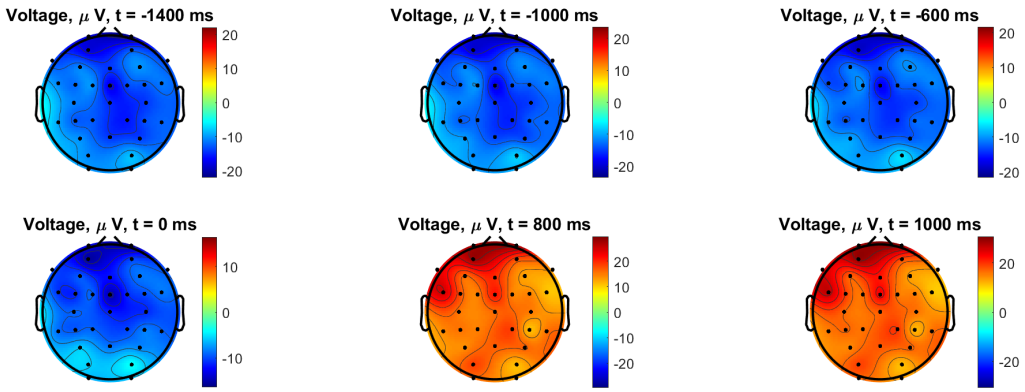

Figure 4.4: Topographies of raw RP that underlines the issue of volume conductance.

4.2 Pre-existent SF

Before exploring spatial filters employed in literature, it is relevant to describe the general idea behind their function. The $\mathrm{RP}(V, t, d)$ is a voltage waveform that depends on three variables: time, space and voltage. Since each electrode is placed at a different distance with respect to the others over the scalp, it is possible to filter each voltage sample recorded at a fixed time instant by considering these inter-electrode distances. By fixing time, it is possible to establish a 2D system characterized by a spatial period and the voltage values and to remove the time dependence, having $\mathrm{RP}(V, d)$. Indeed, every millisecond, it is like an equivalent single electrode measures voltages at different distances. As in time-frequency

domain, it can be found a relationship between spatial period and spatial frequency domains, in which the spatial frequency is defined as:

$$f_z = \frac{1}{d} \tag{4.1}$$

where f_z is the inverse of the inter-electrode distance d between a reference electrode and the other of the helmet.
In order to improve localization, it is essential to attenuate volume conductance, which appears to be huge at low spatial frequencies (or equally at high inter-electrode distances), covering high spatial components, which usually reveal relevant information about motor intention [21]. For that reason, a high pass band spatial filter is required. In literature, spatial filters are also called **surface laplacian spatial filters** because they estimate the second derivative of the instantaneous spatial voltage distribution for each electrode, emphasizing activity of radial sources just below the electrodes. In this thesis, several kinds of surface laplacian filters are analyzed and they have been divided into three families: surface laplacian spatial filters based on inter-electrode distance, common average reference spatial filter and spherical interpolating spatial filter.

1. **Surface laplacian based on inter-electrode distance:**
   The laplacian high spatial filters consists in subtracting the weighted sum of voltage potential differences of neighbouring electrodes to the voltage potential difference of the reference electrode, at each time instant [22]. Typically, four neighbouring electrodes are considered and depending on their distances from the reference electrode, two high pass spatial filter can be obtained:

   - **Small laplacian spatial filter (SLSF):** it considers the four adjacent elctrodes to the reference one.
   - **Large laplacian spatial filter (LLSF):** it takes next four neighbouring electrodes into consideration.

   A clear picture is reported in Figure 4.5. The weights associated to each neighbouring electrode are all equal to:

$$\alpha = \frac{1}{N} \tag{4.2}$$

   where $N = 4$. The fundamental constraint is that:

$$\sum_{i=1}^{N} \alpha_i = 1 \tag{4.3}$$

Indeed, if this is respected, it is possible to remove the common spatial component among RPs of various channels, which represents the DC spatial noise, improving the signal-to-noise ratio of the high filtered signal. The equation that expresses the relationship between the filtered new value v_i, the reference c_i and the neighbouring ones c_j is:

$$v_i = c_i - \sum_{i=1}^{N} \alpha \cdot c_j \tag{4.4}$$

2. **Common average reference (CAR)**
   It is an extension of the laplacian filters. Indeed, every time subtracts the voltages of all the other electrodes of the montage from the reference one. It does not involve the distance as discriminant to filter. In this case, $N = 33$, because the montage employed in this projects counts 34 electrodes.

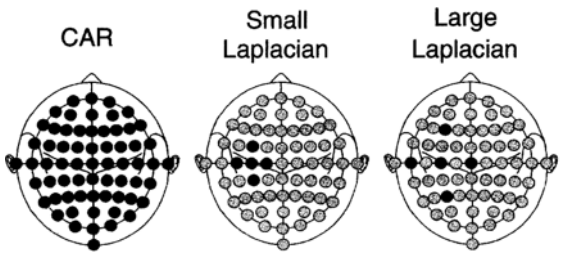

Figure 4.5: Common average reference spatial filter, small and large laplacian spatial filters [23], [24], [25].

3. **Spherical spline interpolation spatial filter (SISF)**
   It is based on a different approach and it is elaborated by Perrin [26], therefore it requires a deeper explanation. First of all, it is a mapping method to estimate scalp current density and it can be used as a spatial filter. In order to design spatial maps of scalp potentials is necessary to choose a surface on which estimates the points retrieved from the second spatial derivative of the voltage samples and what are the projections, firstly between the 3D scalp head surface and the surface of computation, secondly between the surface of computation and the plane on which the final topography is sketched. In this case, a sphere represents the surface of computation. The first projection from real 3D head to sphere is realized by forcing that the polar axis passes through Oz and that the midline through Oz, Pz, Cz, Pz, Cz defines the zero meridian from which degrees of longitude are measured (recall to Figure 3.1). Positions of $T3, Cz, T4$ specify the equatorial plane from which latitude and colatitude

are determined. Recording electrodes are located in terms of longitude ϕ and colatitude θ. Polar coordinates are related to cartesian coordinates by the equations:

$$x = \sin\theta\cos\phi \tag{4.5}$$
$$y = sin\theta\sin\phi \tag{4.6}$$
$$z = cos\theta \tag{4.7}$$

By exploiting these equations, it is possible to retrieve the polar coordinates, considering the scalp a unit sphere. Unfortunately, a little distortion is always introduced when moving from a 3D plane to a 2D representation. In order to minimize it, the back of the head is projected onto a cone [27].
The second projection from the sphere to the 2D plane for the topography starts by estimating a matrix that represents the cosine distance among all pairs of electrodes and it is computed as:

$$\cos(d_{ij}) = 1 - \frac{(X_i - X_j)^2 + (Y_i - Y_j)^2 + (Z_i - Z_j)^2}{2} \tag{4.8}$$

At this point, to calculate the high spatially filtered values, two matrices called G and H must be computed:

$$G_{ij} = \frac{1}{4\pi}\sum_{n=1}^{\text{leg.order}} \frac{(2n+1)\cdot P_n(\cos(d_{ij}))}{(n(n+1))^m} \tag{4.9}$$
$$H_{ij} = -\frac{1}{4\pi}\sum_{n=1}^{\text{leg.order}} \frac{(2n+1)\cdot P_n(\cos(d_{ij}))}{(n(n+1))^{m-1}} \tag{4.10}$$

G and H are squared matrices containing the specific weights that are used to attenuate low spatial information and to enhance high spatial activity. Their values depend on several parameters. The first term is P_n which represents the Legendre polynomial of order n of the cosine of the distance between pairs of different electrodes that is usually employed for spherical coordinate distances. Recalling that the domain of these polynomials is [-1,1], this is the reason why the sphere used as computational surface has been normalized to a sphere with unitary ray. The order of the Legendre polynomial influences the accuracy of final topography after the application of the G and H matrices to the raw data. Larger is this integer number and higher is the accuracy

of final results. Nevertheless, in this project, only thirty-four electrodes are employed, therefore $n > 10$ would slow the computational time of the code without improving topographies because the accuracy of final results would exceed the actual maximum possible accuracy reachable with this number of electrodes. Typically, $n > 10$ are set when sixty-four or more electrodes are present in the montage. The second term is m, an integer number which tunes the filter, changing its behaviour from a low spatial (larger values) to a high spatial (smaller values) filter. The surprising aspect is that G and H are uniquely dependent on the inter-electrode distance. Therefore, if the same montage is used for various patients, their values do not change. At this point, it is possible to estimate the filtered values:

$$lap_i = \sum_{j=1}^{\text{num elec}} C_i H_{ij} \tag{4.11}$$

where lap_i is the Laplacian for electrode i at a fixed time instant and j refers to other electrodes. H_{ij} is the element of the squared H matrix, containing weights. The C matrix is where raw data are inserted and manipulated:

$$C_i = d_i - G_{inv} \cdot \frac{\sum_{j=1}^{\text{num elec}} d_j}{\sum_{j=1}^{\text{num elec}} G_{inv,j}} \tag{4.12}$$

$$d_i = \frac{data_i}{G_s} \tag{4.13}$$

$$G_s = G + \lambda \tag{4.14}$$

$$G_{inv} = \sum_{i=1}^{\text{num elec}} (G_{s,i})^{-1} \tag{4.15}$$

λ is a smoothing parameter inserted in the diagonal of the G matrix to influence the precision of results. In particular, it influences the broadness of voltage spatial distribution in the topographies because it modifies how fast the second spatial derivative varies. In Equation 4.12, a weighted sum of activity registered from all the electrodes is subtracted from the activity of each reference electrode. This operation is performed twice: firstly with G matrix and secondly with H matrix in Equation 4.11. These two passages embody the calculation of the second spatial derivative. In Equation 4.13 data are normalized.

A behavioural algorithm of the spatial filters implementation is provided in the pseudocode shown in 1 and 2.

Algorithm 1 Algorithm to implement spatial filters. Mathematical operations are element-wise. The variable *varargin* contains the information to choose using SLSF, LLSF, CARSF or SISF and the number of neighbouring electrodes.
Input: EEG struct, eeg_channels,varargin
Output: EEGSF

procedure SPATIAL FILTER(EEG, eeg_channels,varargin)
    ▷ Preliminary choice of the filter
    $filter\_method \leftarrow varargin(1)$
    $neigh\_elec\_num \leftarrow varargin(2)$ ▷ in case of CARSF, it is set to 33
    ▷ Transform electrode location in spherical coordinate normalized to a unit-radius sphere
    $X \leftarrow EEG.chanlocs(eeg\_channels).X$
    $Y \leftarrow EEG.chanlocs(eeg\_channels).Y$
    $Z \leftarrow EEG.chanlocs(eeg\_channels).Z$
    $spherical\_radii \leftarrow cart2sph(X, Y, Z)$
    $max\ rad \leftarrow max(spherical\_radii)$
    $X \leftarrow \dfrac{X}{max\ rad}$
    $Y \leftarrow \dfrac{Y}{max\ rad}$
    $Z \leftarrow \dfrac{Z}{max\ rad}$
    $cosdist_{i,j} \leftarrow 1 - \dfrac{(X_i - X_j)^2 + (Y_i - Y_j)^2 + (Z_i - Z_j)^2}{2}$
    $cosdist \leftarrow cosdist + cosdist' + eye(numelectrodes)$
    ▷ Now, each inter-electrode distance is ordered in a descendent way to retrieve neighbouring electrodes. Different ranges of distances are considered for each spatial filter case
    $chan \leftarrow (1:34)$ ▷ Indexes for each electrode
    $curr\_row \leftarrow cosdist(chan_i, :)$
    case SLSF
    $sel \leftarrow sort(curr\_row(curr\_row < 1), descend)$
    case LLSF
    $sel \leftarrow sort(curr\_row(curr\_row < 0.75), descend)$
    ▷ Creating the vector containing only the 4 neighbours for each channel
    $neighbours \leftarrow neighbours(find(curr\_row == sel_i)$
    $all\_neighbours(chan_i,1) \leftarrow neighbours$

Algorithm 2 Part 2. Several constants are employed: $m_G = 2, m_H = 2, leg\_order = 10, \lambda = 1 \cdot 10^{-7}, numelectrodes = 34$.

case CARSF
$all\_neighbours(chan_i,1) \leftarrow neighbours(neighbours \sim= chan_i)$
▷ Computing the laplacian for SLSF, LLSF, CARSF
$\alpha \leftarrow \dfrac{1}{neigh\ elec\ num}$
$neigh\_values \leftarrow EEG.data(all\_neighi, t_i, epoch_i)$ ▷ Voltage samples of neighbours
$center \leftarrow EEG.data(chan_i, t_i, epoch_i)$
▷ $center$ is the voltage sample of the reference value
$laplacian \leftarrow center - \alpha \cdot \sum(neigh\_values)$
case SISF:
$G \leftarrow zeros(numelectrodes)$
$H \leftarrow G$
▷ Compute Legendre polynomial: a number of legendre polynomials equal to leg_order are estimated for each electrode
$leg\_poly \leftarrow zeros(leg\_order, numelectrodes, numelectrodes)$
$leg\_poly_i \leftarrow legendre(leg\_order, cosdist)$
▷ Estimation of G and H matrices
$G_{i,j} \leftarrow \dfrac{1}{4\pi} \sum_{n=1}^{leg\_order} \dfrac{(2n+1) \cdot P_n(\cos(d_{ij}))}{(n(n+1))^{m_G}}$
$H_{i,j} \leftarrow -\dfrac{1}{4\pi} \sum_{n=1}^{leg\_order} \dfrac{(2n+1) \cdot P_n(\cos(d_{ij}))}{(n(n+1))^{m_H-1}}$
$G \leftarrow G + G'$
$H \leftarrow H + H'$
$data \leftarrow EEG.data(eeg\_channels, :, :)$
$Gs \leftarrow G + eye(numelectrodes) \cdot \lambda$
$GsinvS \leftarrow sum(inv(Gs))$
$dataGs \leftarrow -\dfrac{(sum(dataGs,2)}{sum(GsinvS)} \cdot GsinvS$
$C \leftarrow dataGs - \dfrac{sum(dataGs,2)}{sum(GsinvS)} \cdot GsinvS$
$laplacian \leftarrow C \cdot H$
▷ New filtered EEG struct is updated and goes to the output
$EEG.data(chan, :, :) \leftarrow laplacian$
$EEGSF \leftarrow EEG$
end procedure

4.3 Criteria of comparison between SF

At the beginning, the previous high spatial filters have been tested on signals recorded from voluntary healthy individuals subjected to experiments described in protocol 2018-2019 in subsection 3.2.3, in order to highlight their differences and underlines which is the best. Most specifically, SLSF, LLSF with four neighbouring electrodes and CARSF have been tested. The SISF is investigated deeply in successive sections (subsection 4.4.2). In order to judge them, the following parameters have been taken into consideration:

- **Presence of LRP:** since the individuals have been subjected to motor tasks, a major activation of electrodes placed above pre-motor, motor cortex is expected. In particular, the hope is to visualize both the early and the late components of the movement related cortical potential (MRCP), possibly highlighting its lateralization (LRP).

- **Level of localization:** in order to know which filters localize the high spatial frequencies better over the scalp by reducing the broadening effect and attenuating the volume conductance at low spatial frequencies.

- **Improvement of SNR:** since one of the final goals is to improve the RPs signals retrieved at the end of the pre-processing chain, it is relevant to establish which filters more positively contribute to enhance SNR, which is one of the main parameters the machine learning algorithm studies to judge the quality of the RP.

- **Peaks, slope and amplitude of channels:** after filtering, a predominance in the activation of pre-motor, motor areas in one of the two hemispheres involved in the motor tasks should be emphasized. In addition, more distinctive slopes and amplitudes should be highlighted, revealing the channels which measure the highest high spatial activity.

- **Distorsion and oscillations:** attention must be paid to evaluate which filters introduce less distorsion and oscillations in the signal that do not correspond to neural activity and in its baseline after the filtering operation. The baseline consists in the line that theoretically should correspond to $0\mu V$, because it represents time moments where no brain activity has been stimulated. Typically, the baseline represents the first seconds of the epoch of a RP.

- **Transfer function:** it is one of the main features that explain the behaviour of a filter. Unfortunately, it is not trivial to estimate an exact spatial transfer function of these filters, especially because it is strongly influenced by the number of electrodes characterizing the montage and from the high spatial

information that changes at each time instant. Nevertheless, some discussions have been made to compare these filters from this additional point of view.

By comparing with other BCI found in literature, spatial filters are generally placed in two positions: either before the ERP estimation, in order to apply them to the EEG signal continuous in time or after the ERP estimation. Many papers demonstrated that final results are equivalent, because the processes involved to transform the EEG signal in epoched averaged ERP are linear operations. In this project, spatial filters have been used on the EEG signal continuous in time before the epoching and jitter compensation operations described in chapter 3.
After the selection of the menu voice *Spatial filtering*, user can choose among the previous quoted spatial filters and it needs to insert the value *1* to apply their typical version found in literature.

4.4 Updated versions

After employing previous spatial filters on many dataset of voluntary subjects, several doubts regarding the necessity of their presence in the BCI arose. This was because from topographies and graphs of RPs, as shown in successive sections, it was quite often hard to extract meaningful information or verify expected results. Consequently, some updates have been introduced to the previous versions to obtain better results.

4.4.1 Improvements in SLSF, LLSF and CARSF

One limitation of SLSF and LLSF consists in the number of chosen neighbours with which the averaged waveform is subtracted from the reference electrode. In order to reduce statistic uncertainty of the operation, in these new versions eight neighbouring electrodes are considered instead of only four, so that the α weighting coefficients that multiply each voltage wave associated to neighbouring channels are equal to 1/8. Nevertheless, another problem that interests the CARSF as well arises from associating the same α coefficients to all the voltage samples registered from neighbouring electrodes. Indeed, if some neighbouring channels record really noisy signals, they have the same weight of channels that measure clearer signals, leading to possibly wrong filtered results. Since traditional spatial filters relies on distance as unique criteria to filter, an additional level of control has been introduced to try improving their results. The innovative method consists in processing a chosen dataset through each step of the pre-processing chain without applying any spatial filters. After calculation of RPs signal, SNR for each channel is computed and saved. It consists of a matrix containing the linear ratios between signal and noise powers P_s/P_n, whose dimensions are $[number\ of\ channels \times epoch\ samples]$,

where $number\ of\ channels = 34$, $epoch\ samples = 1024$, which represent the number of points that defines an epoch. Then, this vector is sent as feedback to the spatial filter function, where it is extended to be compatible with the EEG signal continuous in time. Here, the spatial filter function has been updated to estimate the α coefficients which now are calculated accordingly to each SNR value referred to each voltage wave of neighbouring electrodes. The criteria prevents to give a higher weighting coefficients to neighbours that show higher SNR values, in order to emphasize them during the filtering operation, attenuating the ones that show a lower SNR. Most specifically, α coefficients correspond to an interval equal to $(0 \div 1)$ and they are estimated as shown in Equation 4.17, after computing the sum in Equation 4.16 of the samples of SNR belonging to each neighbouring channel at each time instant.

$$SNR_{tot} = \sum_{i=1}^{N} SNR_i \tag{4.16}$$

$$\alpha_i = \sum_{i=1}^{N} \frac{SNR_i}{SNR_{tot}} \tag{4.17}$$

$$\sum_{i=1}^{N} \alpha_i = 1 \tag{4.18}$$

where now $N = 8$. Equation 4.18 must be always valid so that DC spatial noise can be filtered out, as well. In terms of code, the function to compute the laplacian has been modified as illustrated in the algorithm 3.

Algorithm 3 Additive function to compute the laplacian for SLSF, LLSF and CARSF, considering the SNR values. Mathematical operations are element-wise.
Input: center, neighbours,snr_neigh,index_neigh
Output: laplacian

```
1: procedure COMPUTE_LAPLACIAN_WITH_SNR(center, neighbours, snr_neigh, index_neigh)
2:     ▷ N is the number of neighbouring electrodes
3:     ▷ Evaluation of coefficients
4:     snr_tot ← sum(snr_neigh)
5:     α ← snr_neigh / snr_tot
6:     ▷ Bubble sort to order vectors in a crescent way
7:     BubbleSort(snr_neigh, α, neighbours, index_neigh, 'crescent')
8:     product ← α · neighbours
9:     laplacian ← center − sum(product)
10: end procedure
```

4.4.2 Tuning of the SISF

The spherical spatial filter presents some tunable parameters, such as λ, m and n (also known as *leg.order*), that can affect the weights contained in the G and H matrices that multiply the raw data, amplifying high spatial components. Since the behaviour of the filter changes, depending on their combinations, they someway characterize its spatial transfer function. Therefore, several tries have been carried out by modifying one of them, leaving the other two constant, in order to establish the best suitable combination to make it work as a high spatial filter, able to localize activity at the level of the dura mater. The tuning has been conducted on the dataset "MI993011-32C18-A18C-UNF-VOL18-RFOF-EMG1-E2-L2". The four cases of study are presented:

- *Varying m*: $\lambda = 1 \cdot 10^{-7}, leg.order = 10$.
  Inspecting Figure 4.6, the weight matrices as functions of inter-electrode distances change a lot by modifying values of m. The vector of the inter-electrode distances is valid for each electrode viewed as the reference from which estimates the distances with other channels. When $m > 2$, by increasing the inter-electrode distance, the weight coefficients are reduced both in G and H. Then, for really higher values of distances (after 100 mm), they slowly start enlarging with a negative sign. This aspect reveals that spherical filters are not precisely high pass selective filters in the range of distances, but they simply accentuate high spatial frequencies more than low ones. As stated in the Mike and Cohen's book [12], m tunes the behaviour from a high to a low pass filter. What counts is the product of the two matrices depicted in Figure 4.7 that affects the quantity subtracted to the original raw data. The most peculiar case is for $m = 1$, where the H matrix presents a lot of oscillations. $G \cdot H$ shows that, up to 70 mm, components at low distances (so high spatial frequencies) are really emphasized, while from 80 mm to 140 mm middle spatial frequencies are really attenuated. After 140 mm some low spatial frequencies are accentuated but far less than higher ones. This value was the first candidate to be kept for the filter to accentuate high spatial frequencies as much as possible. Nevertheless, it has been abandoned because it produced filtered signals with a very low SNR, which were not reliable. Alternatively, even though $m = 2$ present weights that are smaller than the case $m = 1$, it appears to be a great choice because it shows less oscillations and it has a more quite linear trend.

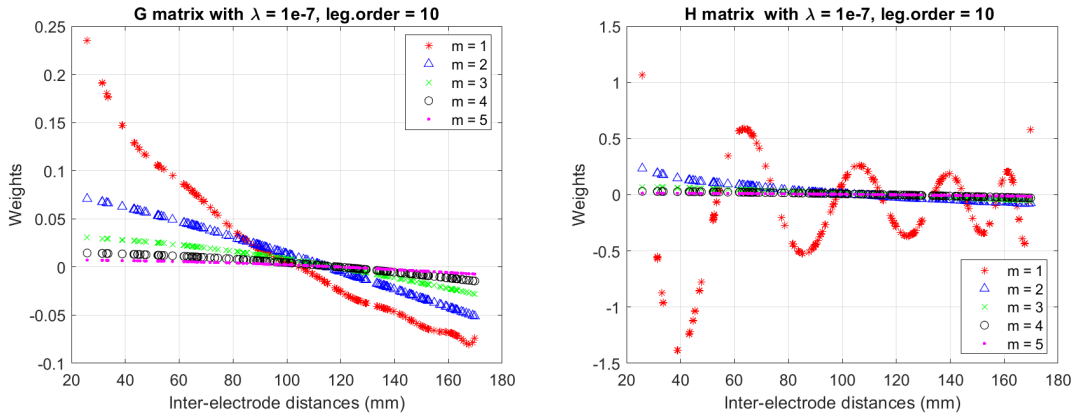

Figure 4.6: G and H matrices as function of inter-electrode distance estimated from the thirty-four electrodes cap by varying m.

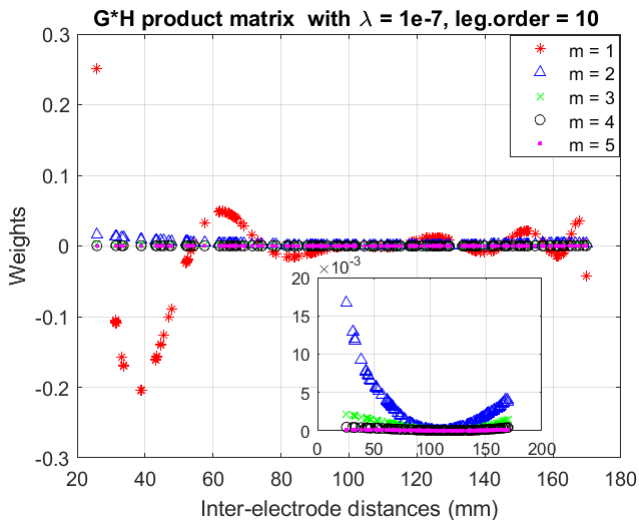

Figure 4.7: Product of G and H matrices by varying m.

- *Varying* λ: $m = 1, leg\_order = 10$.
  In Figure 4.8 are depicted the weight matrices G and H and in Figure 4.9 their product. It can be noticed that varying the smoothing coefficient does not produce significant change in the evaluation of the matrices, whose values appear overlapped. Therefore, it has been set to $1 \cdot 10^{-7}$, because, after several trials, this value appeared to be the best to obtain RPs curves comparable with other spatial filters. Indeed, larger values such as 10^{-3} generates overly smooth results, while smaller values produces more precise topographical results as well [12].

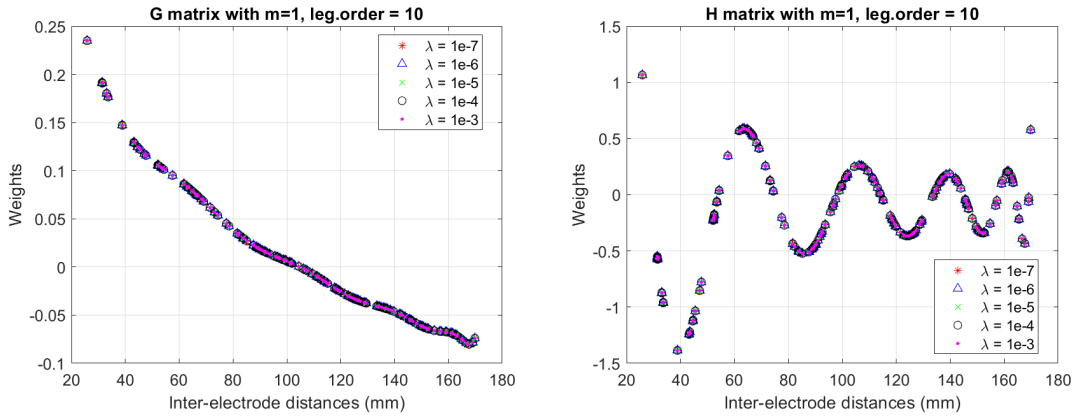

Figure 4.8: G and H matrices as function of inter-electrode distance estimated from the thirty-four electrodes cap by varying λ.

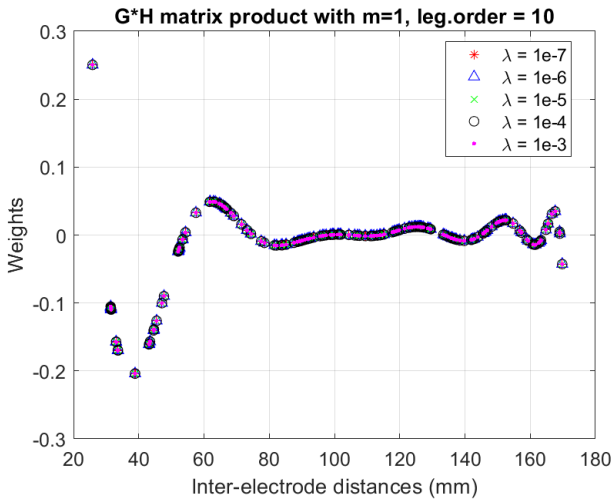

Figure 4.9: Product of G and H matrices by varying λ.

- *Varying n:* $\lambda = 1 \cdot 10^{-7}, m = 2$.
  In this case, $m = 1$ cannot be set, otherwise the H matrices results insensitive to the variations of n, as can be noticed in Equation 4.10. Apart from the case where $n = 1$, little variations are observed in the weight matrices for other values. This parameter represents the order term for the Legendre polynomial, which defines the spatial spherical harmonics frequencies together with m that can detected and which are influenced by each inter-electrode distance, defining the spatial precision of the filter. A demonstration is provided in Figure 4.12. A value equal to 10 increases the accuracy of the weight matrices,

but with larger order, the spatial frequencies exceed the spatial sampling frequency related to the spatial resolution of the montage, which is determined by the number of electrodes, without improving topographies showing useful additional information and increasing the computational time of the algorithm. For more than 100 electrodes in an EEG cap, more benefits with larger order of Legendre polynomials can be obtained.

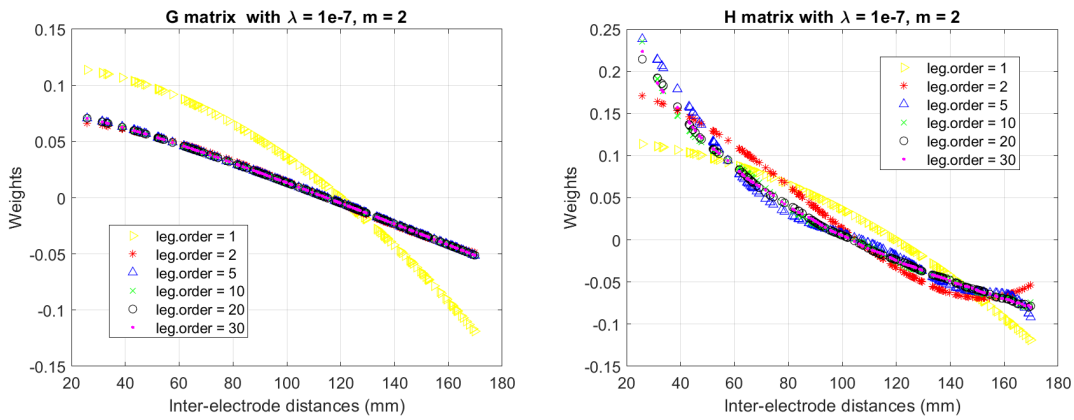

Figure 4.10: G and H matrices as function of inter-electrode distance estimated from the thirty-four electrodes cap by varying n.

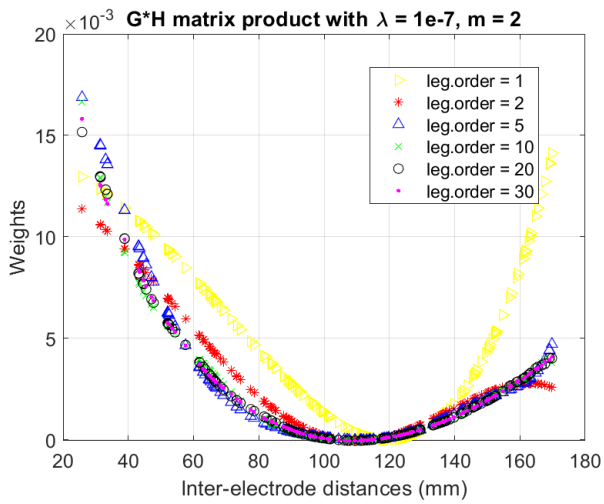

Figure 4.11: Product of G and H matrices by varying n.

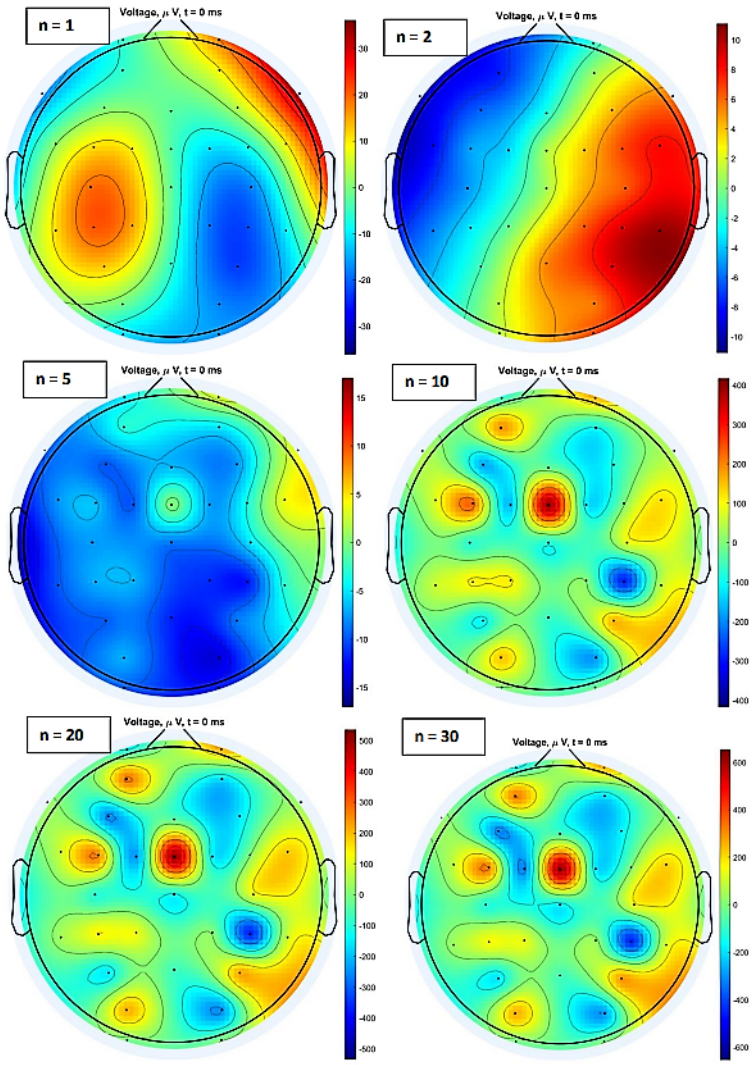

Figure 4.12: Comparison of topographies with different orders of the Legendre polynomials by varying n, with $m = 1, \lambda = 1 \cdot 10^{-7}$.

- *Varying* m_G, m_H:
  Since m is the most influential among the parameters, some attempts have been made on it, but this time differentiating the coefficient present in the Equation 4.19 and in the Equation 4.20, identifying them as m_G and m_H, in order to improve SNR of high spatial filtered channels as well. From Figure 4.13 and Figure 4.14, $m_G = 2, m_H = 1$ is a little worse because it highlights low spatial frequencies more than the previous chosen case ($m_G = m_H = m = 1$). A more interesting case is when $m_G = 1, m_H = 2$, where the values of both

matrices are maximized for high spatial frequencies without maintaining the oscillations of the H matrix. Nevertheless, by analyzing Figure 4.15, this case show less detailed topographies than the other case with $m = 1$ and after several trials, it does not improve the SNR. For these reasons, since using two different values for m_G, m_H did not help to reach optimal results, at the end $m_G = m_H = m = 2$ has been set for the spherical filter.

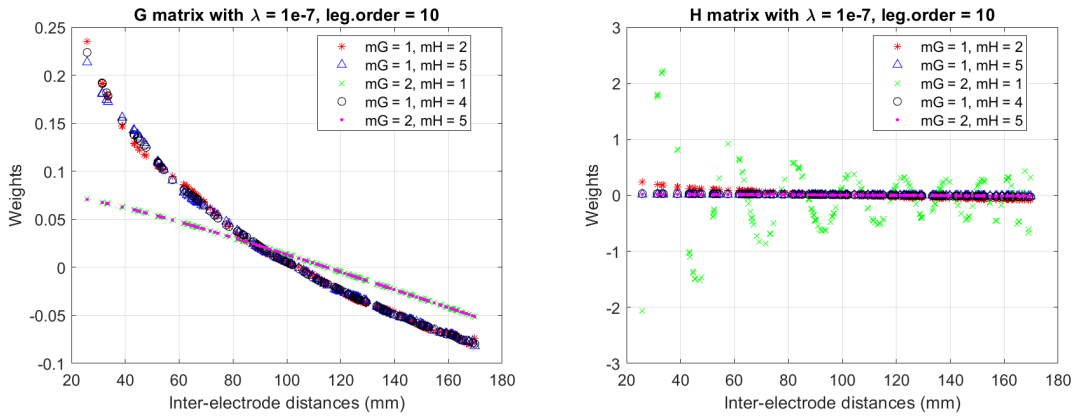

Figure 4.13: G and H matrices as function of inter-electrode distance estimated from the thirty-four electrodes cap by trying two different values for m_G, m_H.

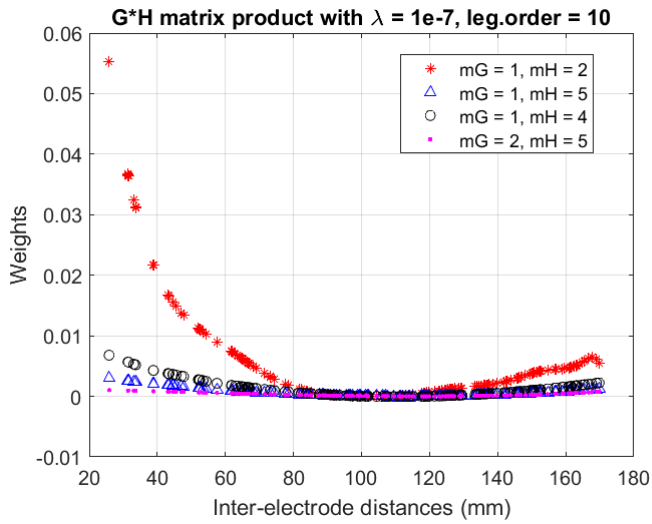

Figure 4.14: Product of G and H matrices by trying two different values for m_G, m_H.

$$G_{ij} = \frac{1}{4\pi} \sum_{n=1}^{\text{leg.order}} \frac{(2n+1) \cdot P_n(\cos(d_{ij}))}{(n(n+1))^{m_G}} \tag{4.19}$$

$$H_{ij} = -\frac{1}{4\pi} \sum_{n=1}^{\text{leg.order}} \frac{(2n+1) \cdot P_n(\cos(d_{ij}))}{(n(n+1))^{m_H-1}} \tag{4.20}$$

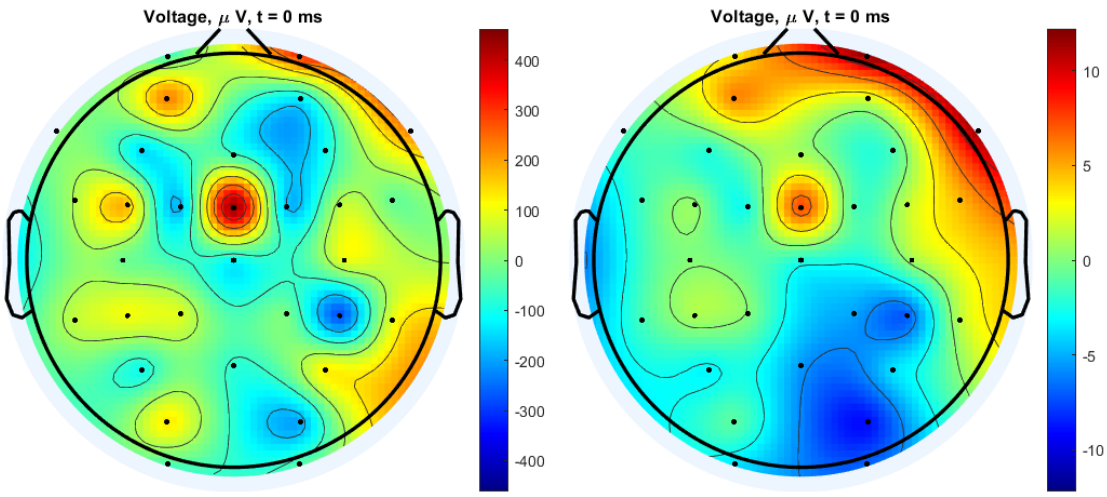

Figure 4.15: (Left) Topography where $m_H = m_G = m = 1$ with more highlighted regions around electrodes but really high values in μV, (right) topography where $m_H = 2, m_G = 1$ where the activity of electrodes is less detailed.

To sum up, the combination employed for the spherical filter in this project is $m_G = 2, m_H = 2, n = 10, \lambda = 1 \cdot 10^{-7}$. These numbers have been compared with other combinations found in literature [28],[29]. Unfortunately, in most of the papers is not specified the reason behind the choice of a particular combination [30]. Several studies suggest $m = 4, n = 7, \lambda = 1 \cdot 10^{-5}$ [26], but using only a montage of nineteen electrodes, while others suggest $m = 3, n = 50, \lambda = 1 \cdot 10^{-8}$, but for sixty-four or EEG-cap richer of channels [28].

The last update inserted in the spatial filter function regards the number of electrodes of the montage. On the whole, spatial filters boost their performances by enlarging the number of electrodes placed in the montage because more electrodes mean more spatial points at each time instant in which they can measure a voltage value. Consequently, more spatial samples improve the spatial resolution of the EEG-cap, allowing the filters to apply higher sampling spatial frequencies with the aim at reaching more accurate results. Considering that many researches may not be able to use a montage rich of electrodes, to make spatial filters applicable for

them as much as possible, in case the dataset imported in the plug-in involves less than thirty-four channels, the lacking ones are filled with an averaged waveform generated from the existent ones, in order to simulate the volume conductance's effect. That procedure allows to obtain better topographies as demonstrated in successive sections.

4.5 Testing High-Pass SF of literature on healthy subjects

In this section, several results are reported after the application of the spatial filters implemented by following examples found in literature. The dataset employed for the simulations is "MI993011-32C18-A18C-UNF-VOL18-RFOF-EMG1-E2-L2", beloging to an healthy individual subjected to voluntary motor tasks, where he was asked to move the index of the right finger.

4.5.1 Voluntary task 2018-2019 Protocol

The following parameters have been considered for analyzing the various spatial filters:

1. **Topographies:**

   - *SLSF:*

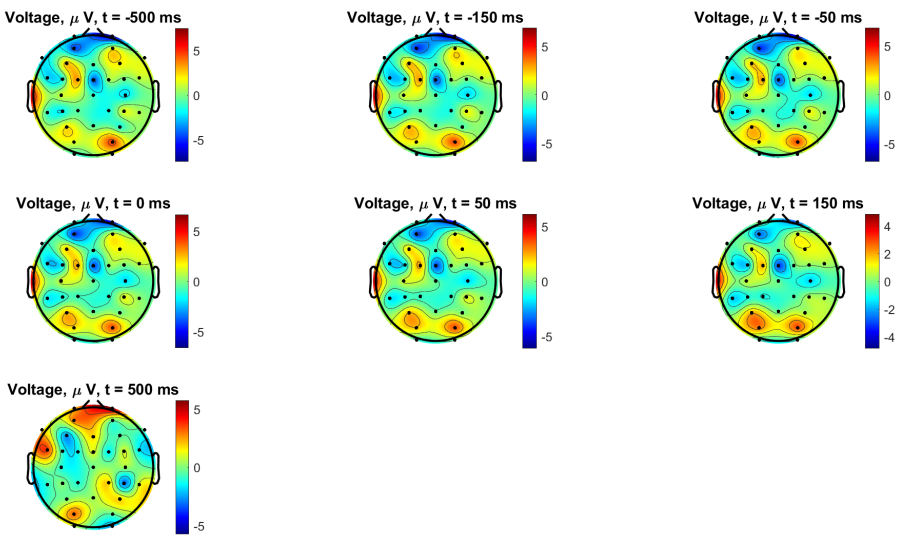

Figure 4.16: Topographies of standard SLSF.

- *LLSF:*

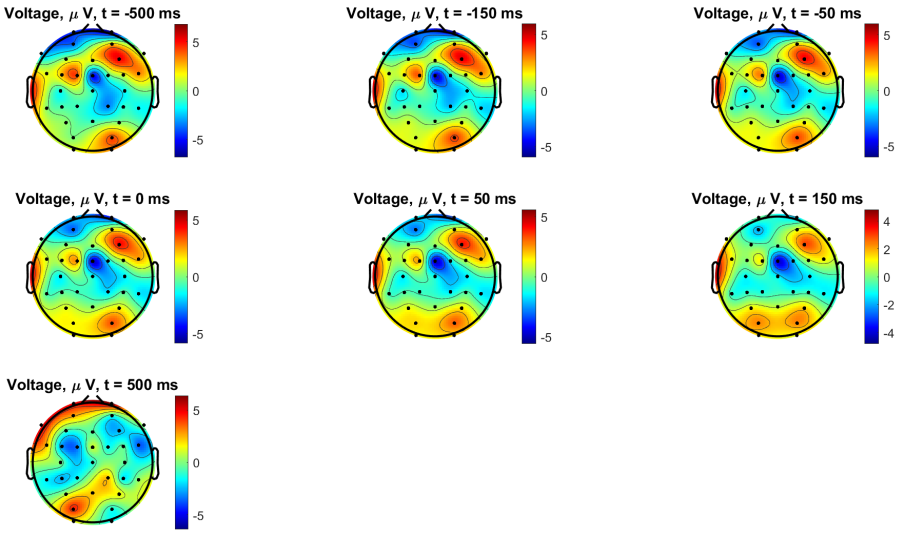

Figure 4.17: Topographies of standard LLSF.

- *CARSF:*

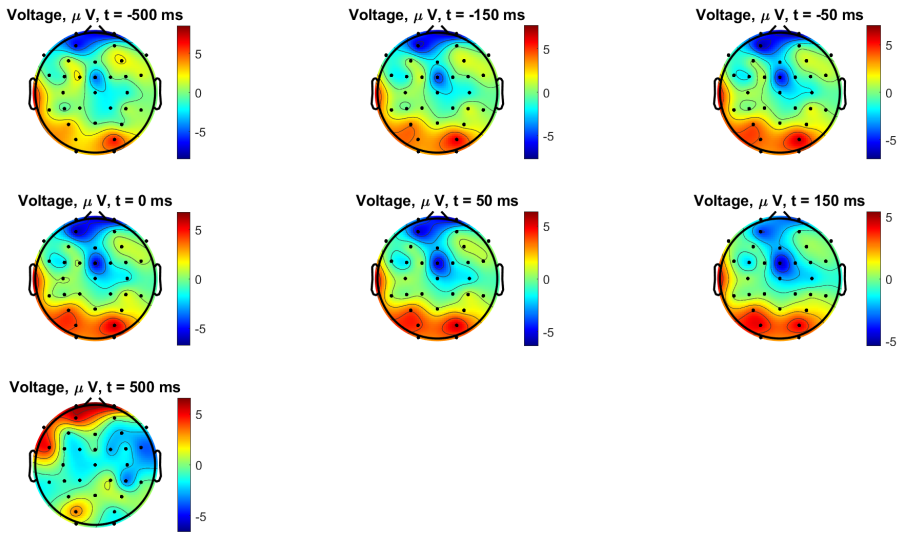

Figure 4.18: Topographies of standard CARSF.

The CARSF shows the worst results. Indeed, even if the activity of Cz is clearly distinguishable, both the early and late components of RP are not clearly visible because the voltage distributions are quite blurred. There is some accentuation around 0 ms, but nowhere else. On the other hand, the

SLSF produces more concentrated regions. It appears to be very specific because, considering the area involving $Fc3, C3, Fc1, Fc5, Fc1$ in the left hemisphere, it is possible to see the lateralization of the RP with details of the activation of the channels, emphasized by their different polarities. The LLSF highlights the lateralization better on electrodes $Fc5, Fc3, Fc1$, without revealing more specific activation regions just like the SLSF.

2. **Activation of pairs C3-C4, Fc3-Fc4**

- *Raw signal:*

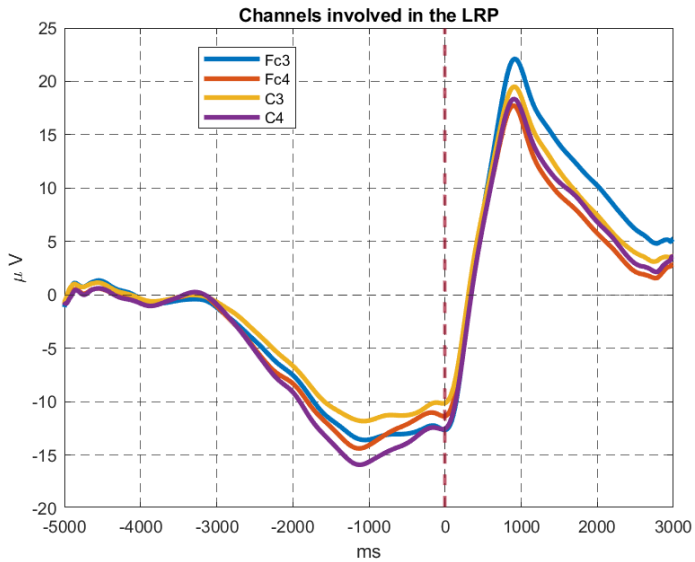

Figure 4.19: Unfiltered channels mostly involved in the pre-motor and motor response.

- *SLSF:*

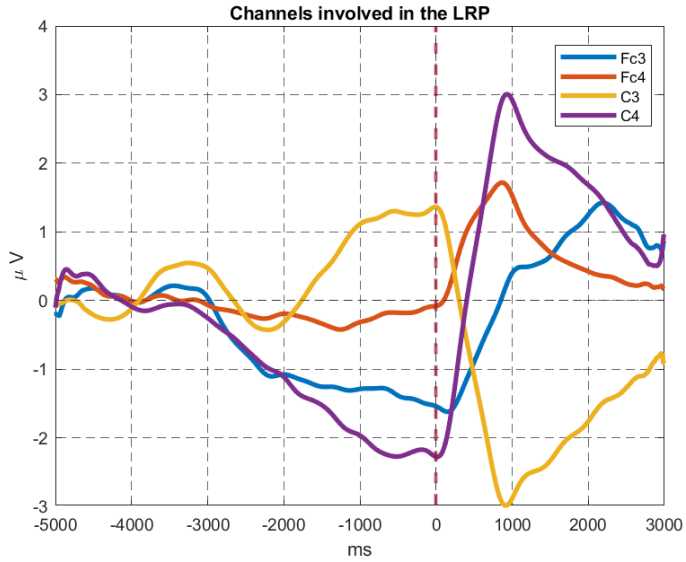

Figure 4.20: SLSF filtered channels involved in the pre-motor and motor response.

$C3, C4$ are the most active channels. Around -1000 ms, $C4$ is more active than $C3$, misleading on the finger moved from the subject. On the other hand $Fc3$ shows greater amplitude than the symmetric $Fc4$ during the phase of intention before the ONSET, revealing the right finger the subject has had the intention to move in the experiment. Around 1,000 ms, $C3$ shows an equal peak with $C4$, which is more reliable to reality, but this time, $Fc3$ is less active $Fc4$, against the predictions. On the whole, it is possible to admire a more pronounced slope in the intention phase between the channels, which makes them more distinguishable, thanks to the removal of the volume conductance. Finally, accordingly to the expectations, while $C3, C4$ exhibit the greater high spatial information during the execution of the movement after the ONSET. The baseline from -5000 ms to -3000 ms presents some noisy peaks.

- *LLSF:* Here, differently from the raw and previous cases, $Fc3$ appears to be the most active channel both in the intention phase around -1000 ms, as predicted and after the end of the execution of the movement around +1000 ms, unexpectedly. Unfortunately, $C3$ is less active than $C4$ in the intention phase, but then it is slightly greater in the execution phase. Since they are quite overlapped, the volume conductance in common between the two is not been efficiently removed as for $Fc3.Fc4$. Indeed, only these two are more distinguishable in amplitude, showing a distinctive slope. Overall, the shapes of the RPs are nice and the baseline from -5000 ms to

-3000 ms appears quite noiseless.

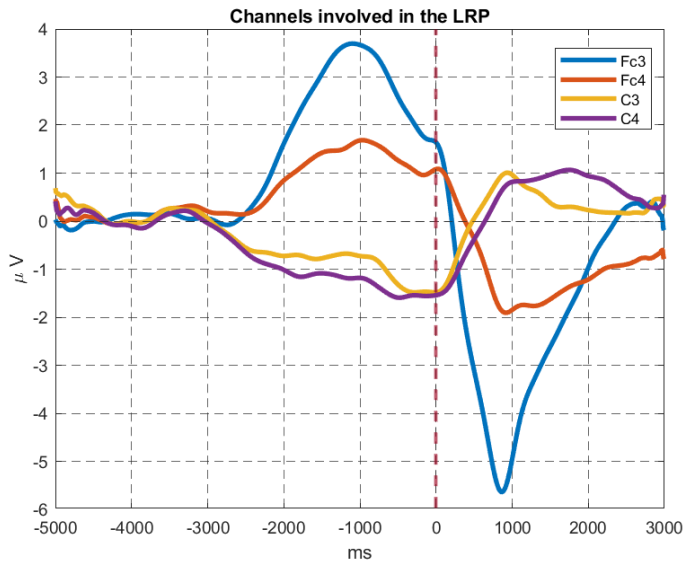

Figure 4.21: LLSF filtered channels involved in the pre-motor and motor response.

- *CARSF:* Near -1000 ms, there are the peaks of $FC3, C3$ which coincide with the peak of intention, shown in the raw form of the signal. They are both more active than symmetric $Fc4, C4$ in that point, confirming that the subject has had the intention to move the right finger. Indeed, in case of right finger motion, neurons located in the left hemispheres start activating. Nevertheless, regarding the peak after the movement of the finger at +1000 ms, both $Fc4, C4$ dominate in terms of amplitude. Excluding $C4$ waveform which does not posses a good shape, the other channels exhibit a quite good RP, even though they have a lot of oscillations and the baseline is noisy.

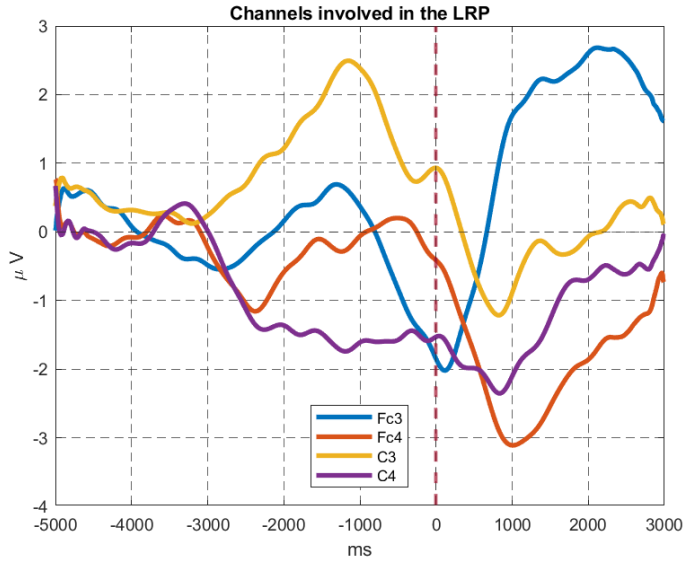

Figure 4.22: CARSF filtered channels involved in the pre-motor and motor response.

3. **Lateralized readiness potential**

- *Raw signal:* The LRP should be visible around -1000 ms, because it represents the major strength of the left hemisphere in the activation of neurons when the subject has the intention to move the right finger. As cited in 2.7, in order to retrieve an accurate LRP, the volunteer should be subjected to two different tasks at least, one in which it is requested to move the right finger and one in which it is requested to move the left one. Unfortunately, dataset regarding the motion of left finger is not available, therefore only the first subtraction between electrodes placed in the contralateral and ispilateral brain regions to the moved finger has been computed. That means the intrinsic bias noise of the two hemispheres may impede the visualization of the motor component. In case of Figure 4.23, the lateralization of the readiness potential cannot be seen for electrodes $C3 - C4$, indeed the positive peak symbolizes the major activation of $C4$ with respect to $C4$, while in $Fc3 - Fc4$ is more evident because it presents a negative trend before the execution of the movement. In the ideal cases, $Fc3, Fc4$ should show greater amplitudes in the intention phase, consequently their subtraction $Fc3 - Fc4$ should give rise to a smaller peak before the ONSET. Viceversa, since $C3, C4$ should show smaller amplitudes than $Fc3, Fc4$ before the ONSET, their subtraction $C3 - C4$ should emphasize a greater peak. Obviously, EEG signals are

rich of components of the superficial scalp and sometimes it is not possible to admire results equal to the ideal case.

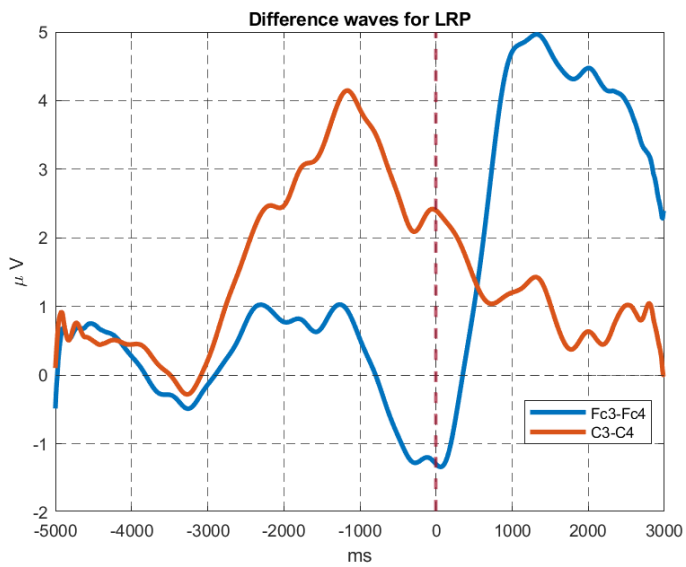

Figure 4.23: Lateralization of Fc electrodes in the raw signal.

- *SLSF:* In this case, it is not possible to appreciate a good LRP in Figure 4.24 around -1000 ms for $C3 - C4$. For $Fc3 - Fc4$, the lateralization is evident in the intention phase and $Fc3$ continues to be more active than $Fc4$ up to +1500 ms.

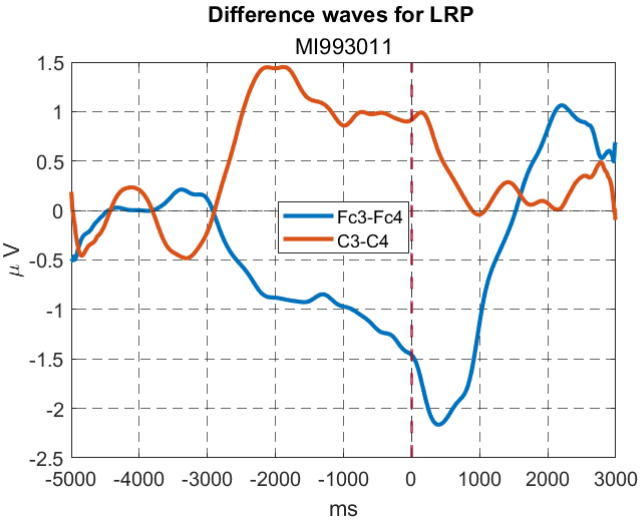

Figure 4.24: LRP after standard SLSF application.

- *LLSF:* Looking at Figure 4.25, this filter highlights the lateralization of readiness potential recorded from $Fc3$, with a positive polarity in this case. Indeed, $Fc3$ is more active than $Fc4$, while no lateralization is evident for the readiness potential recorded from $C3, C4$.

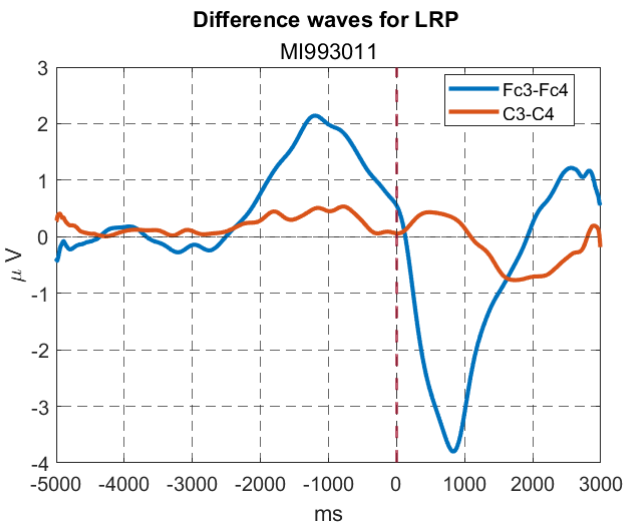

Figure 4.25: LRP after standard LLSF application.

- *CARSF:* The Figure 4.26 shows a lateralization of $Fc3 - Fc4$ and $C3 - C4$ around -1000 ms.

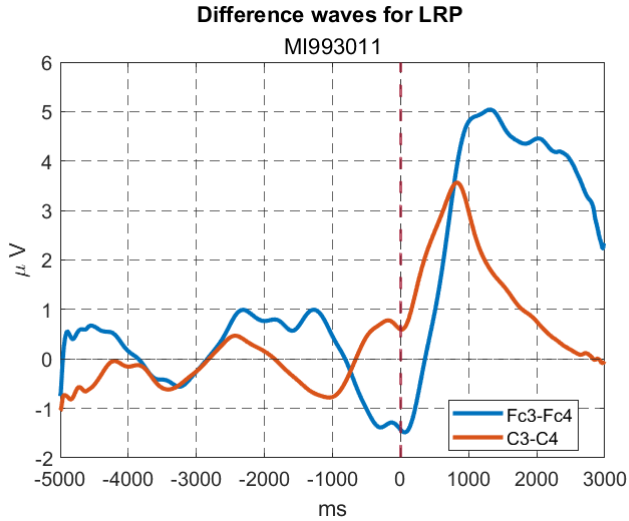

Figure 4.26: LRP after standard CARSF application.

4. **Signal-to-noise ratio:**

   - *SLSF:* The Figure 4.27 shows that only the right and the motor caudal-rost areas report SNR values greater than 3 dB, but less than 6 dB.

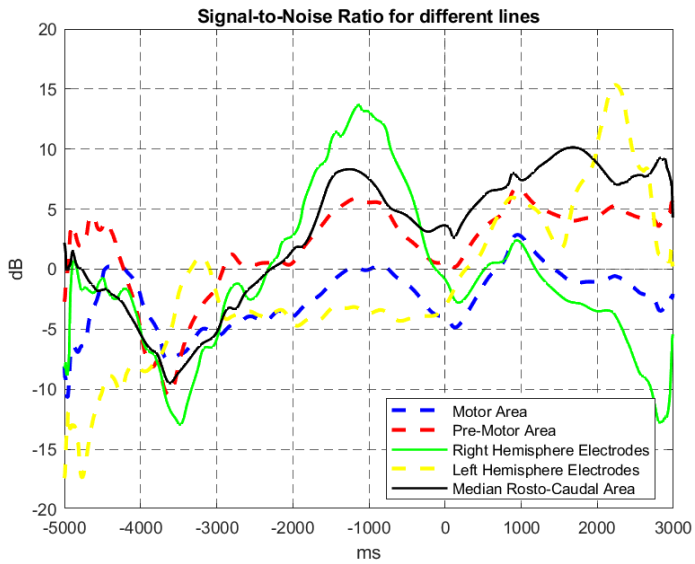

Figure 4.27: SNR of averaged lines on the scalp after standard SLSF application.

   - *LLSF:* In this case, the pre-motor and median rosto-caudal areas present discrete SNR.

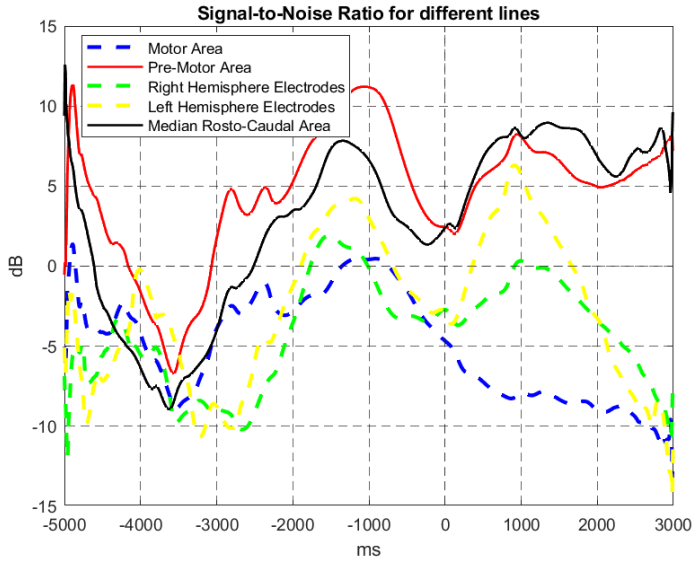

Figure 4.28: SNR of averaged lines on the scalp after standard LLSF application.

- *CARSF:* In Figure 4.29, the motor rosto-caudal area presents SNR values greatet than 6 dB, while the pre-motor between 3 dB and 6 dB.

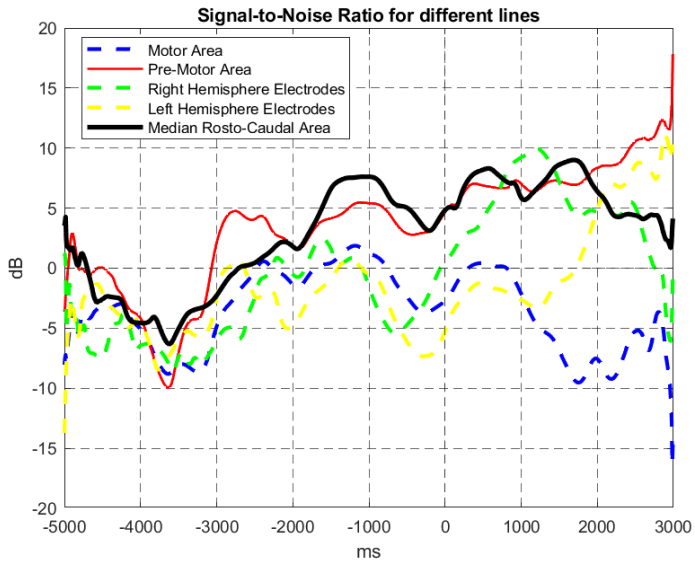

Figure 4.29: SNR of averaged lines on the scalp after standard CARSF application.

5. **Shape of averaged lines:**

- *SLSF:* As shown in Figure 4.30, after the application of this filter, pre-motor and median rosto-caudal areas are the lines with more high spatial energy. Unfortunately, the left hemisphere line has a very low voltage dynamic and it is quite null in correspondence of -1000 *sims*. In addition, it is very less active than the right hemisphere, which is against the predictions. As regards the motor line, it is not so emphasized and its RP is not good.

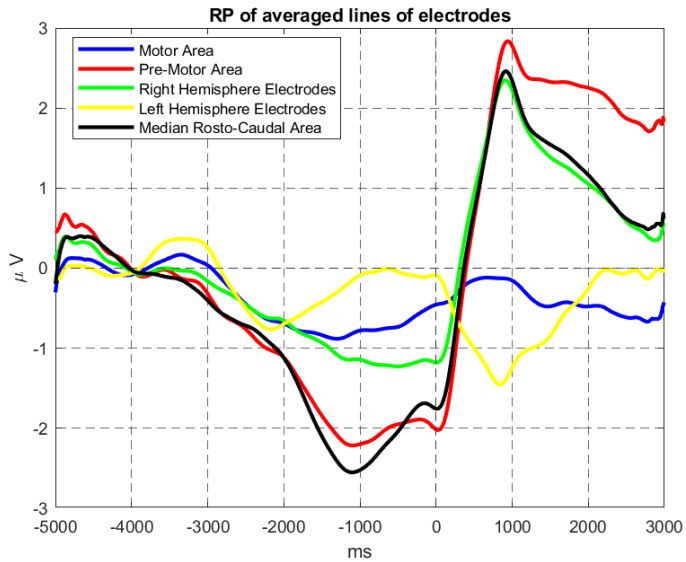

Figure 4.30: RP of averaged lines on the scalp after standard SLSF application.

- *LLSF:* In this case, this filter highlights the high spatial information registered in the motor rosto-caudal area and in the left hemisphere, as expected. Furthermore, the pre-motor and median rosto caudal lines are not overlapped, so that they can be distinguished better and the RP of the motor area is clearer than the case where SLSF were applied. Following the predictions, the right hemisphere is the less active.

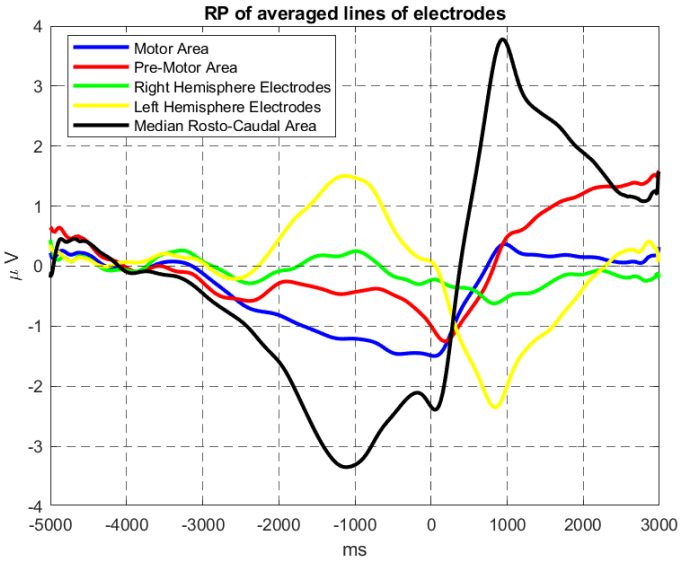

Figure 4.31: RP of averaged lines on the scalp after standard LLSF application.

- *CARSF:* Median rosto-caudal and pre-motor areas reveal to have the greatest high spatial information. Unfortunately, the other RPs are not optimal. In particular, the left hemisphere has an additional peak around +2000 ms, probably due to noise.

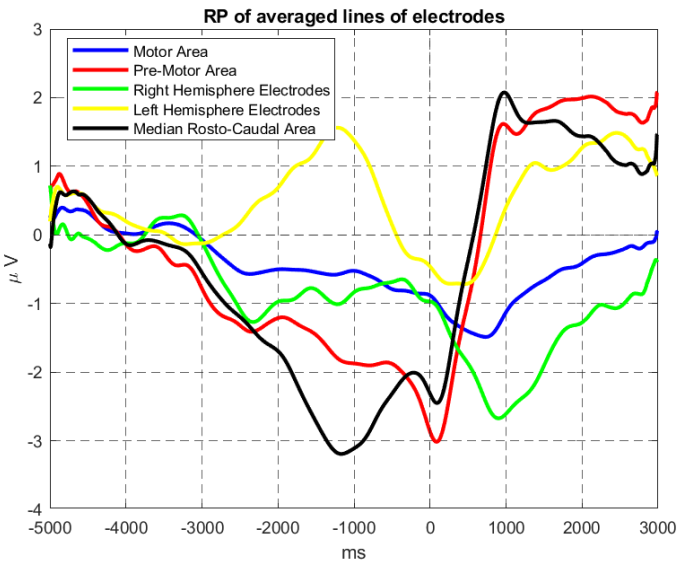

Figure 4.32: RP of averaged lines on the scalp after standard CARSF application.

4.5.2 Issue with small montage

Until now, data recorded from a thirty-four electrodes montage have been utilised for the application of spatial filters. Unfortunately, sometimes researchers prefer to employ a smaller EEG cap, because it is easier to place, especially on patients who are difficult to treat, simplify the recording process, there are less signals to process, it represents a cheaper solution and so on. Nevertheless, less electrodes means less spatial resolution of the EEG-cap. Consequently, if the number of electrodes is equal to seven, as in dataset recorded in the 2015-2018 protocol, the topographies are not precise, as depicted in Figure 4.33. Due to the few number of electrodes, it is not possible to categorize neighbouring and further neighbouring channels, therefore LLSF and CARSF coincide with SLSF, providing similar results, where there are not circumscribed regions of activation anymore.

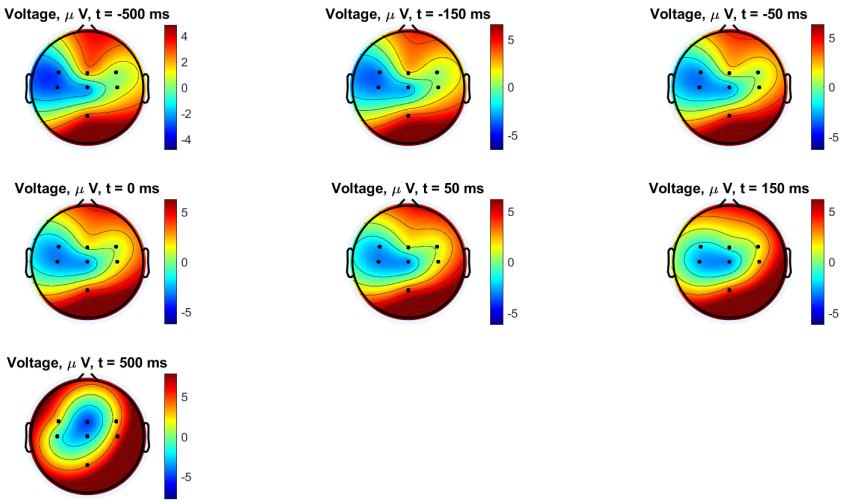

Figure 4.33: Topographies after the application of SLSF which coincide with topographies obtained after employing LLSF and CARSF.

4.5.3 Preliminary discussions

Considering previous results, CARSF appear to be the worst spatial filter, because it provides a quite blurred voltage distribution in the topographies and it does not provide good RPs for $C3, C4, Fc3, Fc4$, even though it shows the highest SNR for the median rosto-caudal area and provides quite good visualization of LRP. SLSF and LLSF have symmetric advantages and disadvantages. The small laplacian selects really high spatial frequencies, since it considers the closest neighbouring channels, showing more detailed topographies. On the contrary, the large laplacian keeps middle-high spatial frequencies from the raw signal, since it considers the

next neighbouring channels, highlighting more the LRP of $Fc3 - Fc4$ and both show similar SNR for the median rosto-caudal area.

4.6 Testing updated High-pass SF on healthy subjects

4.6.1 Voluntary task

Updated versions of spatial filters with innovations explained in 4.4 are applied on the same dataset and on a dataset belonging to the 2015-2018 protocol, where only seven electrodes were available in the montage. At the end of the section, several considerations are treated to compare old and updated versions of spatial filters, trying to highlight at least two filters that are the best among the others.

Results of SLSF

- **Topographies:**

  In this updated version the results of the topographies are preserved. Little differences can be seen in the intensity of some regions in the left hemisphere that are slightly marked better in Figure 4.34.

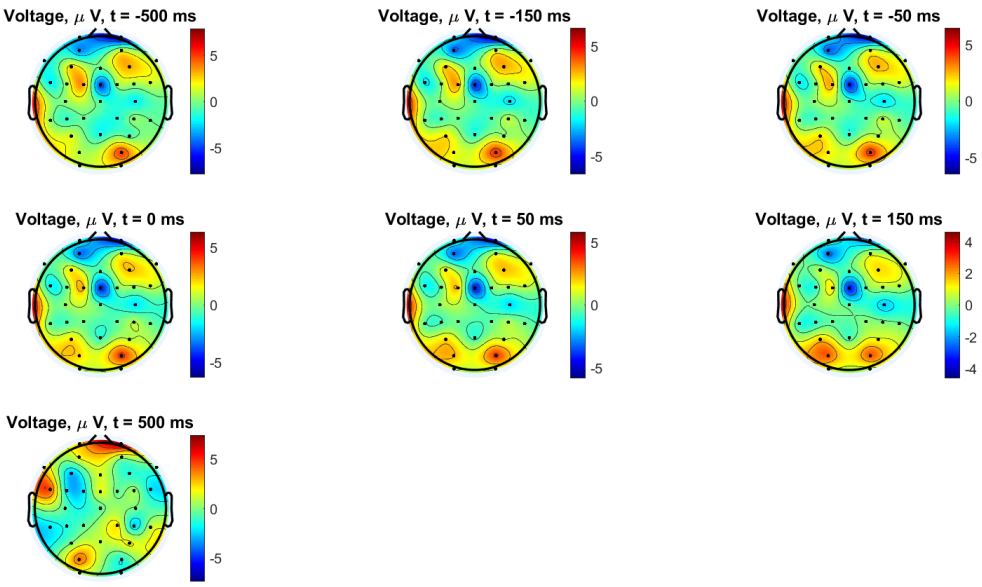

Figure 4.34: Topographies after the application of updated SLSF using eight neighbouring electrodes.

- **Activation of pairs $C3 - C4, Fc3, Fc4$:** In this case, $Fc3$ has a greater amplitude than the symmetric in the right hemisphere, as expected in the intention phase and after the ONSET as well. On the other hand, $C3$ appears to be more attenuated than the symmetrical $C4$ in the intention phase. Nevertheless, they are more involved in the phase of the motor action, indeed around $+1000$ ms, $C3$ has a greater peak in absolute value than $C4$. This is another nice result in comparison with the old spatial filter version, where $C3, C4$ presented the same amplitude after the ONSET. Slopes are accentuated in all the channels.

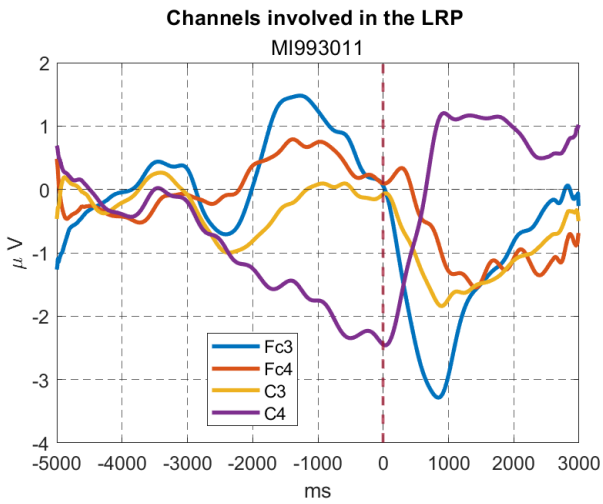

Figure 4.35: Filtered Pre-motor $(Fc3 - Fc4)$ and motor $(C3 - C4)$ channels with updated SLSF.

- **Lateralized readiness potential:** The lateralization shown in Figure 4.36 is worse for both $Fc3 - Fc4, C3 - C4$, in comparison with the old filter.

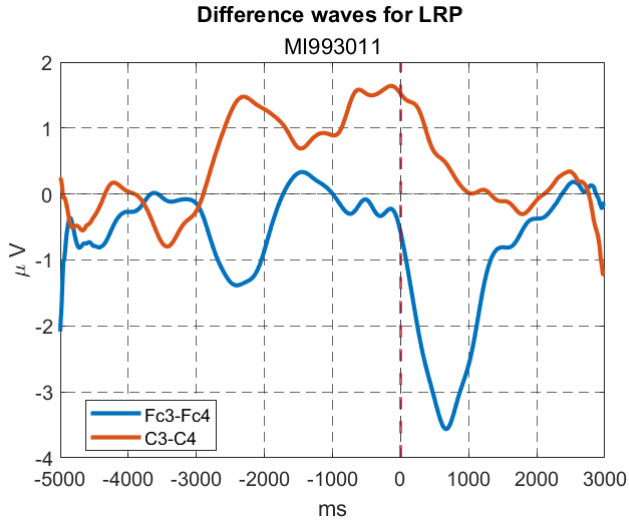

Figure 4.36: Lateralized readiness potentials.

- **Signal-to-noise ratio:** As reported in Figure 4.37, the updated version of the SLSF with the introduction of the SNR feedback shows an improvement for the pre-motor and the median rosto-caudal areas in terms of signal-to-noise ratio. Unfortunately, the right line here is worse than the old filter case, but since that line is less relevant from a point of view of activation, less high spatial energy is encapsulated in that region, justifying the presence of low SNR values.

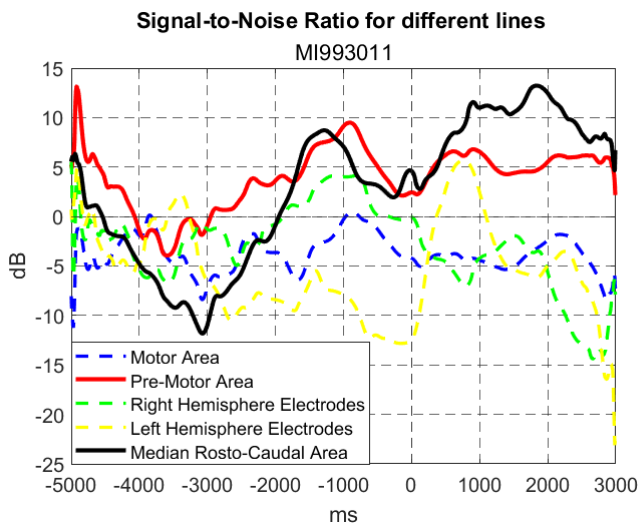

Figure 4.37: SNR of averaged lines more involved during motor tasks after the application of SLSF updated.

- **Shape of averaged lines:** Differently from the old filter case, it can be appreciated a greater voltage dynamic of the left line with respect to the right one, as expected. Median rosto-caudal area continues to show the greatest high spatial energy, while the pre-motor line appears less active in the intention phase. The RPs present a good shape, accentuated slopes and on the whole they are better than the old version case.

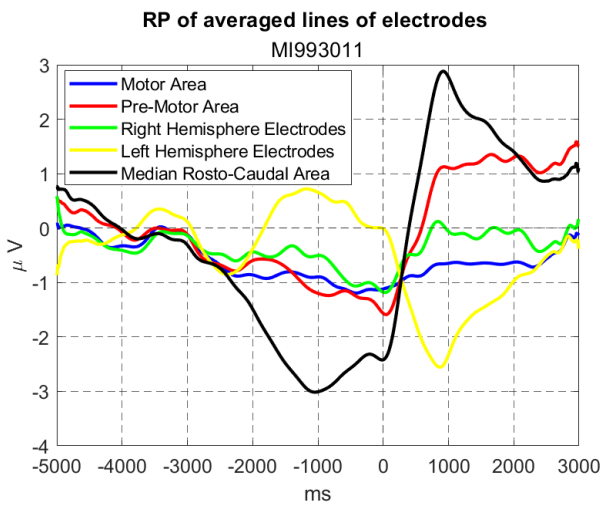

Figure 4.38: Averaged lines of the scalp after the application of updated SLSF.

Results of LLSF

- **Topographies:** Quality of topographies is preserved, as shown in Figure 4.39.

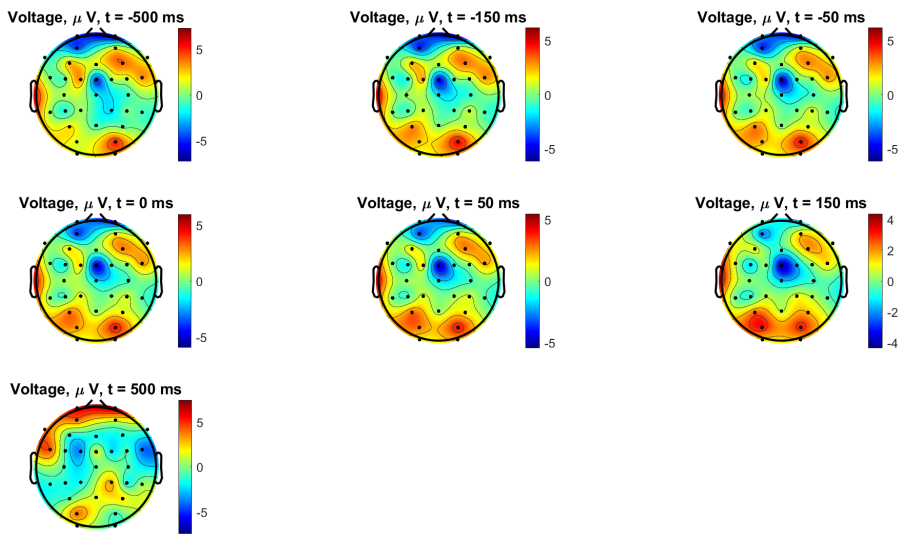

Figure 4.39: Topographies after the application of LLSF using eight neighbouring electrodes.

- **Activation of pairs** $C3, C4, Fc3, Fc4$**:** channel $C3$ is improved because it shows the biggest peak in the intention phase around -1000 ms and because it is cleary distinguishable from $C4$. Unfortunately, this is no longer valid after the ONSET where they are quite overlapped. $Fc3$ results smaller in amplitude than it was in the old filter case.

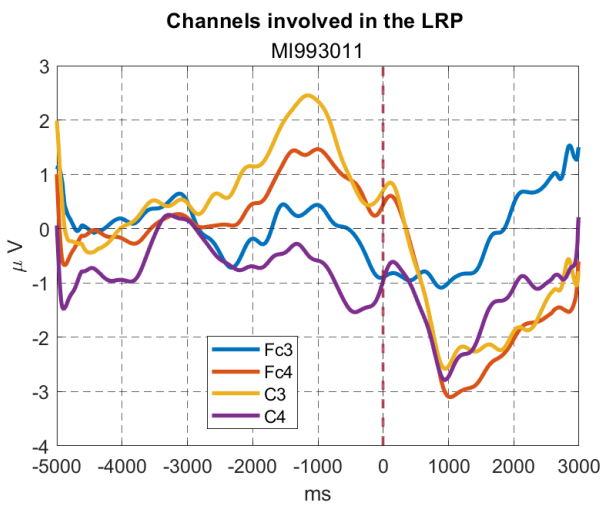

Figure 4.40: Pre-motor $(Fc3 - Fc4)$ and motor $(C3 - C4)$ channels after the application of updated LLSF.

- **Lateralized readiness potential:** The lateralization shown in Figure 4.41 is better for $C3 - C4$, because the peak is in correspondence of the peak of intention at -1000 ms, but $Fc3 - Fc4$ is not good because, since these chanels were both positive, their negative subtraction tells that $Fc4$ is more active than $Fc3$, against the predictions.

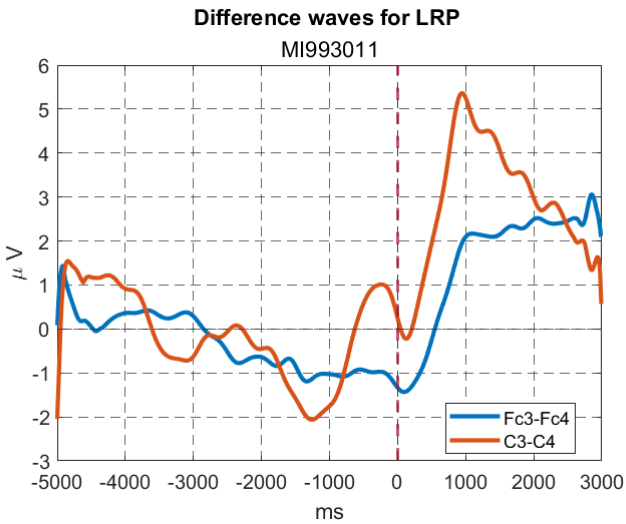

Figure 4.41: Lateralized readiness potentials after the application of updated LLSF.

- **Signal-to-noise ratio:** As reported in Figure 4.42, the updated version of the LLSF with the introduction of the SNR feedback shows a slight improvement for the pre-motor area in terms of signal-to-noise ratio.

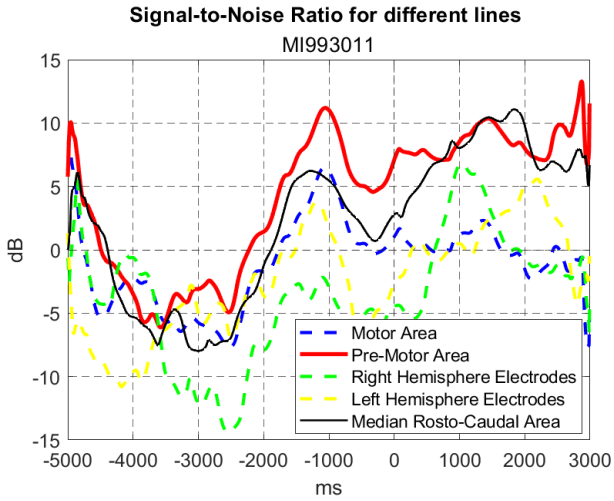

Figure 4.42: SNR of averaged lines more involved during motor tasks after the application of updated LLSF.

- **Shape of averaged lines:** Unfortunately, in this case, the right line appears more active than the left one after the ONSET, against the predictions. As regards the intention phase, all the lines are nice, well distinguishable in amplitudes and slopes.

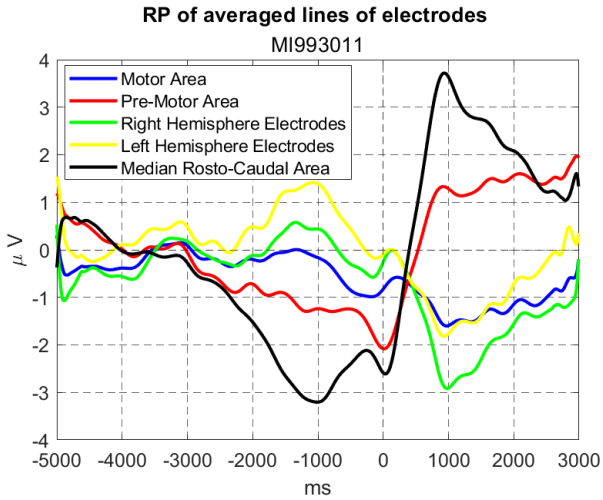

Figure 4.43: Averaged lines of the scalp.

Results of CARSF

In this case, CARSF does not benefit of the update in none of the fields analyzed untill now. This is because it however considers all the electrodes of the montage for the calculus of the laplacian, therefore the α coefficients do not remarkably change, as the final results. For the sake of completeness, graphs to demonstrate this reality are reported.

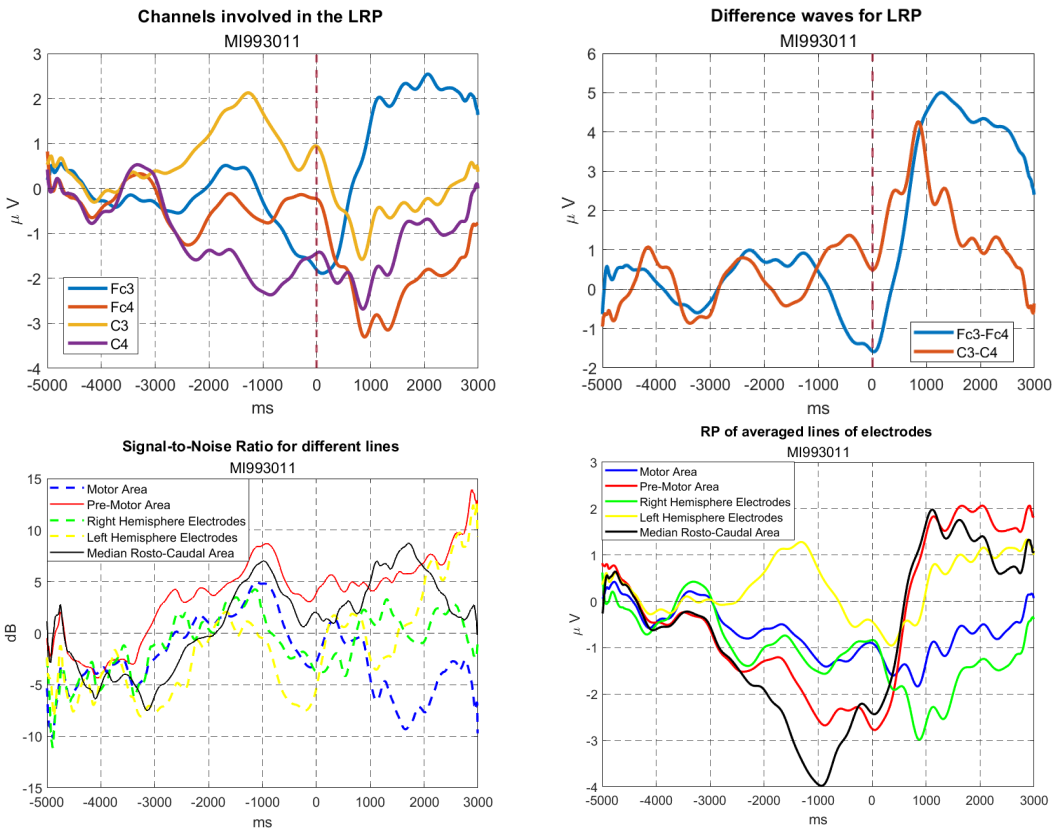

Figure 4.44: Results after applying the updated CARSF.

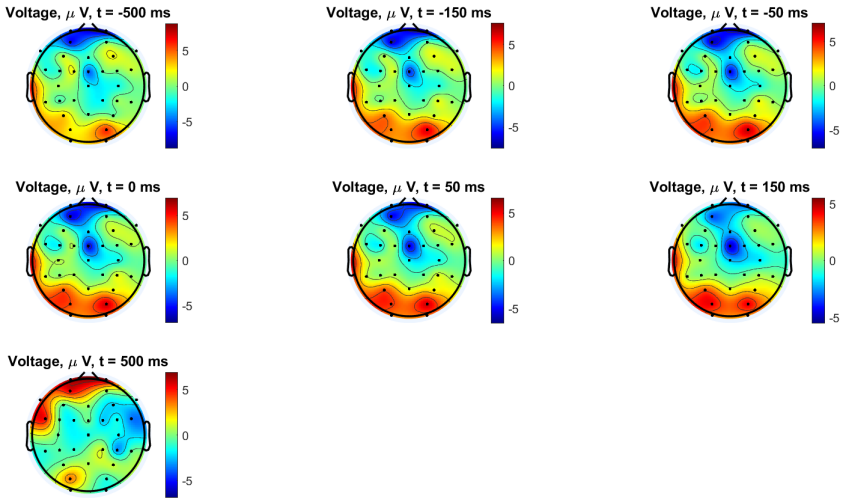

Figure 4.45: Averaged lines of the scalp after the application of updated CARSF.

Results of SISF

For the spherical filter, the following parameters have been set: $m_H = m_G = 2, \lambda = 1 \cdot 10^{-7}, n = 10$. As explained in subsection 4.4.2, the spatial filter tends to amplify the signal recorded from some channels through weight coefficients to make the high spatial frequency information more visible. Nevertheless, in order to obtain voltage dynamics comparable with the ones of the other filters, in the following graphs a normalization has been executed. The normalization consists in dividing the output RPs of the spherical spatial filter with RMS coefficients c_{rms}, retrieved by dividing the root mean square voltage of the high spatially filtered RP signal with the root mean square voltage of the spatially unfiltered RP signal:

$$V_{rms,j}|_{RAW} = \sqrt{\frac{1}{N}\sum_{n=1}^{N}|RP_i|^2_{RAW}} \tag{4.21}$$

$$V_{rms,j}|_{HIGH} = \sqrt{\frac{1}{N}\sum_{n=1}^{N}|RP_i|^2_{HIGH}} \tag{4.22}$$

$$c_{rms,j} = \frac{V_{rms,j}|_{HIGH}}{V_{rms,j}|_{RAW}} \tag{4.23}$$

where i indicates the samples of each channel j that measures a RP, obtained from EEG signal which have been averaged by summing up all the epochs. For the current dataset, c_{rms} values estimated for each channel are reported in Figure 4.46.

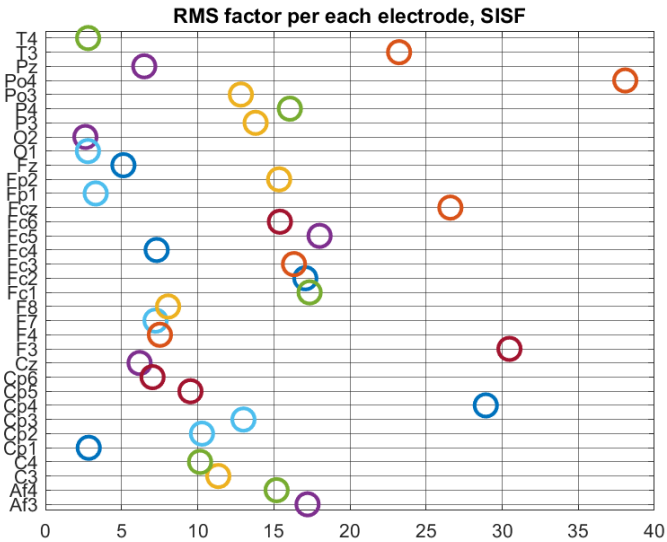

Figure 4.46: RMS coefficients used to normalize the output of the spherical spatial filter.

- **Topographies:** With the spherical filter, really detailed topographies can be obtained, as represented in Figure 4.47.

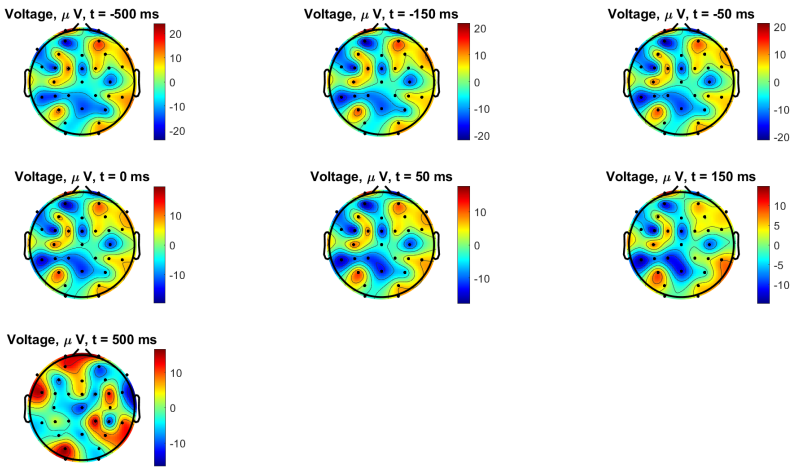

Figure 4.47: Topographies after the application of SISF using eight neighbouring electrodes.

- **Motor and pre-motor electrodes** $C3, C4, Fc3, Fc4$**:** The negative or positive peak before the ONSET is really accentuated. $Fc3$ is more active than $Fc4$, while $C3$ is less active than $C4$.

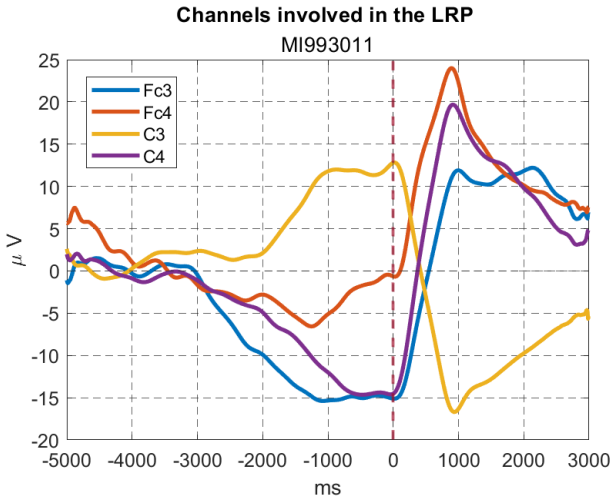

Figure 4.48: Pre-motor $(Fc3 - Fc4)$ and motor $(C3 - C4)$ channels after the application of SISF.

- **Lateralized readiness potential:** From Figure 4.49, a stronger activation of $Fc3$ is evident, since it is more active both in the intention phase and after the accomplishment of the movement. Unfortunately, this is not valid for $C3, C4$.

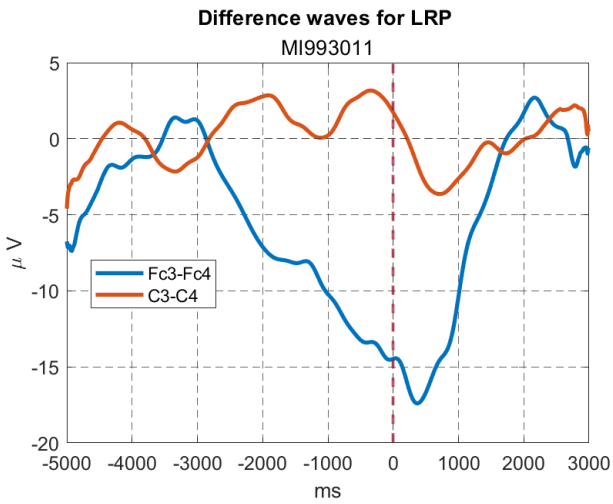

Figure 4.49: Lateralized readiness potentials after the application of SISF.

- **Signal-to-noise ratio:** As reported in Figure 4.50, SISF shows the best signal-to-noise ratio until now, for the pre-motor, median rosto-caudal and right areas.

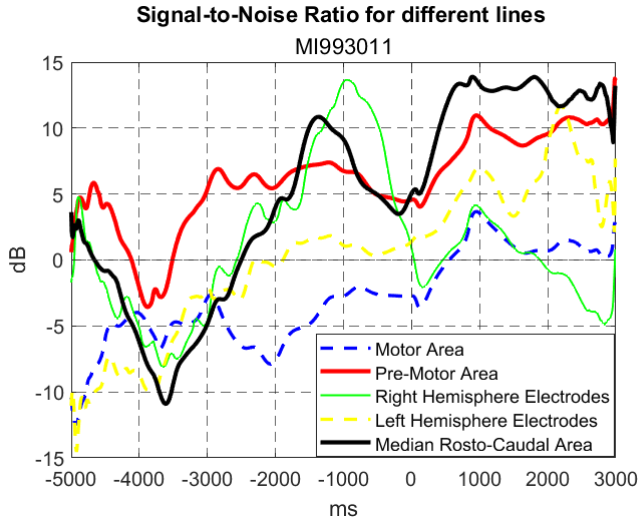

Figure 4.50: SNR of averaged lines more involved during motor tasks after the application of SISF.

- **Shape of averaged lines:** In terms of quality of RP, motor and pre-motor lines have more relevance because they contain Cz, Fcz, which represent approximately a sum of the activity registered from $C3, C4, Fc3, Fc4$ with an additional contribute of energy. In this case, the pre-motor line is very distinctive, while the motor is less relevant in the intention phase and starts raising during the execution of the movement, as expected. Unfortunately, the right line appears more active than the left one.

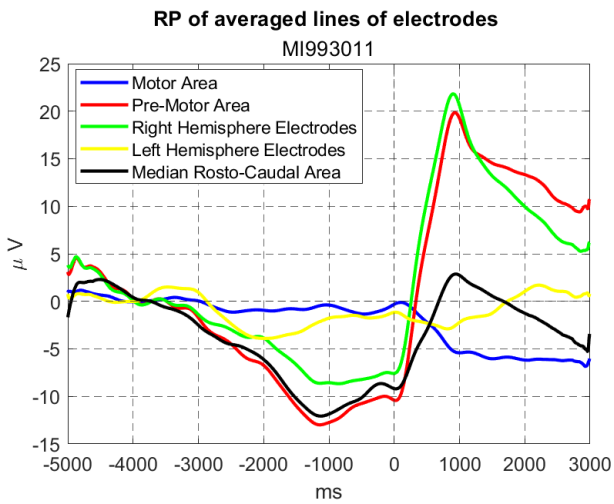

Figure 4.51: Averaged lines of the scalp after the application of SISF.

4.6.2 Comparison between old and updated High-Pass SF

For what has been proposed in previous sections, in general the updated versions contribute to slightly improve the spatial filters. The best choices appear to be the SISF because it assures:

1. High localization on the topographies
2. The highest SNR for the pre-motor, median rosto-caudal and right areas
3. Good shape of $C3, C4, Fc3, Fc4$ with few oscillations and an accentuated negative/positive slope between the phase of intention and the phase of when the movement is executed, in comparison with the unfiltered signal.
4. Shortest computational time for the filtering process, since the weight matrices G and H are the same if the helmet does not change among patients.

The drawbacks are:

1. Identification of the LRP only referred to $Fc3 - Fc4$ and not $C3 - C4$.
2. Lower activation of the left line in comparison with the right one.

As additional information, it provides the amplification factor c_{rms} for each channel. Nevertheless, it often tends to amplify more signal registered from electrodes placed at the edge of the montage, therefore those channels are less reliable in terms of activation. Concerning the other filters, SLSF seems to be a valid candidate to use in alternative or together with SISF, in order to compare the results. SLSF ensures:

1. High localization topographies, involving the nearest eight neighbouring channels. Eight neighbours allow to enlarge the range of spatial frequencies detectable.
2. A slight improvement of the SNR related to pre-motor and median rosto-caudal areas.
3. Better visualization of the averaged lines, underlying the greater activation of the left hemisphere with respect to the right hemisphere.
4. Quite good enhanced slope for $C3, C4, Fc3, Fc4$.

Unfortunately, it does not valorise the lateralization neither of $C3 - C4$, nor $Fc3 - Fc4$ and it requires more computational time than the SISF to elaborate the output filtered signal. The CARSF and LLSF have been excluded because their topographies are less detailed, the channels show a lot of oscillations and a smaller

slope, their SNR are not among the best. Since CARSF always consider all the electrodes of the EEG-cap, it present the largest support in terms of filtering range. As a consequence, it does not filter the high spatial frequencies selectively, but it maintains a mix of middle and low spatial frequencies. Therefore, it is not suitable to extract high spatial components. The LLSF with four electrodes did not provide detailed topographies, but enlarging the neighbouring channels from four to eight, it tends to filter middle-low spatial frequencies, as the CARSF. Consequently, these two are less selective than SISF and SLSF. Therefore, for successive studies, they have been discarded.
Another discussion should be conducted about the SNR. Generally, after using the spatial filters, an improvement of the SNR should be detected. Nevertheless, spatial DC noise may present various correlations in different directions. We have reduced the spatial period of the inter-electrode distances in one dimension, neglecting the other two. This is obviously a simplification. Noise can be linearly or not linearly correlated to one or more directions or uncorrelated, depending on the magnitude of sensors and both environmental and brain noise. It has been demonstrated from L.A. Bradshaw and J.P.Wikswo [31] that, filters like SLSF, LLSF, CARSF manages to remove linearly correlated noise to directions tangential to the surface of the scalp. On the other hand, non linearly correlated noise tends to remain in the output, but it can be extracted and further filtered away. The worst scenario is when noise is uncorrelated to some tangential directions [31]. In this case, those filters may amplify noise as well, leading to very low SNR values. Only if the starting unfiltered raw signal presents a very high SNR, it is possible to measure an acceptable SNR in the output filtered signal. This condition is hard to reach and these aspects may explain why, by using spatial filters with the current dataset, SNR does not improve for all the averaged lines. Implementing the filters at the hardware level may lead to slightly improved SNR, but this solution does not eliminate the spatial correlation of noise.
Other results have been obtained by using a seven electrodes EEG cap, analyzing the dataset "MS593051-OBE12-B18C-UNF-VOL18-RFOF-EMG1-E2-L0", belonging to the 2015-2018 protocol.

4.7 Results of best High-Pass SF on healthy subjects

Before viewing the results, a brief introduction is provided in order to clarify the criteria took into consideration for choosing the dataset that have been spatially filtered. In the section treating the voluntary task has been used an EEG signal recorded from a montage characterized by only seven electrodes, so that it was possible to test the updated spatial filters. As far as the other sections are concerned,

semi-voluntary and involuntary data have been chosen by their quality, which has been evaluated by considering SNR values of channels, the shape of the RPs and the noise on the baseline. Table 4.2 summarizes their qualitative classification.

Table 4.2: Qualitative classification of dataset analyzed. The parameters considered are shape, baseline and SNR. From positive to negative, the markers are "Good", "Discrete", "Bad". The final quality can be "High" for very good dataset, "Mediocre" for nice dataset that do not show high quality in all the parameters and "Bad", for poor signals.

Dataset	Task	Shape	Baseline	SNR	Quality
AL	Vol.	Good	Discrete	Discrete	High
GO	Semi-vol.	Discrete	Good	Discrete	Mediocre
GO	Invol.	Good	Discrete	Discrete	High
LB	Invol.	Discrete	Discrete	Bad	Mediocre
MI	Vol.	Good	Good	Good	High
MS	Vol.	Good	Good	Good	High
TC	Vol.	Discrete	Bad	Discrete	Mediocre
TC	Semi-vol.	Good	Bad	Bad	Low

4.7.1 Voluntary task with smaller EEG montage

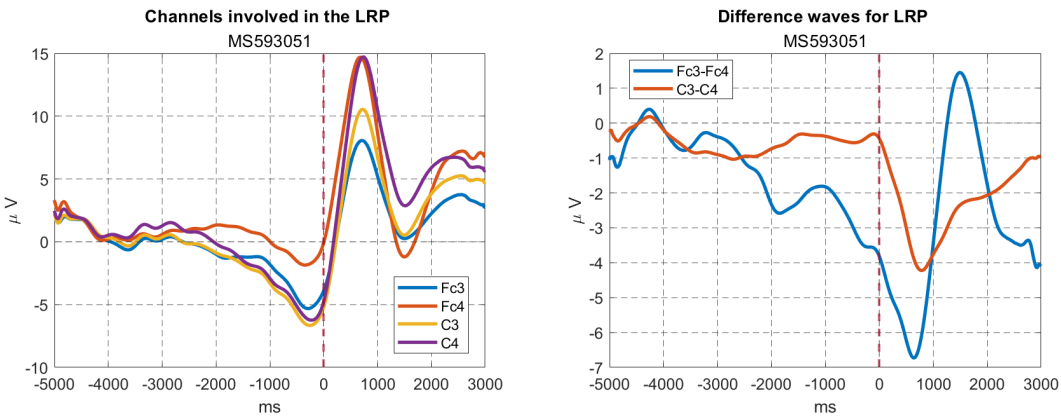

Figure 4.52: (Left) Pre-motor and motor channels, (right) pairs of subtraction between symmetrical electrodes in right and left hemisphere of the brain of the unfiltered signal.

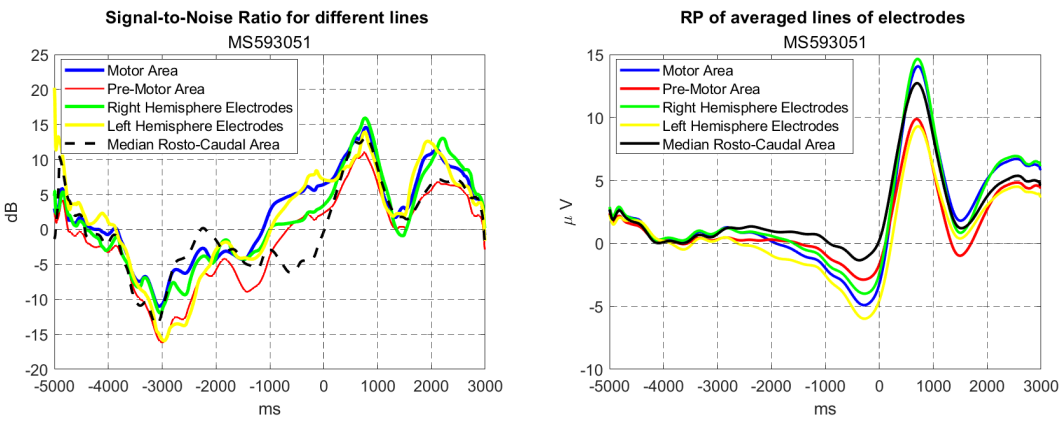

Figure 4.53: (Left) Signal-to-noise ratio in time of averaged principal lines, (right) averaged lines in time of the unfiltered signal.

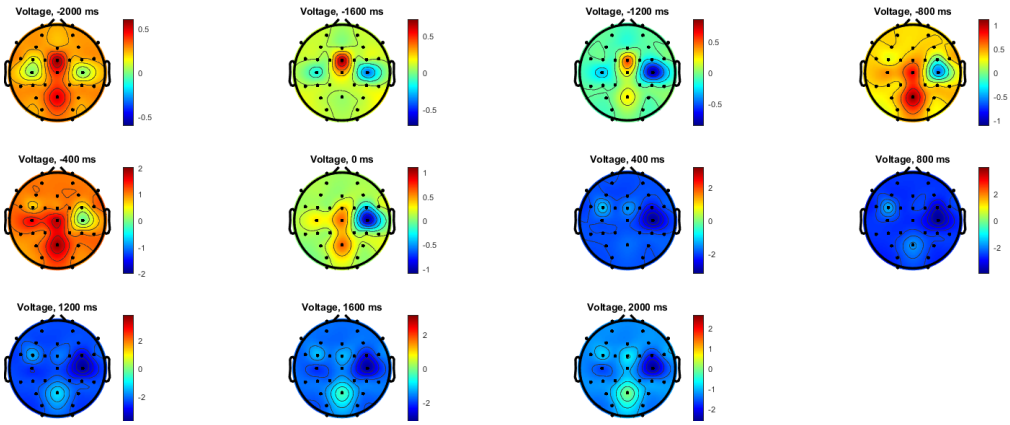

Figure 4.54: Topographies at various time instants of the unfiltered signal.

- *SLSF:*
  In this case, from Figure 4.55, accentuated slopes can be distinguished for the channels and $Fc3$ appears to be more active than $Fc4$, both in the phase of the intention and during the execution of the muscular contraction. $C3$ is more active than $C4$, only during the execution of the movement and not before. From Figure 4.56 compared to Figure 4.53, the SNR is clearly increased, while as regards the averaged lines, the left line shows a greater negative peak in the phases of intention. In the phase of the movement, the left line does no longer exhibit a positive peak. On the whole, each line is more distinguishable from the others. In addition to that, from Figure 4.57, it can be appreciated the opposite polarities between the contralateral region of the brain where there is the activation of the intention and the ipsilateral region, which is the less active if the subject moves the right finger. This image is more detailed and clear in comparison with the previous one, retrieved with the standard filters found in literature.

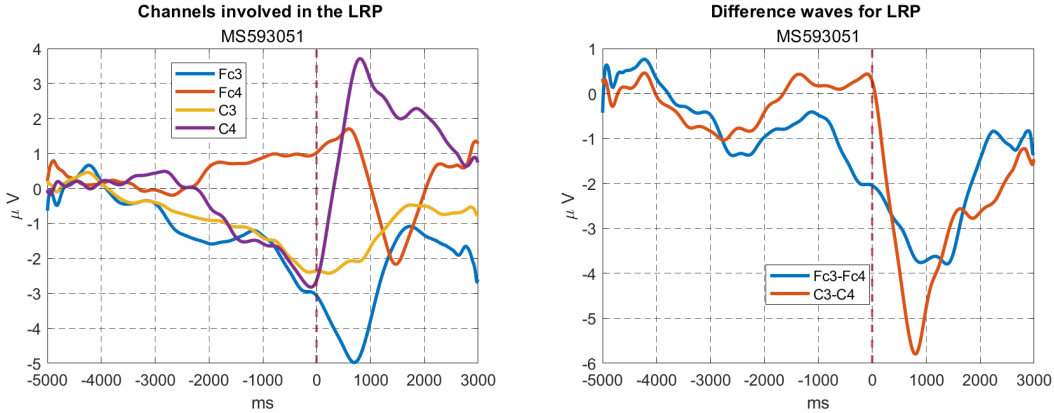

Figure 4.55: (Left) Pre-motor and motor channels, (right) pairs of subtraction between symmetrical electrodes in right and left hemisphere of the brain.

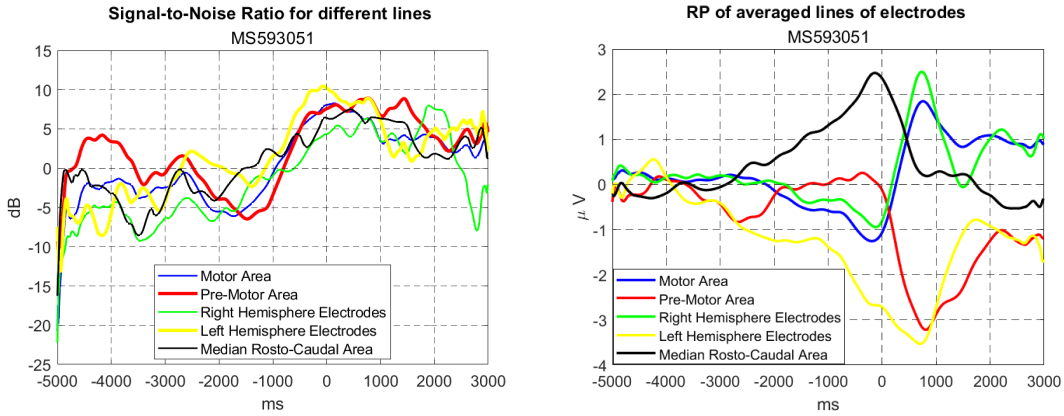

Figure 4.56: (Left) Signal-to-noise ratio in time of averaged principal lines, (right) averaged lines in time after the application of the SLSF.

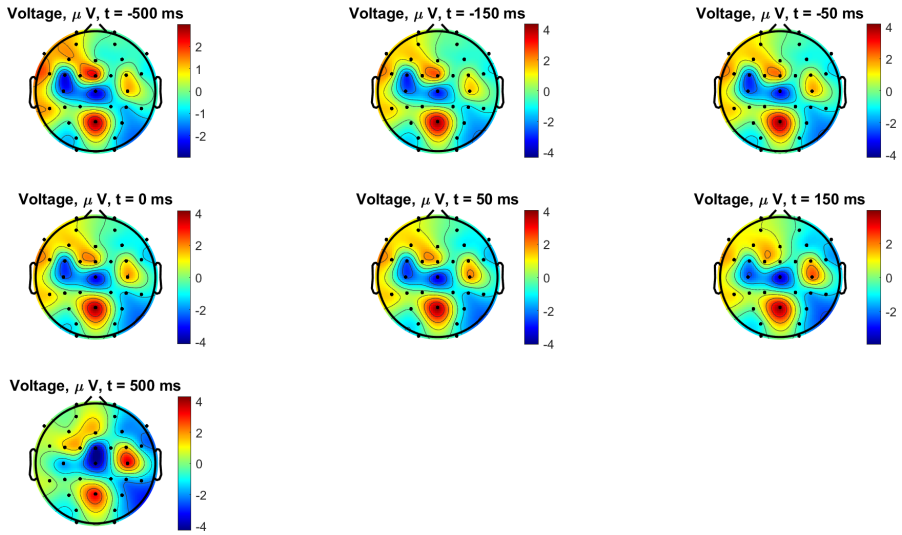

Figure 4.57: Topographies at various time instants.

- *SISF:*
  Even in this case, slopes are more accentuated, which is a good aspect for the machine learning algorithm. A small negative trend is visible in Figure 4.59 during the phase of intention and during the execution of the movement, representing the dominance of $C3$ over $C4$, while $Fc3$ only dominates during the phase of the muscular contraction. In Figure 4.60, motor and left areas have good SNR, indeed they are the lines which are more active. Furthermore, in Figure 4.61, very detailed topographies can be admired, with the opposite polarities for the contralateral and ipsilateral regions of the brain related to the motion of the right finger.

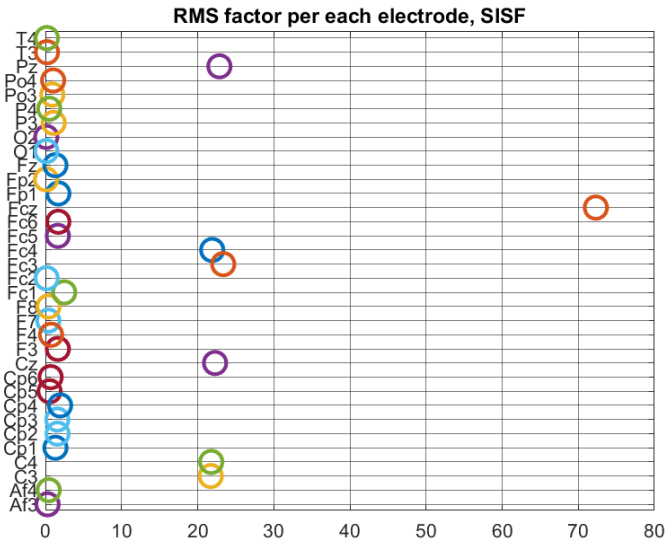

Figure 4.58: c_{rms} coefficients used to normalized the voltage waveforms which are the outputs of the SISF.

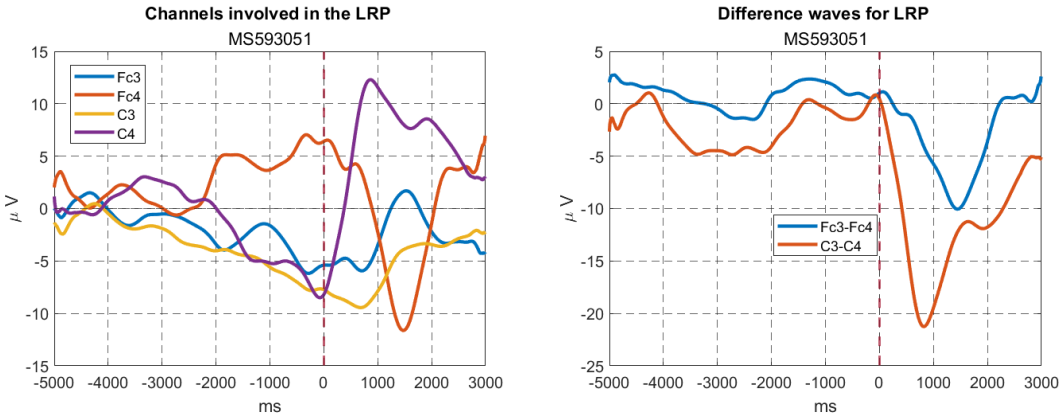

Figure 4.59: (Left) Pre-motor and motor channels, (right) pairs of subtraction between symmetrical electrodes in right and left hemisphere of the brain after the application of the SISF.

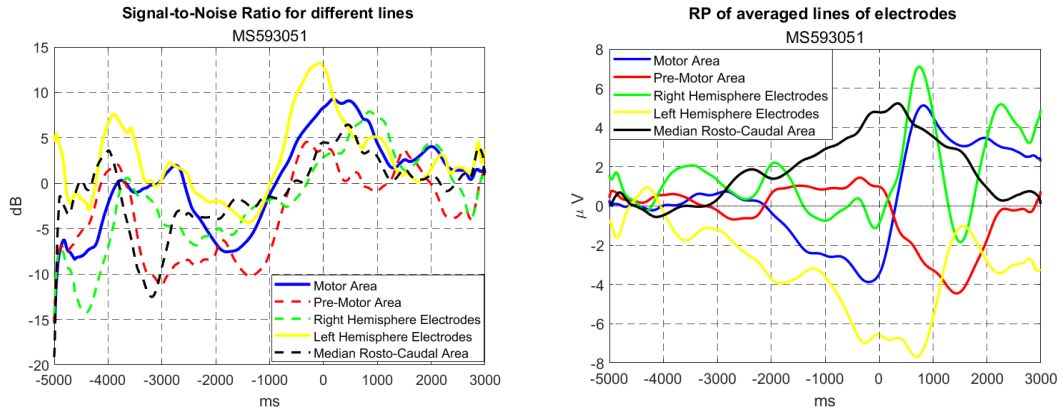

Figure 4.60: (Left) Signal-to-noise ratio in time of averaged principal lines, (right) averaged lines in time after the application of the SISF.

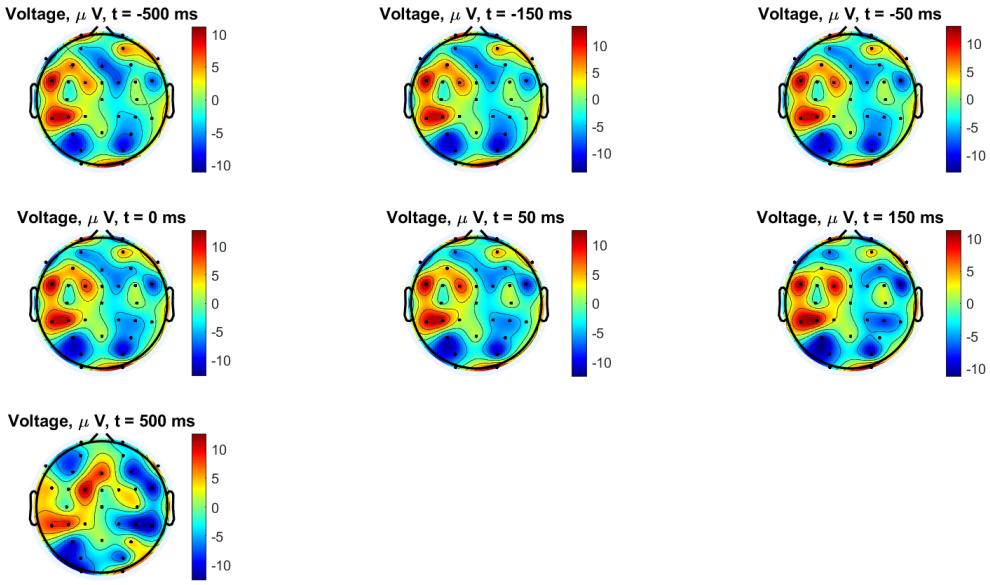

Figure 4.61: Topographies at various time instants after the application of the SISF.

4.7.2 Semi-voluntary task

Semi-voluntary and involuntary experiments present RPs where the peak of the intention is more attenuated because the brain has less time to prepare itself to accomplish the motor tasks. For that reason, it is more important in these cases to extracting high spatial information, emphasizing the peak of intention.

- *Raw signal:*

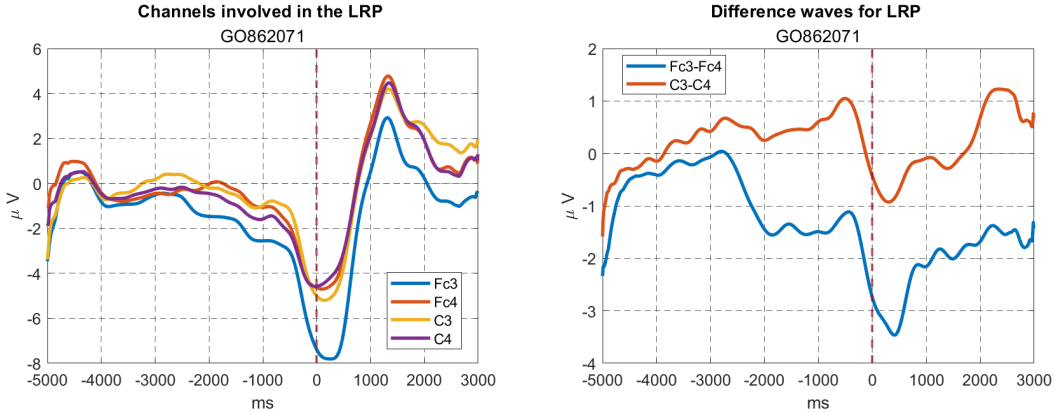

Figure 4.62: (Left) Pre-motor and motor channels, (right) pairs of subtraction between symmetrical electrodes in right and left hemisphere of the brain of the unfiltered signal.

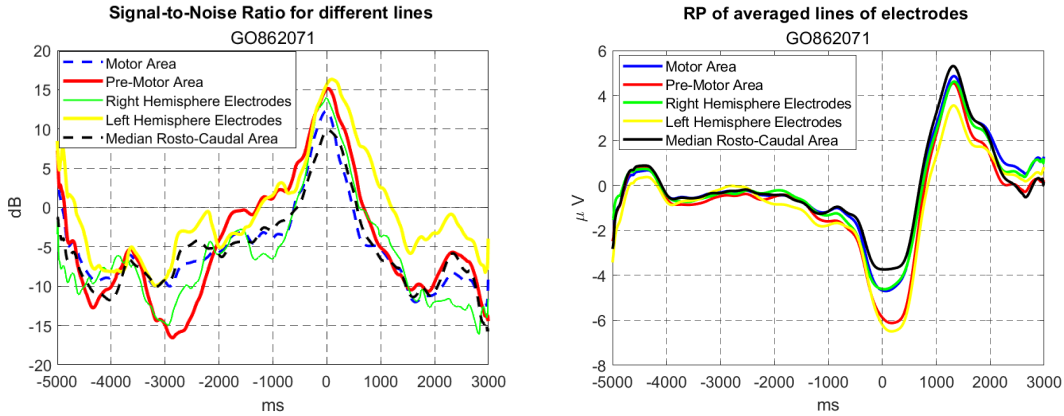

Figure 4.63: (Left) Signal-to-noise ratio in time of averaged principal lines, (right) averaged lines in time of the unfiltered signal.

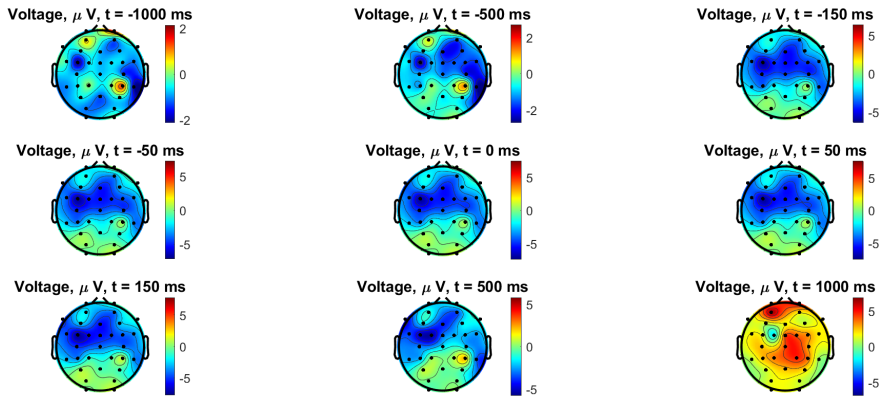

Figure 4.64: Topographies at various time instants of the unfiltered signal.

- *SLSF:*
  After the employment of the filter, it is more clear in Figure 4.65 the distinction between the various levels of activation of the channels, each of which presents an accentuated slope from the initial baseline to the negative peak of the intention. $Fc3$ has higher amplitudes than $Fc4$, while the opposite happens for $C3, C4$. The SNR is not optimal, while the right line shows up the greatest amplitudes around 0 ms and after, highlighting the movement of the right finger in Figure 4.66. From Figure 4.67, particular activity in correspondence of the left hemisphere where $Fc3, C3$ are placed is emphasized.

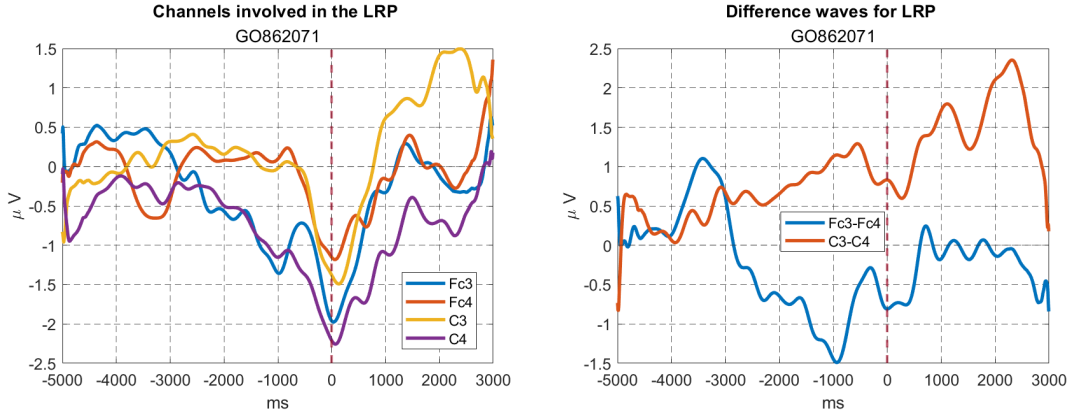

Figure 4.65: (Left) Pre-motor and motor channels, (right) pairs of subtraction between symmetrical electrodes in right and left hemisphere of the brain.

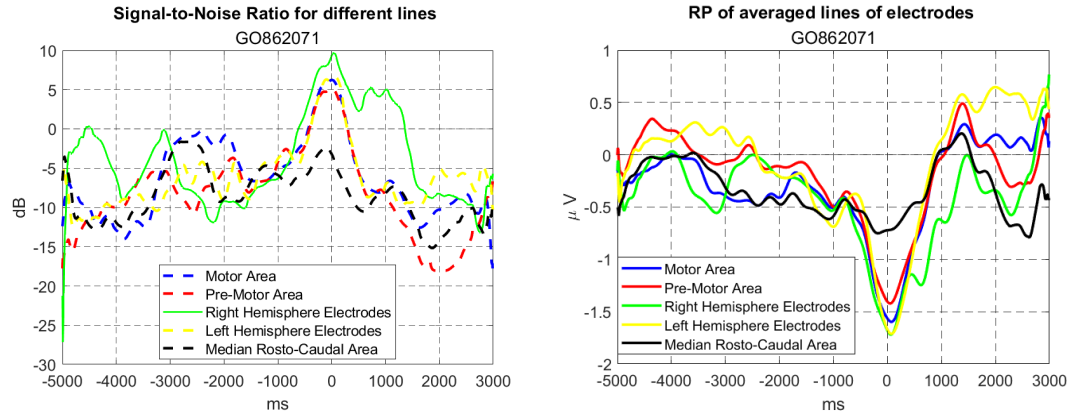

Figure 4.66: (Left) Signal-to-noise ratio in time of averaged principal lines, (right) averaged lines in time after the application of the SLSF.

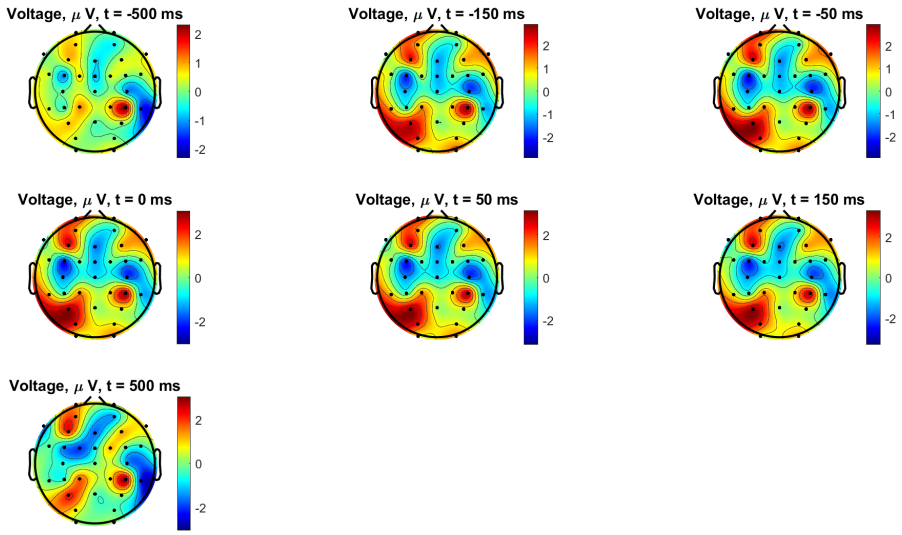

Figure 4.67: Topographies at various time instants after the application of SLSF.

- *SISF:*
  From Figure 4.68, a greater LRP is obtained for $Fc3 - Fc4$. The slopes are not so emphasized for $C3, Fc4$. In Figure 4.69, the pre-motor line dominates during the phase of intention, followed by the median rosto-caudal and the left areas. In the phase of the execution of the movement, the motor and the left areas dominate, as it is expected. Finally, the spherical filter highlights the activity of $C3, Fc3$ better in the topographies in Figure 4.71.

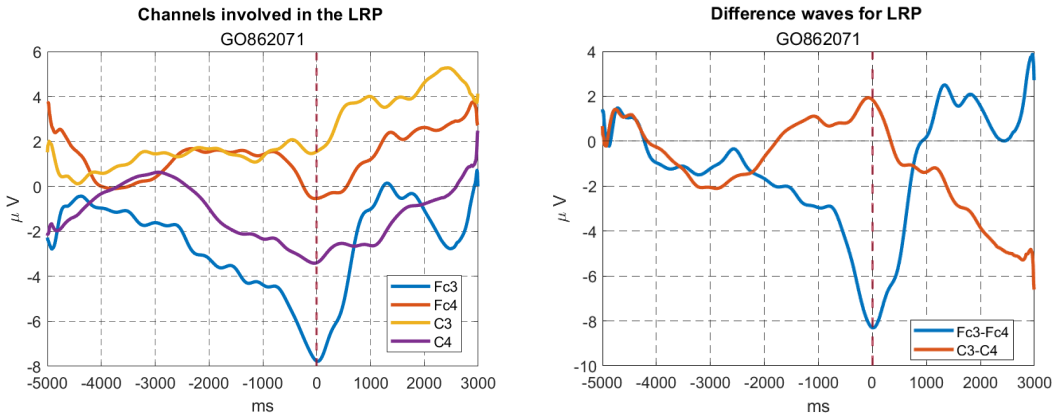

Figure 4.68: (Left) Pre-motor and motor channels, (right) pairs of subtraction between symmetrical electrodes in right and left hemisphere of the brain.

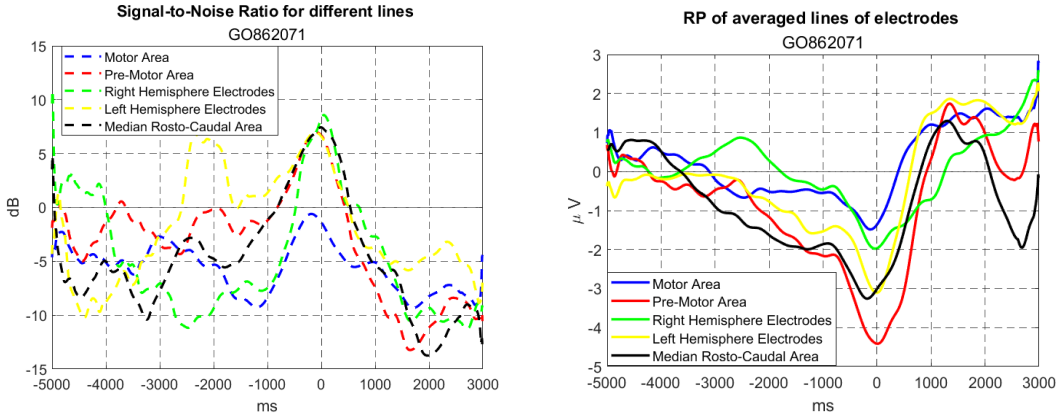

Figure 4.69: (Left) Signal-to-noise ratio in time of averaged principal lines, (right) averaged lines in time after the application of the SLSF.

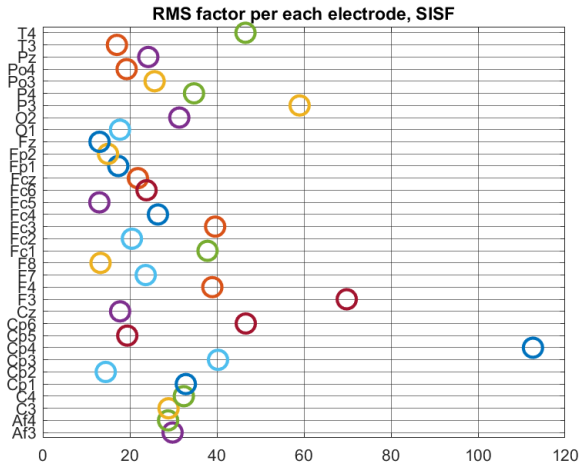

Figure 4.70: c_{rms} estimated for GO semi-voluntary dataset.

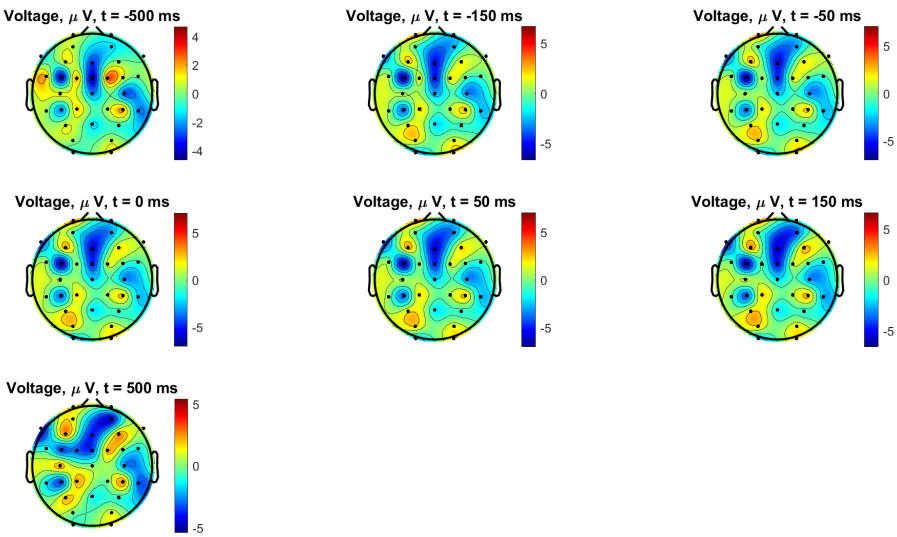

Figure 4.71: Topographies at various time instants.

4.7.3 Involuntary task

Besides the smaller peak to emphasize, another issue with involuntary tasks is the very low SNR.

- *Raw signal:*

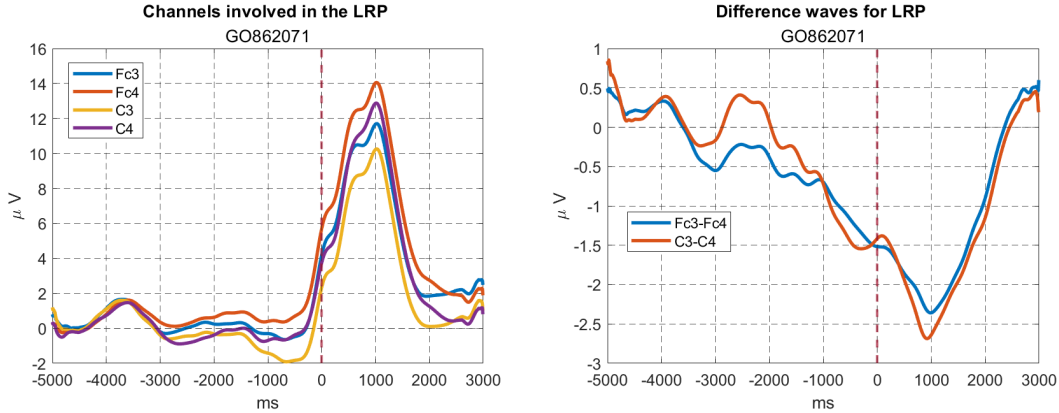

Figure 4.72: (Left) Pre-motor and motor channels, (right) pairs of subtraction between symmetrical electrodes in right and left hemisphere of the brain of the unfiltered signal.

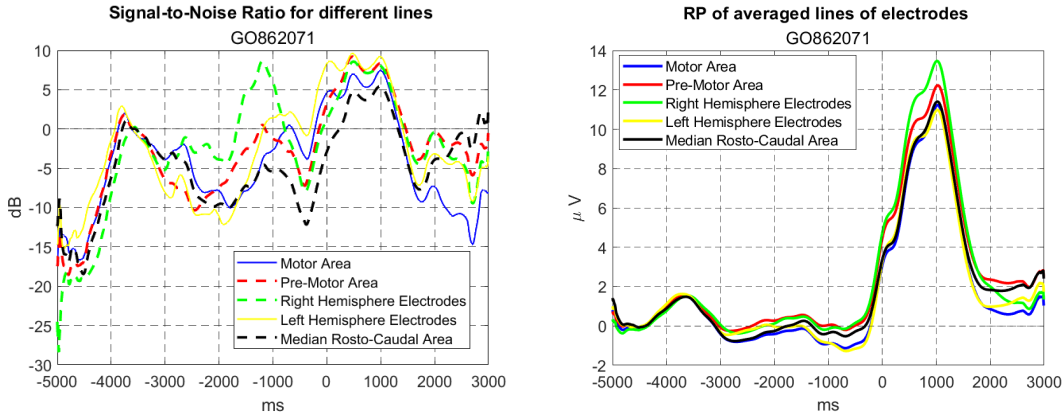

Figure 4.73: (Left) Signal-to-noise ratio in time of averaged principal lines, (right) averaged lines in time of the unfiltered signal.

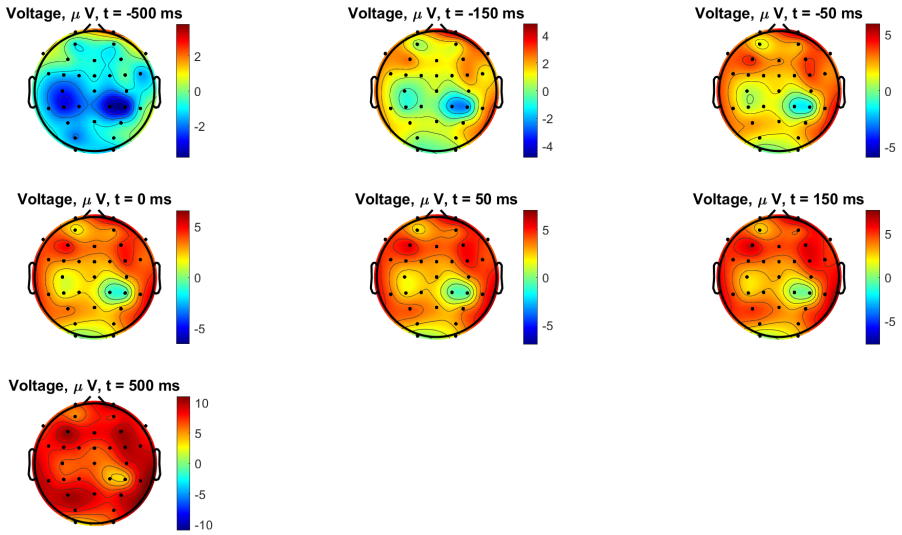

Figure 4.74: Topographies at various time instants of the unfiltered signal.

- *SLSF:*
  In Figure 4.75, it can be seen the major activation of $C3$ with respect to $C4$, aspect that is not valid for $Fc3, Fc4$. All channels show a different and distinct slope. In Figure 4.76, the SNR is improved for the pre-motor area, but in terms of averaged lines, the right area is the more emphasized, even though it does not show an optimal shape being a RP. In Figure 4.77, a nice localization is showed, even though same regions in the right hemisphere appear more active.

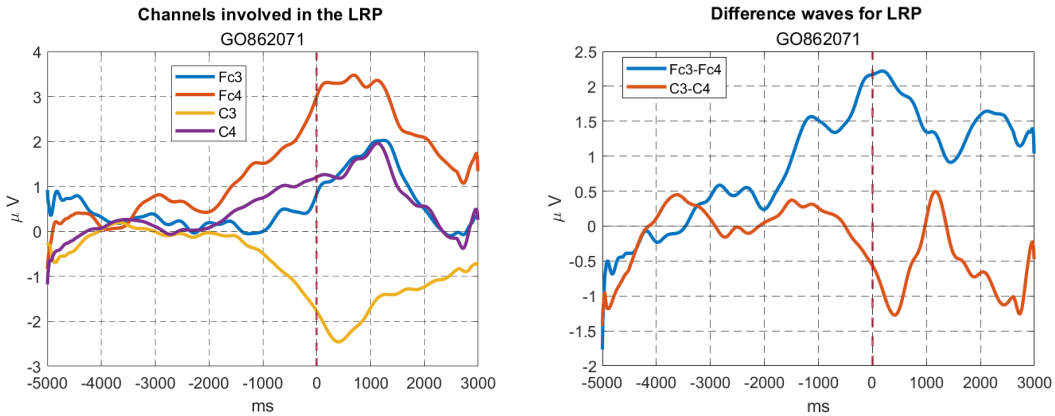

Figure 4.75: (Left) Pre-motor and motor channels, (right) pairs of subtraction between symmetrical electrodes in right and left hemisphere of the brain after the application of SLSF.

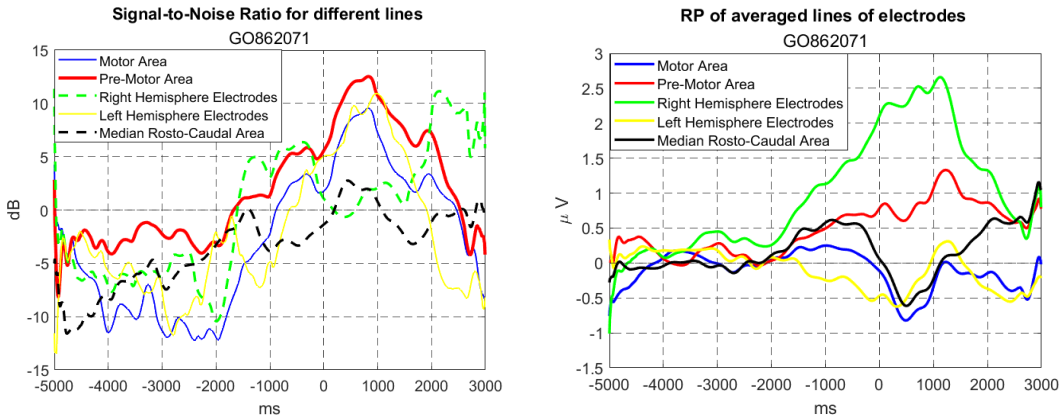

Figure 4.76: (Left) Signal-to-noise ratio in time of averaged principal lines, (right) averaged lines in time after the application of the SLSF.

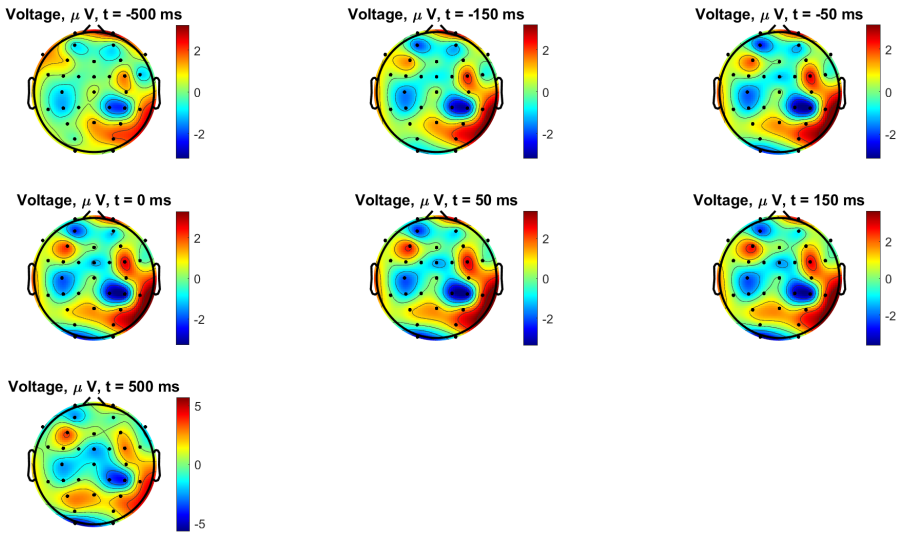

Figure 4.77: Topographies at various time instants after the application of SLSF.

- *SISF:*
  Looking at Figure 4.78, both $Fc3, C3$ are more active than the symmetrical $Fc4, C4$, but only after 0 ms. In Figure 4.79, the SNR for the left area is improved and it shows a great voltage dynamic. The topographies reported in Figure 4.81 highlights a great lateralization of the readiness potential in the left hemisphere for both its early and late components.

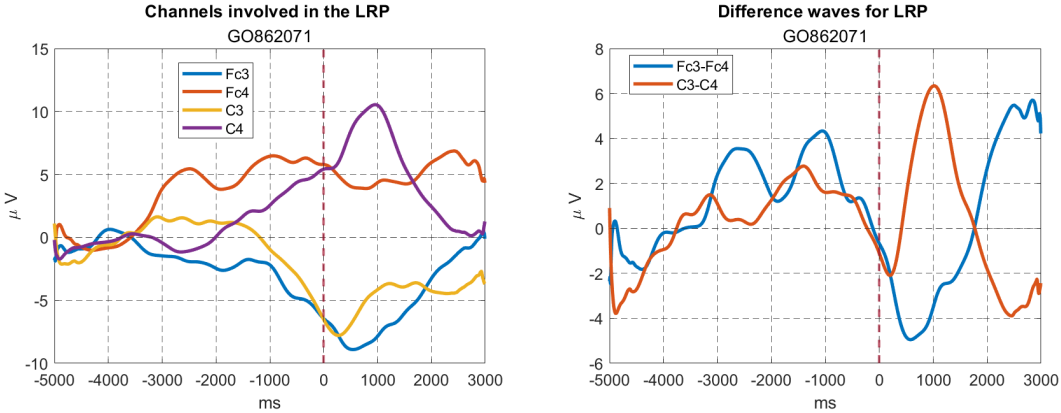

Figure 4.78: (Left) Pre-motor and motor channels, (right) pairs of subtraction between symmetrical electrodes in right and left hemisphere of the brain.

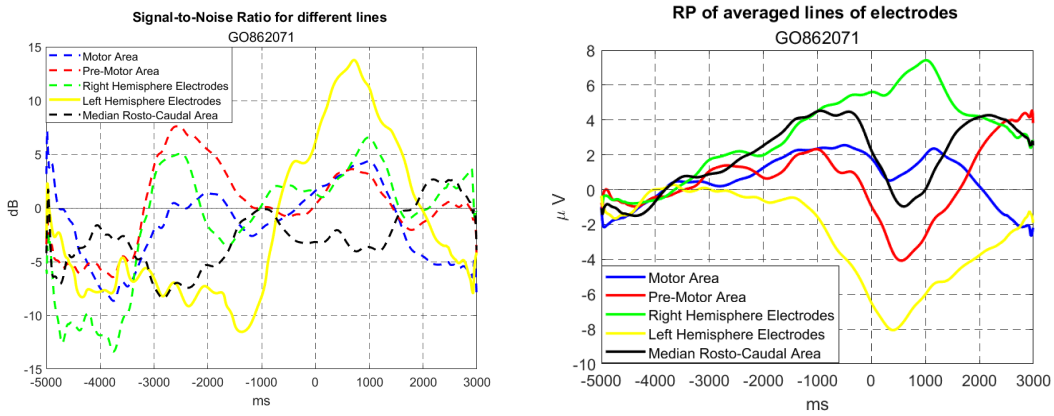

Figure 4.79: (Left) Signal-to-noise ratio in time of averaged principal lines, (right) averaged lines in time after the application of the SISF.

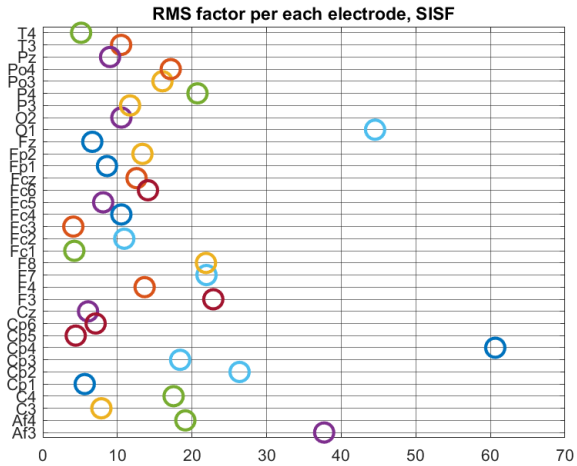

Figure 4.80: c_{rms} estimated for GO involuntary dataset.

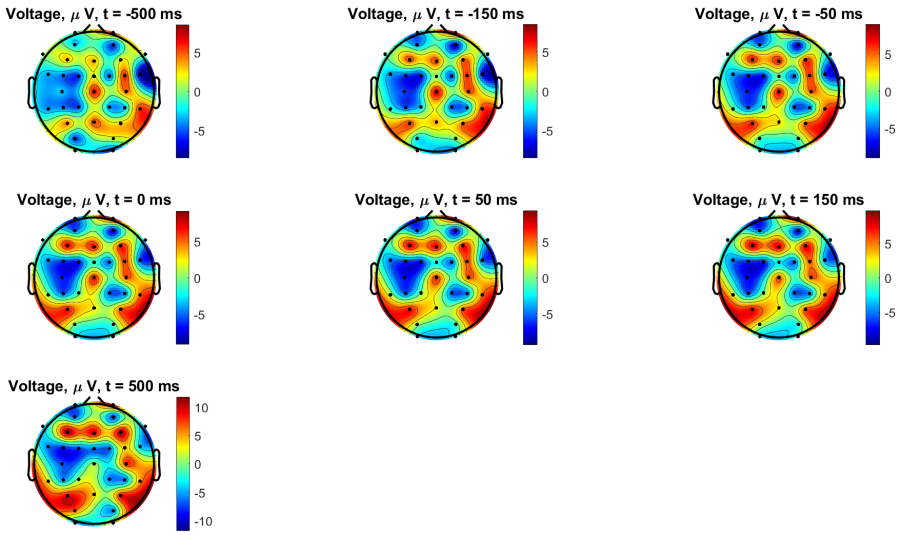

Figure 4.81: Topographies at various time instants after the application of SISF.

4.7.4 Discussion of results

From the amount of information analyzed in the previous sections, it is possible to claim that high spatial filters are necessary in the pre-processing chain in order to visualize through topographies the voltage distribution without volume conductance to distinguish the different regions of activation. In addition to that, they contribute to substantially modify the slope and the amplitude of single channels, making them more distinguishable between them, even though they sometime introduce additional oscillations in the signals [22]. Unfortunately, they strongly depend on the quality of the initial raw signal and they do not often succeed in improving the SNR of all the averaged lines of the scalp. Sometimes, from a mediocre or bad dataset, they manage to emphasize the major activity of $C3, Fc3$ in the phase of intention, but sometimes they fail, emphasizing only $Fc3$ or $C3$ and the correspondent LRP as a consequence. In the next section, the SLSF will be used in its low spatial version, in order to improve the SNR. The low spatially filtered signal has been obtained as:

$$\mathrm{RP}_L = \mathrm{RP}_{raw} - \mathrm{RP}_H \tag{4.24}$$

where they respectively represent the low spatially filtered, the unfiltered and the high spatially filtered signals.

4.8 Results of Low-Pass SF on healthy subjects

Since with high pass spatial filters, globally the SNR did not improve so much for all the channels and the lines on the scalp, in this section, the updated version of SLSF has been used as low spatial filter to improve the SNR of the dataset.

4.8.1 Voluntary task

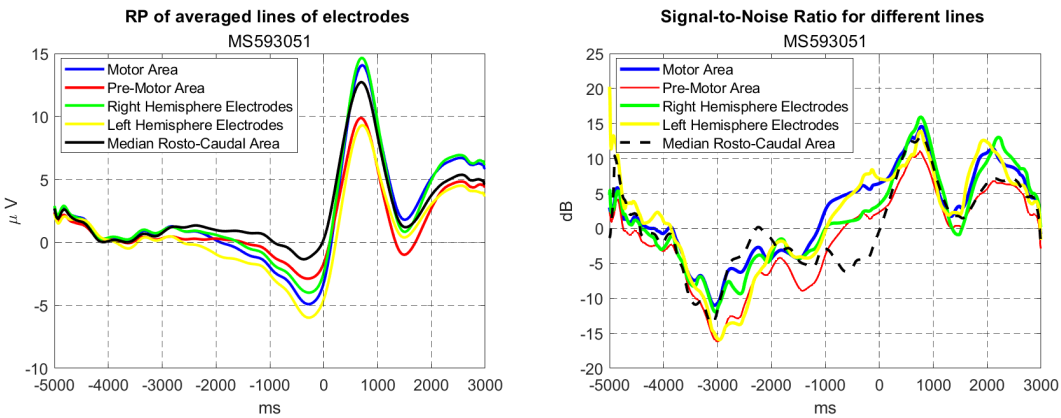

Figure 4.82: (Left) RPs of averaged lines, (right) SNR of averaged lines of the raw signal.

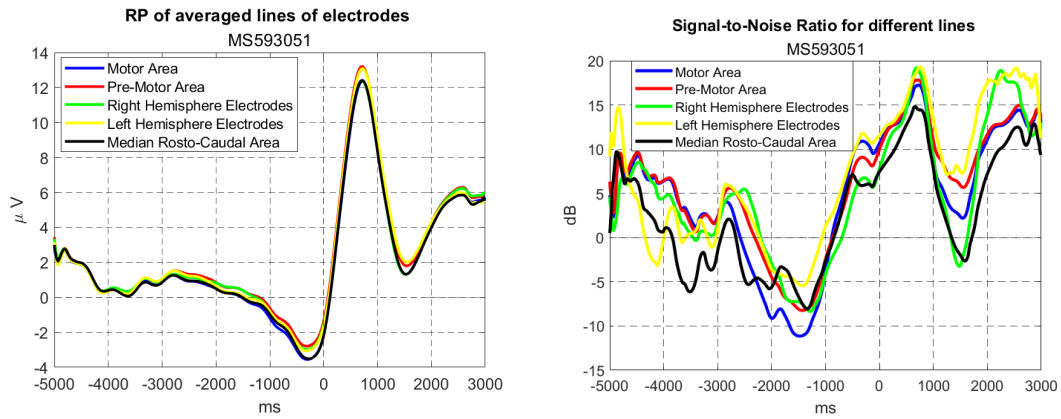

Figure 4.83: (Left) RPs of averaged lines, (right) SNR of averaged lines of the low-pass filtered signal.

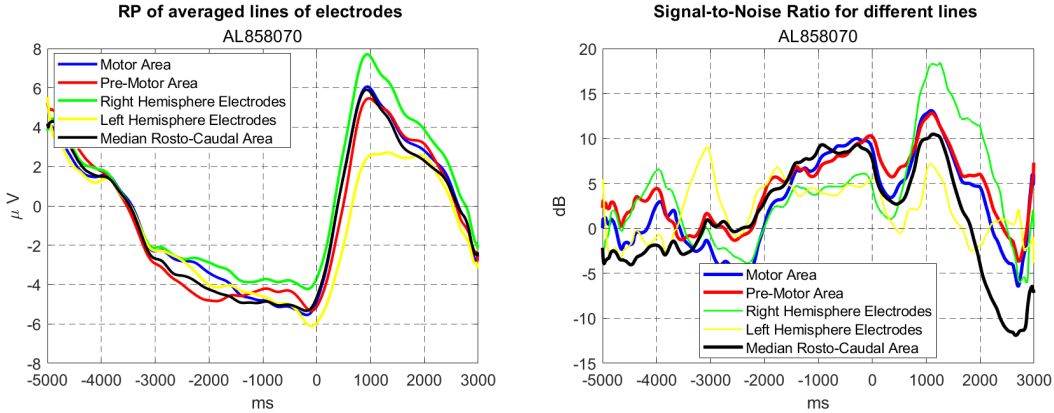

Figure 4.84: (Left) RPs of averaged lines, (right) SNR of averaged lines of the raw signal.

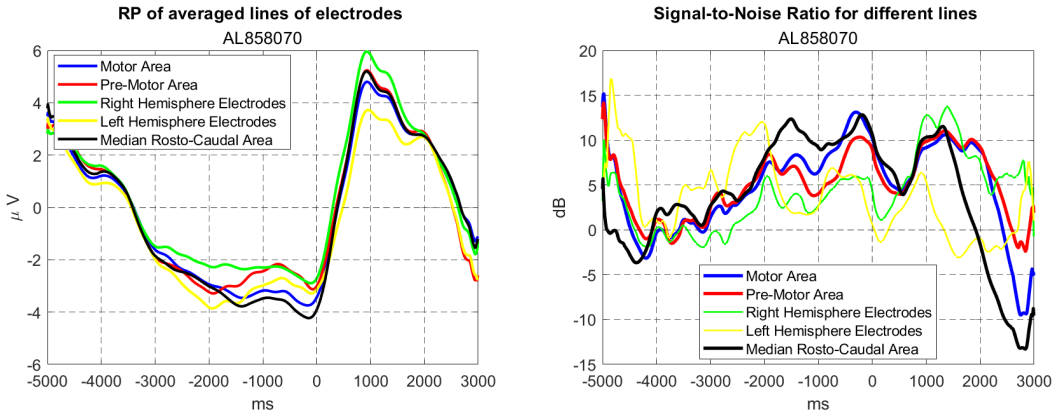

Figure 4.85: (Left) RPs of averaged lines, (right) SNR of averaged lines of the low-pass filtered signal.

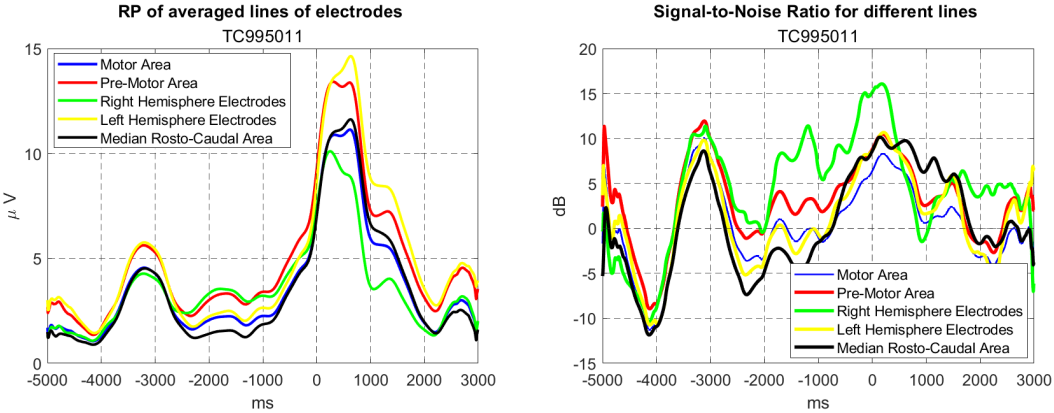

Figure 4.86: (Left) RPs of averaged lines, (right) SNR of averaged lines of the raw signal.

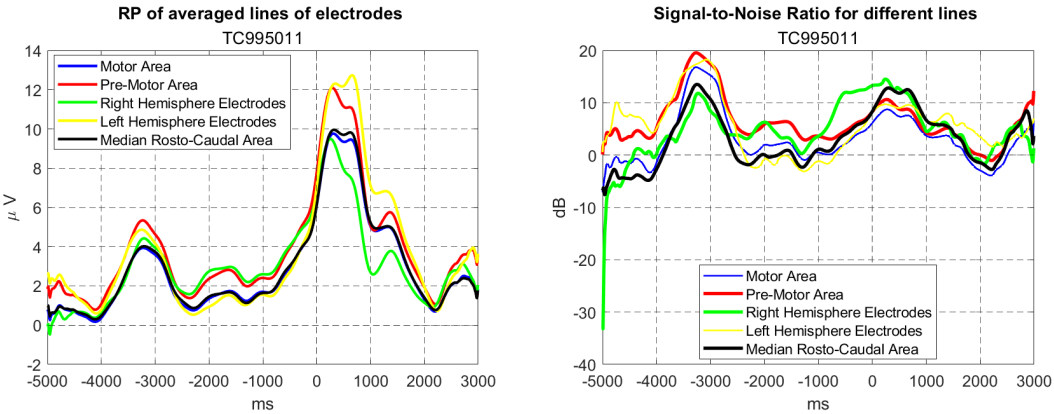

Figure 4.87: (Left) RPs of averaged lines, (right) SNR of averaged lines of the low-pass filtered signal.

4.8.2 Semi-voluntary task

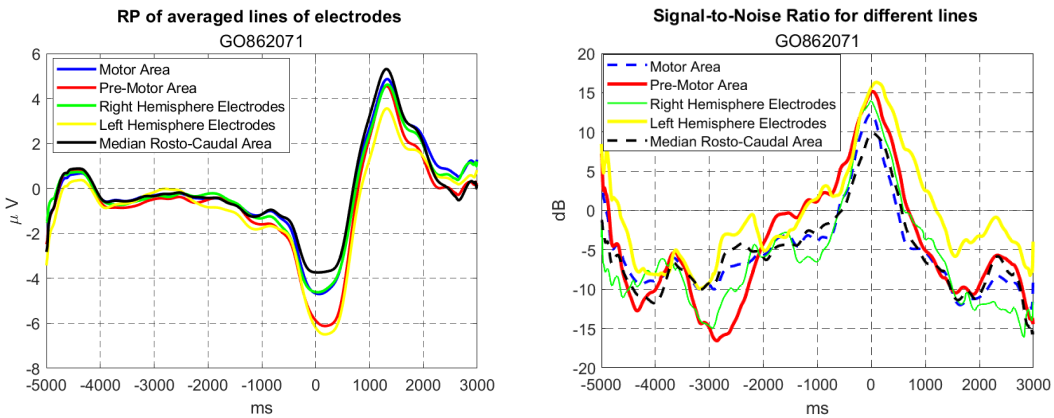

Figure 4.88: (Left) RPs of averaged lines, (right) SNR of averaged lines of the raw signal.

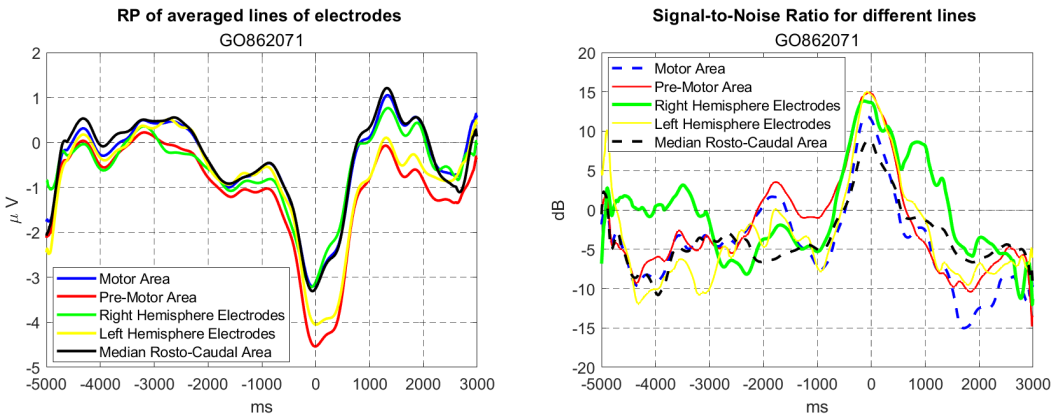

Figure 4.89: (Left) RPs of averaged lines, (right) SNR of averaged lines of the low-pass filtered signal.

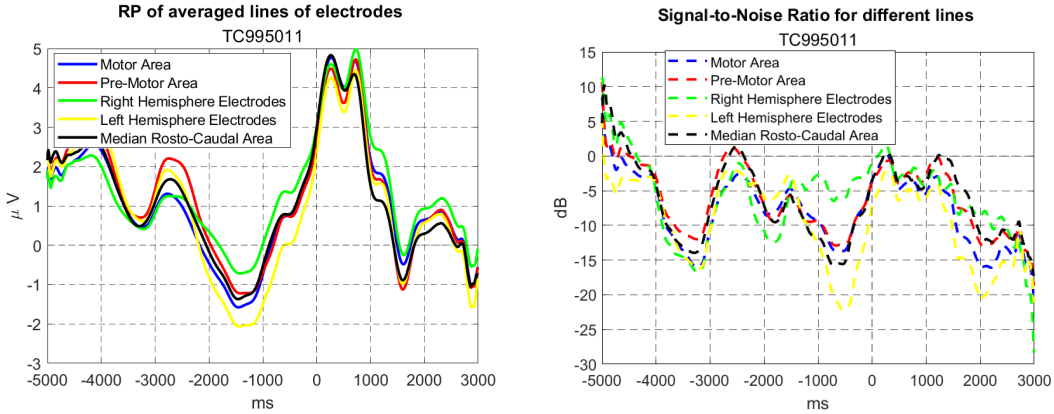

Figure 4.90: (Left) RPs of averaged lines, (right) SNR of averaged lines of the raw signal.

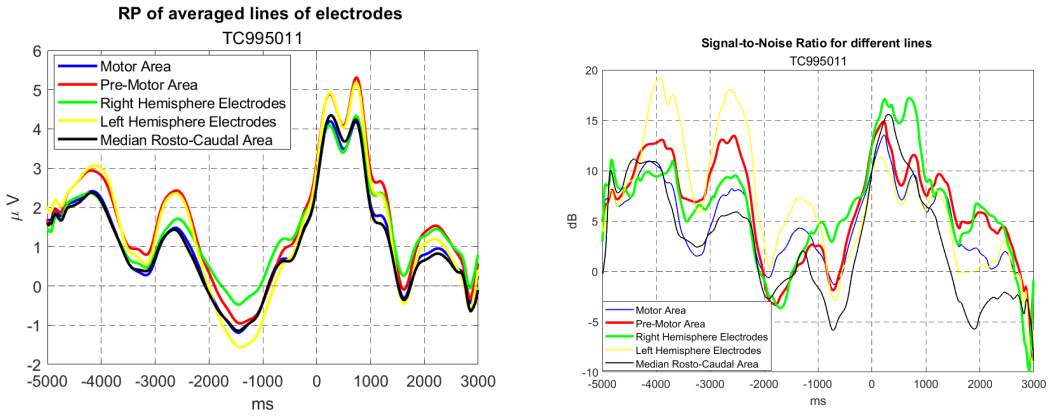

Figure 4.91: (Left) RPs of averaged lines, (right) SNR of averaged lines of the low-pass filtered signal.

4.8.3 Involuntary task

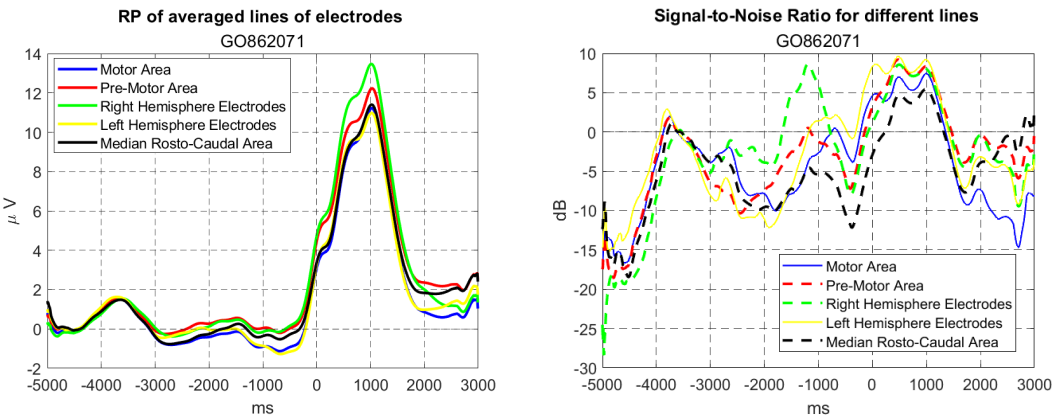

Figure 4.92: (Left) RPs of averaged lines, (right) SNR of averaged lines of the raw signal.

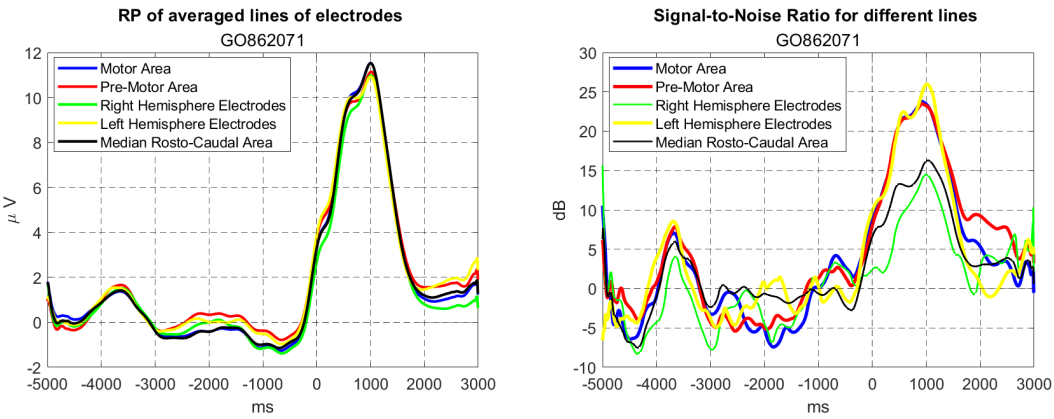

Figure 4.93: (Left) RPs of averaged lines, (right) SNR of averaged lines of the low-pass filtered signal

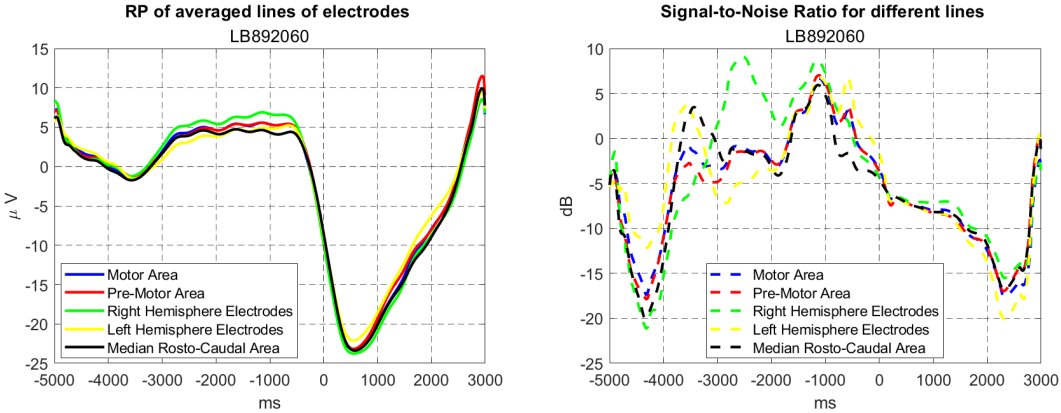

Figure 4.94: (Left) RPs of averaged lines, (right) SNR of averaged lines of the raw signal.

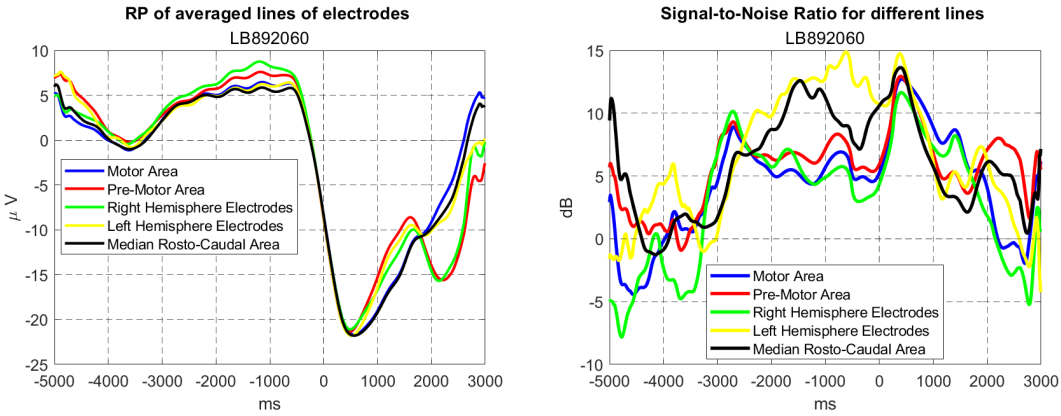

Figure 4.95: (Left) RPs of averaged lines, (right) SNR of averaged lines of the low-pass filtered signal

4.8.4 Discussion of results

It can be noticed from the previous results that inserting the updated SLSF in the pre-processing chain as low spatial filter can improve the signal-to-noise ratio of the EEG signal by removing the noise, increasing the quality of mediocre or bad dataset, as well. Sometimes, it also helps providing better shapes for the final RPs to send to the machine learning algorithm. The spherical spatial filter does not provide the same improvements of the SLSF as low spatial filter, for that reason it has been discarded for this application.
An another advantage of this two filters is the low energy encapsulated in the double product between the high spatially filtered and the low spatially filtered RPs. Indeed, from an energy point of view, the energy of the raw RP can be approximated as:

$$\mathrm{RP}_{raw} = \mathrm{RP}_H + \mathrm{RP}_L \tag{4.25}$$

$$E_{raw,i} = |\mathrm{RP}_{raw,i}|^2 = |\mathrm{RP}_{H,i}^2 + \mathrm{RP}_{L,i}^2 + 2 \cdot \mathrm{RP}_H \mathrm{RP}_L| \tag{4.26}$$

where i indicates each channel. If the contribute $2 \cdot \mathrm{RP}_H \mathrm{RP}_L \approx 0$, then the spatial filters are very selective, because all the energy has been divided between the high and the low spatial filtered signals. In Figure 4.96 are reported the $\sqrt{2 \cdot \mathrm{RP}_H \mathrm{RP}_L}$ for some principal channels: since the RP_H and RP_L seen before are in the range of μV in terms of amplitude and the square root of the double product is of the order of pV, the two spatial filters show a great selectivity, since only a negligible energy is lost in the filtering process.

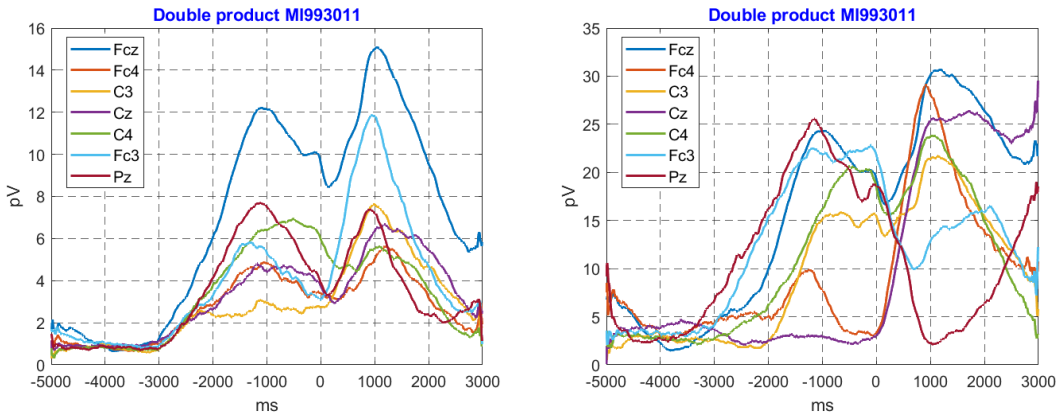

Figure 4.96: Square root of the double product estimated for the SLSF (left) and the SISF (right) from the MI dataset.

To conclude, spatial filtering demonstrated to be an essential block in the preprocessing chain of the BCI to study deeply the intention of healthy subjects and patients, because, thanks to high pass and low pass spatial filtering is possible to improve the RPs, their SNR, extract useful information, compare the different activity of channels to simplify the search of specific neural populations stimulated during motor tasks.

Chapter 5

Hemiplegic patients

In this chapter, results regarding signals recorded from hemiplegic patients are reported. In particular, the subjects manifest a damage in the right hemisphere that impedes to let them move the left hand. In subsection 5.2.1 and subsection 5.2.2 there are the results retrieved after the application of the spatial filters. In section 5.1 are explained the procedures followed to deal with hemiplegic dataset.

5.1 Issues in detection of ONSETs

Unfortunately, the automatic algorithm for the detection of the onset of the EMG signal in the plugin does not work efficiently with the dataset of hemiplegic patients. Consequently, it has been necessary to manually select the events from the raw EMG signal and discard some of them that showed potentially low quality. Since it is not trivial to stabilize which points pick to identify the onsets, for simplicity, the maximum peaks of each spike of the EMG signal has been considered, since the EMG exhibits a discrete clarity. This decision ensures the alignment of signals measured from the channels, even though the maximum peak of the intention is shifted leftwards, since the points picked up from the EMG do not correspond to the real onsets. The final RPs have been estimated by averaging the epochs that have been generated manually, fixing each peak of the EMG at 0 ms. Generally, the criteria employed to produce RP of hemiplegic takes into consideration:

- **Quality of EMG raw:** it must have distinctive peaks with small lateral voltage lobes and the events must be at a reciprocal distance greater than 1024 samples, which is the number of points to describe an epoch for the final RPs. These two conditions may be broken owing to noise that increases lateral lobes or due to the patient that perhaps executed two movements in a short time period causing an overlap of events or a too slow movement which is not registered as a single spike. In these last cases, events can be discarded.

- **Quality of final RPs**: the SNR is related to the number of trials which coincide with the number of events selected from the EMG signal through the following relationship:

$$\text{SNR} \propto \sqrt{\text{number of trials}} \tag{5.1}$$

  That means doubling the number of trials allows to increase SNR of 41%. But, this is valid even in the opposite case: by reducing the number of events of the 50%, the SNR decreases of the 30%. This means is easier to worsen the SNR rather than improving it [11]. For that reason, it is not possible to discard too much events, otherwise, the final RPs will be too noisy to detect the peaks of intention and of the motor movement.

In Figure 5.1 are reported the EMG raw signals for MC and DV datasets considered in the study. Too much smaller or closer peaks with respect the neighbouring ones have been neglected.

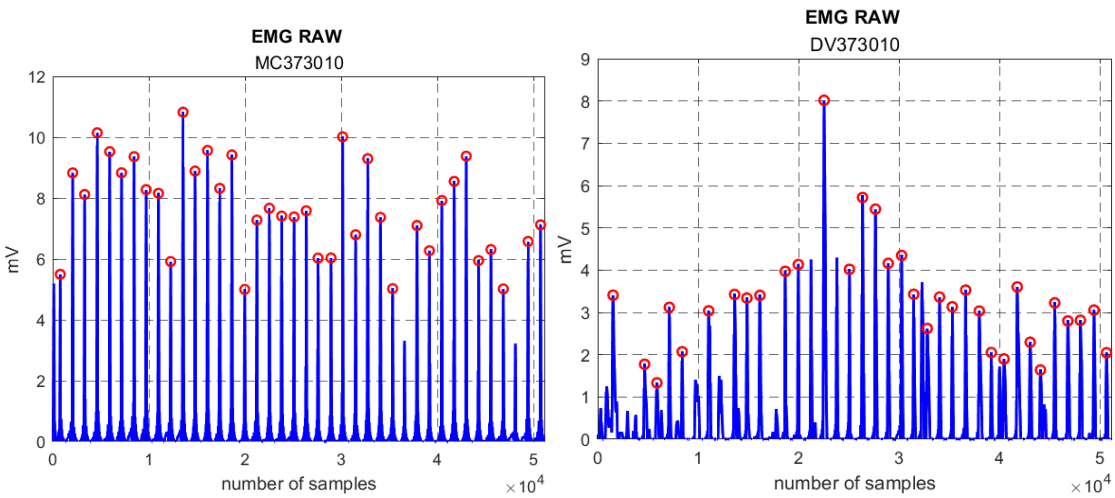

Figure 5.1: (Left) MC raw EMG, (right) DV raw EMG.

5.2 Hemiplegic results

The studied dataset belong to hemiplegic patients subjected to bimanual voluntary tasks. For the MC dataset, 38 events have been detected from the EMG raw signal and none of them has been discarded. On the contrary, for the DV dataset, the epochs number 6 and 8 shown in Figure 5.2 have been removed, since they presents broader peaks, ending up with 31 events. Even epoch number 7 should be removed because it presents a little broadness on the peak, but, remembering Equation 5.1, at the end it has been kept.

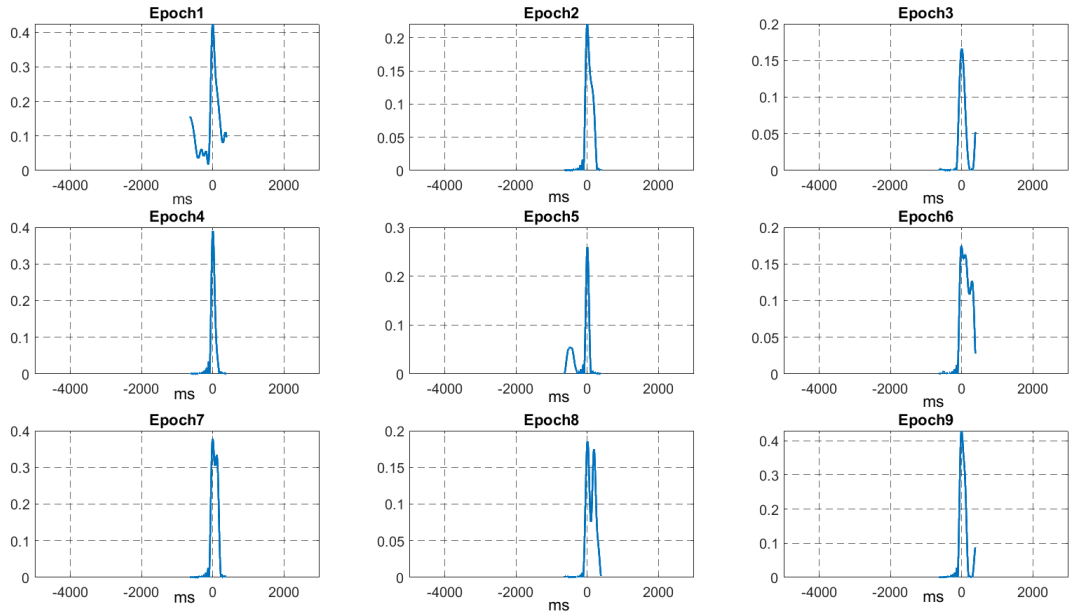

Figure 5.2: First nine peaks of the EMG raw of the DV dataset normalized with the absolute maximum peak.

5.2.1 High-pass SF applications

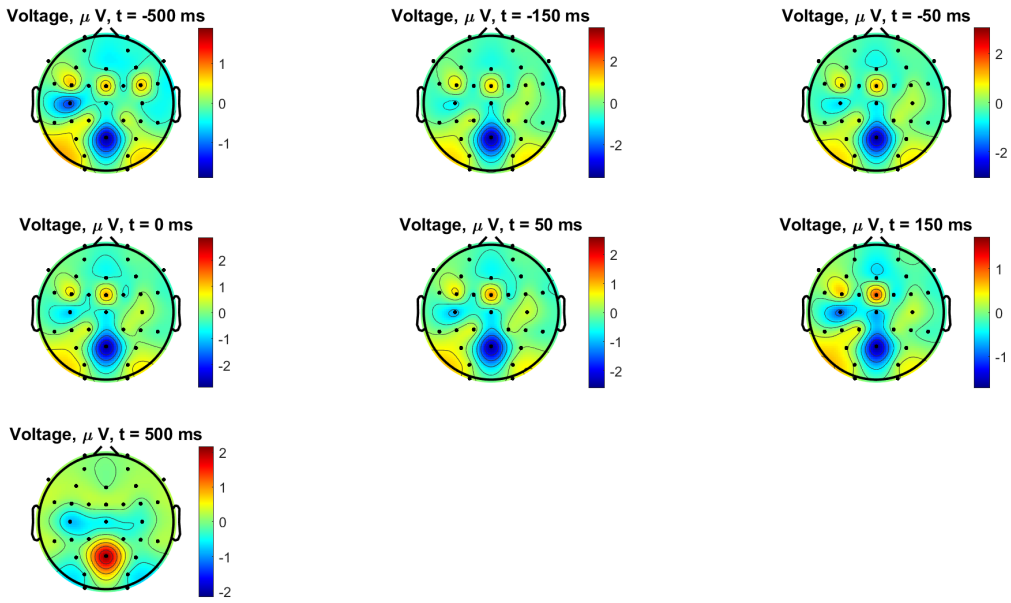

Figure 5.3: Topographies after the application of the SLSF updated on dataset MC.

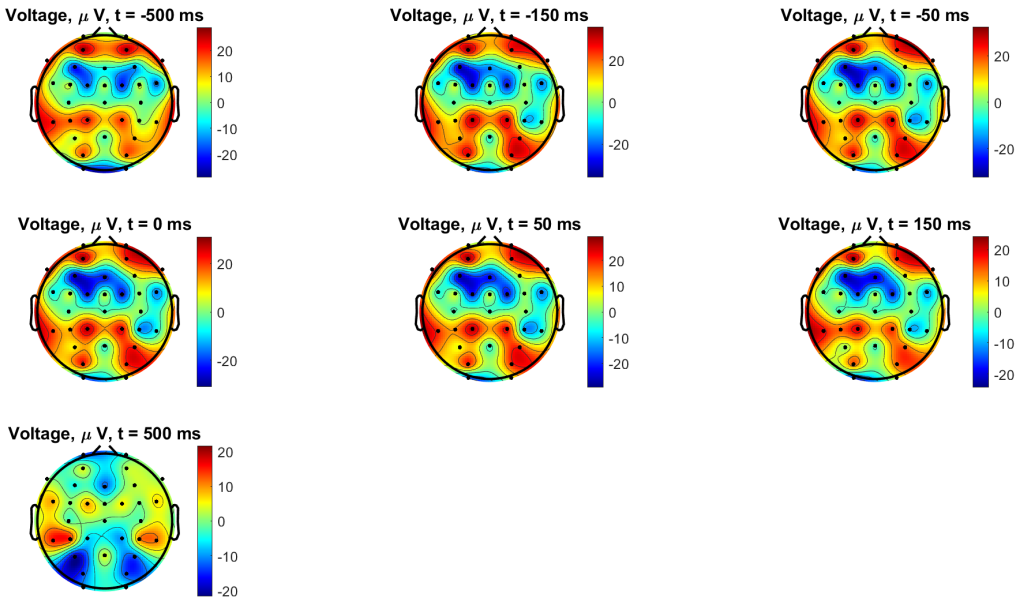

Figure 5.4: Topographies after the application of the SISF updated on dataset MC.

The topographies show activity in both the hemispheres. In particular, there are some moments where right and left electrodes have a similar activation just like at 0 ms.

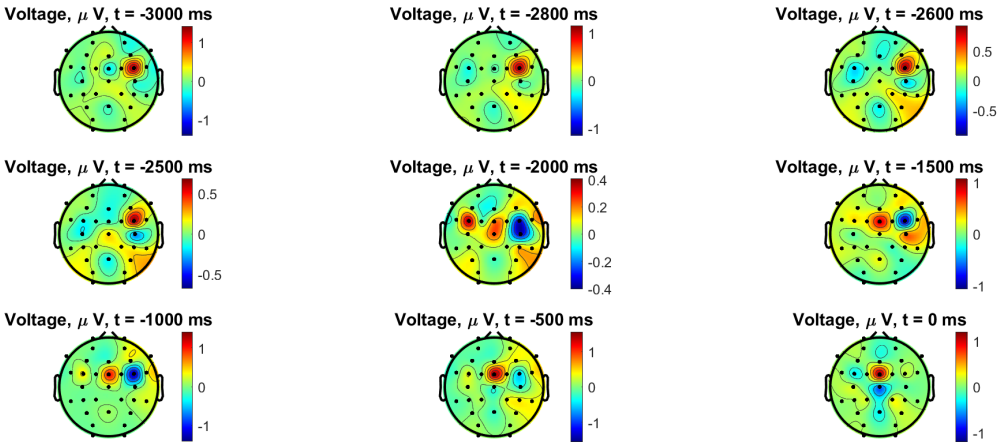

Figure 5.5: Topographies after the application of the SLSF updated on dataset DV.

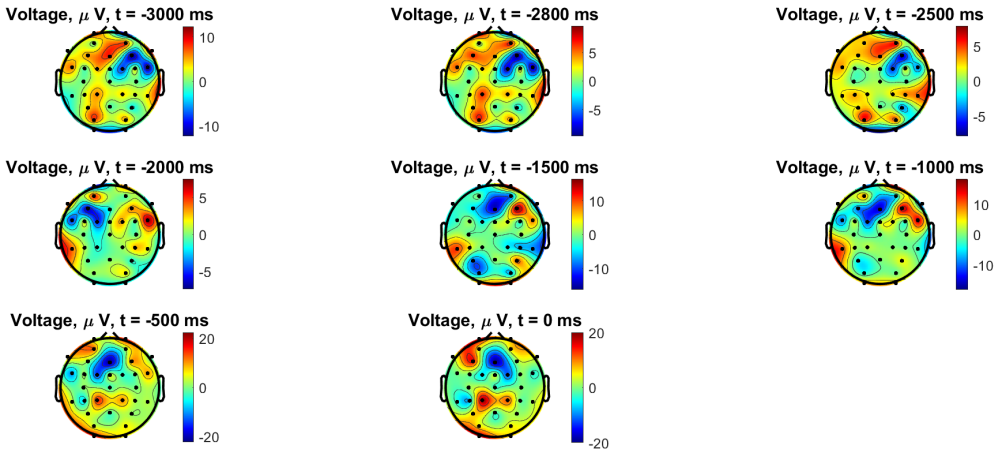

Figure 5.6: Topographies after the application of the SISF updated on dataset DV.

Even for the DV dataset, the topographies emphasize the activity of both left and right electrodes. The spherical spatial filter in both cases is more detailed in the results.

5.2.2 Low-pass SF applications

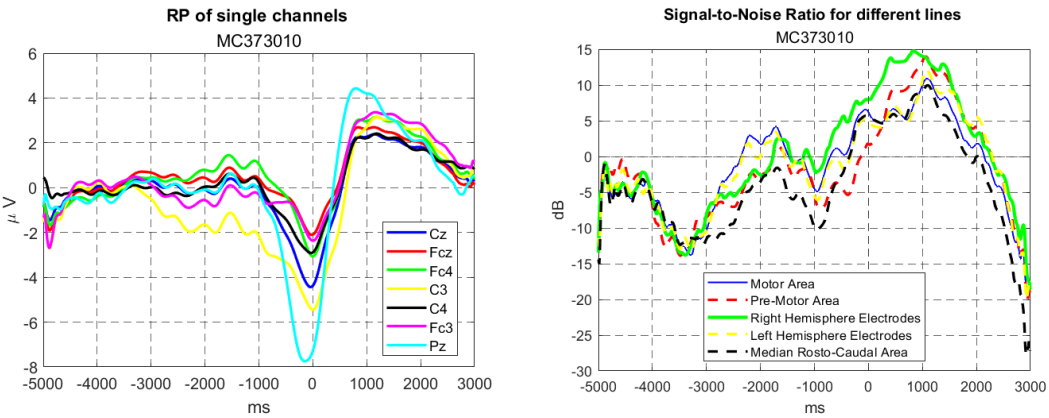

Figure 5.7: (Left) RPs of single channels, (right) SNR of averaged lines of the spatial unfiltered signal.

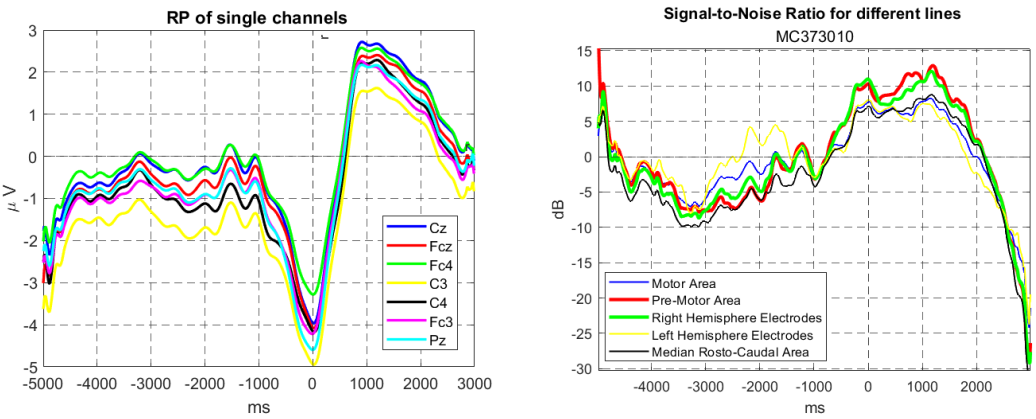

Figure 5.8: (Left) RPs of single channels, (right) SNR of averaged lines of the low spatial filtered signal.

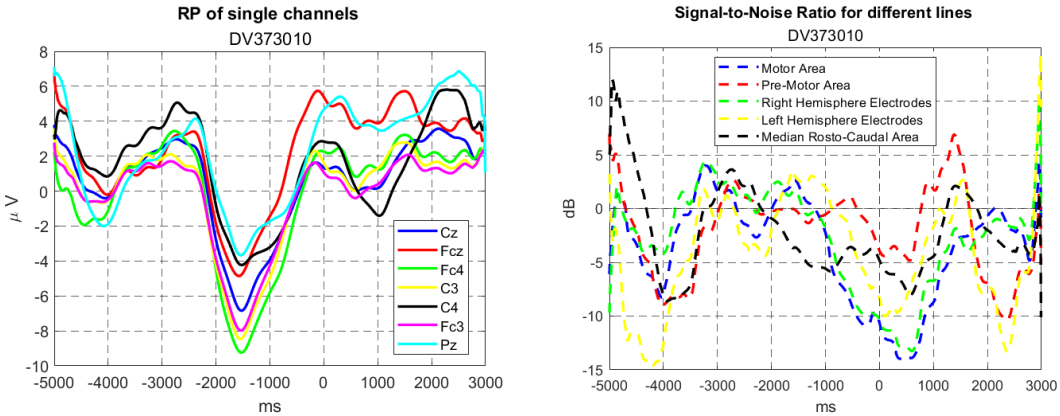

Figure 5.9: (Left) RPs of single channels, (right) SNR of averaged lines of the spatial unfiltered signal.

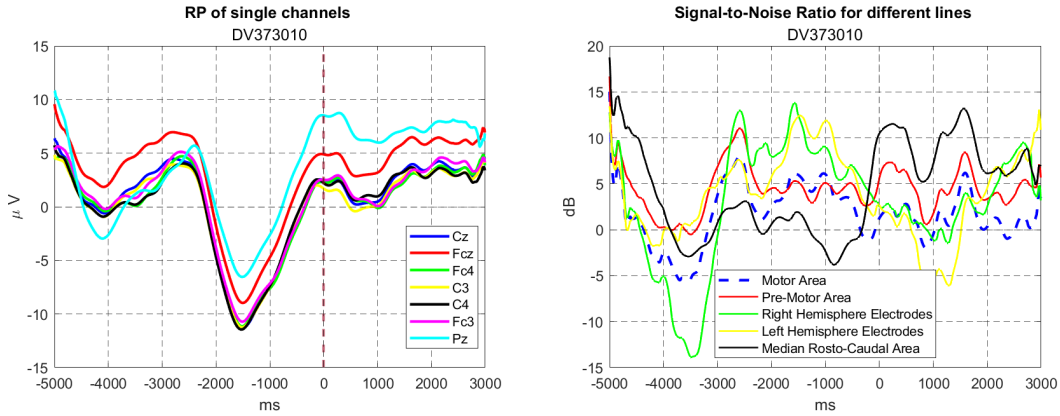

Figure 5.10: (Left) RPs of single channels, (right) SNR of averaged lines of the low spatial filtered signal.

Even with the hemiplegic, the low pass spatial filter helps enhancing the SNR thanks to the removal of noise and potential EOG artifacts. Comparing the two patients, the MC results are better, since the raw signal has a good quality, while unfortunately the DV signal begins with a very low SNR.

5.3 Conclusions & Future ideas

Spatial filters have demonstrated to be essential in the pre-processing chain of this brain-computer interface, especially because they provide topographies that show regions of activation on the scalp by removing the blurring effect of volume conductance and because they can enhance the signal-to-noise ratio of readiness potentials measured both with large and small EEG-cap. Unfortunately, their effectiveness is strongly dependent on the number of electrodes, the noise present in the raw signal and especially in the case of the high spatial filters, they may alter the RPs making difficult their interpretation. Indeed, it has been clarified from this thesis that it does not exist a perfect spatial filter that showcases optimal performances with each dataset analyzed. Furthermore, they are not immune to artifacts, so they risk worsening the final RPs if the raw signal is not properly cleaned up. Doubtless, performance of spatial filters will boost by employing a larger montage (i.e more than 100 electrodes) to improve the spatial resolution and, speaking about the quality of the input signals, the development of a denoising block and an improvement of the artifact correction processes put before the block of spatial filtering will valorize the output RPs of the spatial filters. Furthermore, a challenge for the future may be to realize a spatial filter using elliptic coordinates to approximate a 2D or even a 3D head, in order to obtain more precise results regarding the localization of superficial neuronal activities. Nevertheless, it is important to remember that the poor spatial resolution remains a limitation of the EEG signals. For that reason, recording them together with MEG (magnetoencephalographic) signals may increase the quality of topographies, circumscribing better the regions of activation. Regarding the hemiplegic patients, a lot of work is necessary to define an automatic algorithm to find the onsets and to perform the artifact corrections, in order to allow spatial filters to produce more reliable results.

Bibliography

[1] G. Brunetti. «La coscienza, alla ricerca di una propria identità». In: (2020). URL: http://www.neuroscienze.net/la-coscienza-alla-ricerca-di-unapropria-identita/ (cit. on p. 1).

[2] D. Chalmers. «The Blackwell Companion to Consciousness». In: (2007) (cit. on p. 1).

[3] Adrian M. Owen, Nicholas D. Schiff, and Steven Laureys. «The Assessment of Conscious Awareness in the Vegetative State». In: (2009) (cit. on p. 1).

[4] M. Manfredi. «La coscienza e i suoi fondamenti biologici». In: (2010) (cit. on p. 3).

[5] A. G. Casali et al. «A Theoretically Based Index of Consciousness Independent of Sensory Processing and Behavior». In: (2013) (cit. on p. 3).

[6] Springer Science and Business Media LLC. «Sleep Disorders Medicine». In: (2017) (cit. on p. 4).

[7] Istituto Superiore di Sanità. «Coma». In: (2013). URL: https://www.issalute.it/index.php/la-salute-dalla-a-alla-z-menu/c/coma?highlight=WyJkaWFiZXRlIl0=#sintomi (cit. on p. 4).

[8] K. Maiese. «Vegetative State and Minimally Conscious State». In: (2020) (cit. on p. 4).

[9] Carol Di Perri, Lizette Heine, Enrico Amico, Andrea Soddu, Steven Laureys, and Athena Demertzi. «Technology-based assessment in patients with disorders of consciousness». In: (2014) (cit. on p. 6).

[10] C. Di Perri, L. Heine, E. Amico, A. Soddu, S. Laureys, and A. Demertzi. «Technology-based assessment in patients with disorders of consciousness». In: (2014) (cit. on p. 6).

[11] Steven J. Luck. «An introduction to Event-Related Potential Technique, second edition». In: (2014), pp. 4–5 (cit. on pp. 13, 15, 19, 122).

[12] Mike X Cohen. «Analyzing Neural Time Series Data». In: (2014), pp. 26–27 (cit. on pp. 22, 58, 59).

[13] Chiara Botrugno. «Enhancement of Readiness Potentials' Pre-Processing Chain in a Brain-Computer Interface for nonresponsive patients». In: (2022), pp. 3–5 (cit. on p. 23).

[14] M. Bracale. «Elettromiografia». In: (2002), pp. 20–22 (cit. on p. 24).

[15] Springer Science and Business Media LLC. «The Bereitschaftspotential». In: (2003) (cit. on p. 28).

[16] C.Tandonneta, B.Burlea, T.Hasbroucqa, and F. Vidal. «Spatial enhancement of EEG traces by surface Laplacian estimation: comparison between local and global methods». In: (2004), pp. 4–5 (cit. on p. 28).

[17] P. Haggard. «Conscious Intention and Motor Cognition». In: Cognitive Science 9 (June 2005), pp. 290–295 (cit. on p. 30).

[18] Sasivimol Virameteekul1 and Roongroj Bhidayasiri. «We Move or Are We Moved? Unpicking the Origins of Voluntary Movements to Better Understand Semivoluntary Movements». In: (2022) (cit. on p. 30).

[19] «Trans Cranical Technologies ldt». In: (June 2012), pp. 1–2 (cit. on p. 33).

[20] In: (). URL: `https://eeglab.org/tutorials/#III.Advanced_Topics` (cit. on p. 39).

[21] Davide Rigoni, Marcel Brass, Clémence Roger, Franck Vidal, and Giuseppe Sartori. «Top-down modulation of brain activity underlying intentional action and its relationship with awareness of intention: an ERP/Laplacian analysis». In: (2012) (cit. on p. 49).

[22] C. Tandonneta, B. Burlea, F. Vidala, and T. Hasbroucqa. «The influence of time preparation on motor processes assessed by surface Laplacian estimation». In: (2003) (cit. on pp. 49, 112).

[23] Dennis J. McFarland, Lynn M. McCane, Stephen V. David, and Jonathan R. Wolpaw. «Spatial filter selection for EEG-based communication». In: (1997) (cit. on p. 50).

[24] Mads Jochumsen, Imran Khan Niazi, Natalie Mrachacz-Kersting, Ning Jiang, Dario Farina, and Kim Dremstrup. «Comparison of spatial filters and features for the detection and classification of movement-related cortical potentials in healthy individuals and stroke patients». In: (2015) (cit. on p. 50).

[25] Simone Rumac. «Single-Trial Analysis of Readiness Potentials using Empirical Mode Decomposition». In: (2018) (cit. on p. 50).

[26] O. Bertrand F. Perrin J. Pernier and J.F. Echallier. «Spherical splines for scalp potential and current density mapping». In: (1998), pp. 1–2 (cit. on pp. 50, 64).

[27] Uzgalis Estras. «Computerized Display of Spatio-temporal BEG Patterns». In: (1969), pp. 1–2 (cit. on p. 51).

[28] Timothy J. Lano Seung Suk Kang and Scott R. Sponheim. «Distortions in EEG interregional phase synchrony by spherical spline interpolation: causes and remedies». In: (2015), p. 15 (cit. on p. 64).

[29] Thomas C. Ferree. «Spherical Splines and Average Referencing in Scalp Electroencephalography». In: (2006) (cit. on p. 64).

[30] C. Tandonneta, B. Burlea, T. Hasbroucqa, and F. Vidala. «Spatial enhancement of EEG traces by surface Laplacian estimation: comparison between local and global methods». In: (2004) (cit. on p. 64).

[31] L. A. BRADSHAW1 and JR. J. P. WIKSWO. «Spatial Filter Approach for Evaluation of the Surface Laplacian of the Electroencephalogram and Magnetoencephalogram». In: (2001), pp. 7–8 (cit. on p. 91).